71

A Systematic Approach to Station-Keeping of Constellations of Satellites

by

Brian Kantsiper

Submitted to the Department of Aeronautics and Astronautics
in partial fulfillment of the requirements for the degree of

Doctor of Philosophy in Aeronautics and Astronautics

at the

MASSACHUSETTS INSTITUTE OF TECHNOLOGY

Feb 1998

Author .....
Department of Aeronautics and Astronautics
11 Dec 1997

Certified by ... .
Stanley Weiss
Visiting Professor, Department of Aeronautics and Astronautics
Thesis Supervisor

Certified by ....
Paul Cefola
Technical Supervisor, Draper Laboratory
Thesis Reader

Certified by ....
Jack Kerrebrock
Professor, Department of Aeronatics and Astronautics
Thesis Reader

Certified by ....
Richard Battin
Adjunct Professor, Department of Aeronautics and Astronautics
Thesis Reader

Accepted by ....
Jaime Peraire
Chairman, Departmental Committee on Graduate Students

A Systematic Approach to Station-Keeping of Constellations of Satellites

by

Brian Kantsiper

Submitted to the Department of Aeronautics and Astronautics
on 11 Dec 1997, in partial fulfillment of the
requirements for the degree of
Doctor of Philosophy in Aeronautics and Astronautics

Abstract

The recent proliferation of satellite networks for personal communication systems has led to an increase in interest in understanding the dynamics of constellations of satellites. One of the problems associated with constellations of satellites is the determination of the control requirements of each individual satellite in order to meet a top level requirement. The most common metric for analysis of constellations is the percent coverage. The goal of this work was to develop a systematic, extensible approach to determining the station-keeping requirements on individual satellites based on a coverage requirement for the constellation.

An analytical approach to calculating the coverage of a constellation was developed. This approach contrasts with more typical numerical algorithms, which are often too slow for detailed analysis. The analytical method is based on integrating the area in the regions defined by the overlap of satellite footprints. The constellation coverage is assembled from these overlap areas using basic combinatorics. The coverage may be determined over any region on a sphere which can be defined by the intersection of circles on the surface. This approach proves to be faster than numerical approaches for reasonable precision for most constellations.

An algorithm for determining the best orbital element limits on individual satellites to meet a coverage requirements was developed. The uncontrolled dynamics of the satellite orbits was examined to determine in what way the coverage of the constellation fails. That pattern was used to systematically vary the configurations of the constellation, and the coverage was calculated for each perturbed configuration. This approach produces coverage contours. The position on the contour which minimizes the fuel usage for station-keeping was chosen as the requirement for the constellation. These results were validated for the Ellipso constellation using the ASKS system developed by Naresh Shah [27]. The results of the simulations confirmed the qualitative behavior predicted by the analysis.

Thesis Supervisor: Stanley Weiss
Title: Visiting Professor, Department of Aeronautics and Astronautics

Acknowledgments

As always, there are an immense number of people who should be acknowledged, and I doubt very much that I can cover all of them without this section being longer than the rest of the dissertation. If you're the sort of person who reads acknowledgments and get offended if you're not listed, tell me and I'll send you a personalized acknowledgment and a surplus thesis.

First, I must thank Prof. Stanley Weiss, whose constant efforts to drum up support for and interest others in this project and other efforts on my behalf. I must also thank Dr. Paul J. Cefola and Dr. Ronald J. Proulx for taking me in to Draper and acting as extra advisors, despite their already overloaded schedules. It is often hard enough to find one advisor, but I had three.

Special thanks to the other two members of my thesis committee, Prof. Jack Kerrebrock and Prof. Richard Battin, for time spent discussing my work, reviewing the document, and their support.

Further thanks are owed to Ross Jones of the Jet Propulsion Laboratory, Chuck Rudiger of Lockheed-Martin Missiles and Space, and Byong Ahn and John Sweeney of the Charles Stark Draper Laboratory for their generous financial support of this work. Also, thanks are due to John Draim of MCHI, Nino Pino of Globalstar, and Dennis Diekelman of Iridium for information necessary to this work.

Thanks to all the guys at Draper, Naresh Shah, Jack Fischer, and Joe Neelon. To Marvin, for not blowing up the world until I was done. To Tim, because the Huskers suck. To Min, for all the encouragement when I stressed and the kicks in the rear the rest of the time.

And, finally, most of all to my parents and family, because they would kill me if I didn't put them in and because of everything.

This thesis was prepared at The Charles Stark Draper Laboratory, Inc., with support from the DFY 97 and 98 Draper IR & D Program, with further support from Lockheed-Martin and the Jet Propulsion Laboratory.

Publication of this thesis does not constitute approval by or the sponsoring agency

of the findings or conclusions contained herein. It is published for the exchange and stimulation of ideas.

Permission is hereby granted by the Author to the Massachusetts Institute of Technology to reproduce any or all of this thesis.

Author .....

Brian Kantsiper

Contents

List of Figures

List of Tables

Chapter 1

Introduction

One of the more striking trends in the space industry is the tendency toward mission designs utilizing more than one spacecraft. This trend is the result of several factors. The current NASA credo of "faster, better, cheaper" has driven the industry toward production of smaller and simpler satellites, with less redundancy and shorter development times. For a given size of instrumentation, decreasing the size of the satellite limits what may be accomplished with a single spacecraft. Distributing the payload across several spacecraft takes advantage of the cost savings inherent in these smaller spacecraft, as smaller satellites are typically cheaper to launch, transport, and test. Distributing the payloads on multiple platforms also mitigates the increased risk which results from the shorter development times and decreased redundancy.

In addition, increasing numbers of scientific missions and industrial initiatives require instantaneous access to a large portion of the surface of the earth. Scientific missions (such as those studying global climatic change) are becoming more demanding in that they require measurement of such parameters as atmospheric pressure and temperature on a high precision global grid. In industry, the ever growing "information superhighway" is creating a demand for global satellite telecommuncations. These demands also require a large number of spacecraft.

The types of multiple satellite configurations may be divided into three classes.

The first is known as "formation-flying" and just consists of two or more satellites orbiting in the same plane with a relatively small fixed distance between them. The second class is a "cluster", which is a group of satellites in slightly different orbits. These configurations tend to be unstable and typically have been proposed to study local variations (such as in the earth's magnetic field) for short durations. The final class is a "constellation," which consists of a number of widely spaced satellites in similar orbits. Constellations can provide visibility of the entire surface of the earth for extended periods of time. The wide range of applications of multiple spacecraft configurations fall into these classes and can be treated similarly.

The use of these configurations all place new demands on satellite design. For formation-flying and clusters, high-precision position and pointing information are often critical. And all of them require new approaches to navigation and control of the spacecraft. This work attempts to study the dynamics of constellations, in particular, and to develop a systematic approach to the determination of the control requirements for individual satellites necessary to meet a system objective.

1.1 Description of Constellations

Despite the immature state of our understanding of their dynamics and control, there are already a number of constellations which are either in orbit or approaching completion. These satellites fall into three categories: global navigation, satellite telecommunications, and scientific studies of global change. These categories are listed in roughly the order of their development.

1.1.1 Navigation

Global navigation systems utilize multiple spacecraft to determine the user's position precisely. The Global Positioning System (GPS) is the best known example of this type of constellation, although the former Soviet Union also operates a similar satellite navigation system (GLONASS). Each GPS satellite contains a high precision atomic

	GPS
Number of Planes	6
Number of Satellites	24
Semi-major Axis (km)	26561.75
Eccentricity	≤ 0.02
Inclination (deg)	55
Argument of Perigee (deg)	–

Table 1.1: Key parameters for the Global Positioning System

clock, and the signal the satellite emits contains a time signature. The GPS receiver determines from this signal the current distance to the satellite (as the signal travels at the speed of light). With simultaneous data from at least four satellites, the three position elements of the receiver may be determined precisely. The fourth satellite is necessary in order to correct the imprecision in the receiver clock.

The program began in 1973, and the first satellite was launched in 1978. The operational GPS constellation, the GPS block II satellites, consists of 24 satellites placed in circular 12-hr orbits. The orbital data for the GPS constellation is listed in Table 1.1 [30].

1.1.2 Telecommunications

The telecommunications industry is responsible for most of the effort put into studying satellite constellations over the past several years. The success of cellular phone technology has led to a number of proposals for handheld telephone service provided via satellite. In addition, the ever increasing demand for instantaneous access to information has led to several similar proposals for providing data transmission. Some of these constellations are discussed below. There are also a number of constellations which intend to provide high-speed data transmission in a similar fashion, such as ORBCOMM and Teledesic, but these will not be considered here.

	Iridium
Number of Planes	6
Number of Satellites	66
Semi-major Axis (km)	7158
Eccentricity	0.0013
Inclination (deg)	86.4
Argument of Perigee (deg)	90.0

Table 1.2: Key parameters for the Iridium System

Iridium

Iridium is the name of a satellite telecommunications service developed by Motorola Corporation. Originally designed to have 77 satellites, it was named after the element with an atomic number of 77, although, in the current design, there are only 66 satellites. The satellites are distributed into 6 planes, evenly spaced in longitude of the ascending node. They are in circular polar orbits at an altitude of 780 km. The orbital information for Iridium is listed in Table 1.2 [11].

Because of the low altitude of the Iridium satellites, each satellite can only see a small portion of the surface at a time. In addition, the low altitude leads to a short orbital period. This indicates that each satellite travels across the sky at a large angular rate. Iridium relies on satellite cross-links and rapid call hand-offs to try to resolve these issues.

Iridium received its FCC license in 1995. With 33 satellites on-orbit, Iridium is currently the largest constellation in existence.

Globalstar

Globalstar is another low earth orbit (LEO) satellite telecommunications constellation. It is the property of Loral Corporation and will consist of 48 satellites in 8 orbital planes. The constellation is a Walker delta pattern [32] inclined at 52 degrees. The orbital data for Globalstar is listed in Table 1.3 [24]. The Globalstar program was formed in 1991. Initial service is expected to be available in August, 1998, and the constellations will be fully operational by January, 1999.

	Globalstar
Number of Planes	8
Number of Satellites	48
Semi-major Axis (km)	7792
Eccentricity	0.05
Inclination (deg)	52.0
Argument of Perigee (deg)	90.0

Table 1.3: Key parameters for the Globalstar System

Ellipso

Ellipso is the MCHI Corporation personal communication network. It consists of three planes of satellites with apogees which are much higher than the other two discussed above. The first plane, known as Concordia, contains seven satellites in a circular equatorial orbit. The other two planes, collectively known as Borealis, are more interesting. They are moderately elliptical and critically inclined, which allows the argument of perigee of the orbits to be fixed. For Borealis, it is set to be 270 degrees, which fixes the apogee of the orbits above the northern hemisphere. Since satellites spend more time at apoapsis than at periapsis, this focuses the coverage of the Borealis planes on the northern hemisphere, where the potential market for the system is greatest. The Borealis constellation provides the primary coverage for the northern hemisphere, while Concordia provides coverage in the southern hemisphere to 55 degrees south and supplements Borealis in the north.

In addition, the Borealis planes are sun-synchronous, which simplifies the satellite design, and have fixed ground-tracks (8:1 repeat cycle), which simplify the ground station operations. The data for the two components of Ellipso are shown in Table 1.4 [8]. The parameters listed for the Borealis constellation actually vary slightly between the planes, in order to maintain both sun-synchronicity and critical inclination. Ellipso received its FCC license in 1997.

	Ellipso (8:1)	
	Borealis	Concordia
Number of Planes	2	1
Number of Satellites	10	7
Semi-major Axis (km)	10559	14440
Eccentricity	0.3457	0.0
Inclination (deg)	116.5	0.0
Argument of Perigee (deg)	270.0	–
Minimum Elevation Angle (deg)	25	10

Table 1.4: Key parameters for the Ellipso constellation

1.1.3 Earth Observing Constellations

In addition to the systems described above, which are all in existence already or well along in their design, there is also unrealized potential for the use of constellations in studying global change. The Earth Observing System (EOS), which will have its first satellite launched in 1998[2], will provide a massive amount of data on the earth system, but to truly understand the long-term physical and chemical processes in the earth's atmosphere and oceans, global real-time data covering an extended period of time is necessary. In order to obtain this information, a satellite network is required. Presumably, as global change and climatic variations become hotter issues, there will be proposals for constellations to study them.

1.2 Metric for Constellations

As has already been mentioned, the move from individual satellites to constellations creates new challenges in satellite control. These challenges are primarily in the field of system engineering, in that they pertain more to deciding how to budget the top-level constellation requirements down to individual satellites rather than to the process of meeting the requirements at a satellite level. Regardless of whether the satellite is part of a constellation or operating independently, the control methodology is the same. A maximum allowable deviation from some reference trajectory is defined,

and, if there is a violation, some velocity correction is determined to eliminate the violation and, if the methodology is designed properly, to maximize the time between such violations. The new issues concern the proper definition of that control box.

As an example, consider a group of satellites spaced evenly in the same orbital plane. If these satellites are all displaced evenly in mean anomaly, i.e. the entire plane is rotated, there is no impact on what part of the earth is visible to the plane as a whole, although, of course, what each individual satellite covers does vary. If we were to consider each satellite individually, they would all require position corrections, in this case costly mean anomaly burns. When the plane is viewed as whole, however, no corrections are necessary.

The deviation from nominal trajectories is therefore not a good measure of the performance of the constellation. What is important is how much the constellation as a whole sees, not what the contribution from any individual satellite is. The parameter which quantifies this measure of performance is the percent coverage of the constellation. The percent coverage C is defined as the ratio of the area which is visible to at least one satellite to the total area of interest:

$$C(t) = \frac{Area\ Visible}{Total\ Area}$$

As noted above, the coverage is a function of time, a snapshot of the area visible to the constellation at a given instant. As such, it depends only on the position of the satellites at that time, not their velocities. If we are interested in the overall performance of the constellation, we must take the time average of the coverage over one orbital period, or perhaps over one repeat cycle of the constellation.

There are a large number of varieties of coverage-like parameters. Multiple coverage, or the percent of the area visible to n or more satellites, may also be calculated. This is of interest for navigation systems such as GPS which require four or more satellites to provide complete information. We can determine coverage as a function of latitude and/or longitude. There are also other parameters which attempt to include time information (such the average duration of lapses in coverage) along with

visibility to improve over pure coverage. See Wertz [19] for a discussion of the value of these different parameters. Despite the existence of these different approaches, the percent coverage is by far the most commonly used metric for the evaluation of constellation performance. Some of the theory involved in calculating this metric is discussed in the next chapter.

1.3 Overview

Chapter 2 gives a brief description of the history of constellation design. Chapter 3 develops an analytic approach for determining the coverage area of a given constellation configuration. It develops the theory for integrating the area defined by the overlap of satellite footprints. Chapter 4 describes the algorithm by which the analytic coverage theory is implemented. It also discusses the advantages and disadvantages of the method, including extensions to the theory and a comparison to more typical approaches to calculating coverage. Chapter 5 develops the systematic approach for deriving requirements for individual satellites based on an overall requirement for the constellation. In Chapter 6, numerical simulations are utilized to test the requirements derived in the preceding chapter. Finally, Chapter 7 discusses future work which is suggested by this work and provides a conclusion.

Chapter 2

Literature Review

This chapter examines the history of the design and analysis of constellations of satellites. It begins with the early work of J. G. Walker and others in the development of symmetrical circular constellations through more complicated elliptical orbit constellations. Descriptions of the various methods and metrics used to analyze constellation performance are developed.

2.1 Constellation Design

Early work in constellation design focused on developing configurations for global coverage with a minimal number of satellites [1]. These configurations were, of course, symmetric polyhedra with various number of vertices. These configurations were not practical, in that given the dynamical system, the satellites would not remain evenly distributed, as they were static designs and did not take into account the dynamics of the the system. Gradually, the constellation designs became more practical.

2.1.1 Early Work

Some of the earliest work in the field of satellite constellations was done by Frank Gobetz [12]. He considered two types of configurations: polar and polyhedral. The first class consists of a set of evenly distributed orbital planes which all intersect at two points at antipodal points of the earth. The choice of these points was limited to the north and south poles as a result of earth oblateness effects. This class of constellation is therefore known as a polar constellation.

The second class of orbits consist of planes parallel to the regular polyhedra. As it was known that the best configurations for instantaneous coverage are these regular polyhedra, it was natural to model constellations on these geometries. Gobetz analyzed the minimum altitude required for a given number of satellites in each configuration, utilizing the natural symmetries of the constellations to determine the worst-case configurations. His analysis demonstrated that for a given number of satellites the minimum altitude required for complete global coverage was larger for the polyhedral constellations than for the polar constellations. He concluded that polar constellations were a more efficient approach for providing earth coverage. He further developed a symmetric constellation containing six satellites in two orbits with altitude of 5260 nmi which provided complete coverage. He also developed a five satellite constellation in three planes which also provided global coverage, but dismissed it because it required a much larger satellite altitude.

The defining work in the design of constellations was contributed by J. G. Walker in a series of papers from 1971 through 1984. In an early paper [32], he develops the constellation configuration which has come to be known as the Walker delta patterns. While Walker was not the first to recognize the possible advantage of the delta pattern configuration, he was the first to provide a thorough analysis of the coverage obtained through such constellations.

His analysis begins by identifying the primary weakness in polar constellations, that because all of the satellite orbits converge at a point, coverage is not distributed evenly across the surface of the earth. His solution was to create a configuration in

which the orbital planes all had a fixed inclination relative to some plane, taken in practice, again because of earth oblateness effects, to be the equatorial plane. In such a configuration, no more than two orbits intersect at any one point; therefore, the coverage of the constellation is more evenly distributed. The inclination of the orbits relative to the reference frame was referred to as δ in his nomenclature. These constellations are therefore referred to as delta patterns.

He then determined that five satellites in circular orbits was the minimum number to provide global coverage. Any four satellites must, at some point, lie all in the same plane, and, at this point, cannot provide complete coverage for less than infinite altitude. He then develops minimal constellations for single and double global coverage, consisting respectively of five and seven planes with one satellite per plane. In addition, he details a constellation of six satellites in two planes which provides global coverage in a wide range of configurations. A similar constellation consisting of nine satellites in three planes is also developed.

In later works [33], he developed the classic TPF nomenclature for describing delta pattern constellations. T is the number of satellites in the constellation, and P is the number of orbital planes in the constellation. The satellites are evenly divided amongst the orbital planes. F is the angle, in units of $2\pi/T$, from one satellite to its ascending node when a satellite in the adjacent plane is at its node. Walker tabulated the coverage performance (in terms of minimum elevation angle) for various TPF values for different degrees of coverage.

2.1.2 Elliptical Orbits

The Walker and polar patterns both rely on circular orbits. Some improvements may be made through the use of elliptical orbits. Specifically, the minimum number of satellites necessary to provide continuous coverage may be reduced. For elliptical orbits, orbits may be chosen such that four satellites do not ever fall into one plane. Draim [9] develops a set of constellations consisting of four satellites in four satellite planes which provide continuous global coverage. The orbits must have period of at

least 26.5 hours, but such constellations may be designed for a range of eccentricities and inclinations. Draim focuses on one with a 48 hour period and inclination of 28.5 degrees, to correspond with the latitude of Kennedy Space Center for ease of launch.

Such constellations provide an intriguing alternative to geostationary orbits. Geostationary orbits are becoming quite overpopulated. They do not cover polar regions adequately. The Draim orbits populate a wide range of orbital parameters, allowing flexibility in design (in choice of a repeat groundtrack, for example), without the high satellite density in the geostationary belt. These orbits could, in principle, be applied for communications, weather, or other earth-viewing missions.

Constellations consisting entirely or partially of elliptical orbits are becoming more and more popular. They may be developed in ways similar to polar or delta patterns, but, through judicious design, may be used to focus the coverage over particular regions. One example of such a design is the Borealis planes of the Ellipso constellation [26], discussed previously, which is designed to focus its coverage on the northern hemisphere during daytime hours. Another example is the well-known Molniya satellite orbit, which uses the long dwell-time near apogee to provide coverage of high latitudes over Europe and the former Soviet Union. Recently, Palmerini [23] has been doing some more general analysis of elliptical orbits, in particular for regional coverage, based on superimposition of coverage "streets," which are the locus of all points a satellite can view through a period of its orbit. The study of constellations based on elliptical orbits is young, and much more analysis is necessary.

2.2 Coverage Analysis

In the past, there have been a number of different methods used to evaluate coverage. For most applications, numerical methods have been utilized, although one analytical approach will be described. The numerical methods have fallen into one of two categories, depending on the way they approximate the surface: the grid or the meridian methods. These two methods will be discussed, but, in the interest of

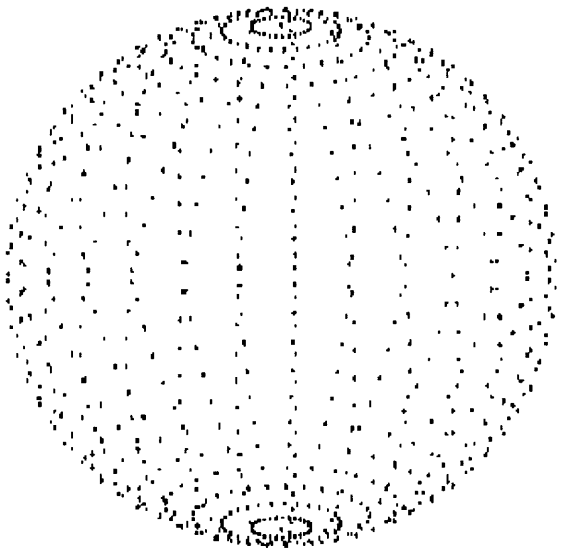

Figure 2-1: Typical grid

brevity, no discussion of the numerous hybrid methods which have been employed will be attempted.

2.2.1 Grid-based Methods

The grid based method is the most basic numerical technique. This method has been used extensively in coverage analyses [19, 31]. In this method, the earth is represented by an array of points on its surface. Typically, the grid is chosen to have fixed number of points at each latitude, as shown in Figure 2-1. The coverage as a function of latitude can be obtained simply from the ratio of the number of points at a given latitude for which a satellite is visible to the number of points at that latitude.

If we are interested in the total coverage, we have to be a little more careful. As can be seen in Figure 2-1, a grid which consists of points evenly spaced in latitude and longitude covers the polar regions more densely than the equatorial regions. If we assume a spherical earth, this is easily remedied by weighting the contribution of each grid point by the sine of its colatitude (or polar angle) θ. In this case, the coverage is simply

$$C(\theta) = \frac{\sum_{i=1}^{N} Vis(\theta_i, \phi_i, \epsilon) \cos\theta_i}{\sum_{i=1}^{N} \cos\theta_i} \tag{2.1}$$

where θ_i and ϕ_i are the colatitude and longitude of point i, ϵ is the minimum elevation angle, and *Vis* represents the visibility function , which has value 1 if a satellite is in view above the minimum elevation angle, and value 0 if there is no satellite visible. A similar but more complicated equation may be written for the case in which the ellipticity of the earth is included.

The advantages of the grid method are its simplicity and flexibility. A grid can be generated for an arbitrarily complex surface. There is, however, a rather severe drawback to this method. Being a numerical method, the results are not exact. There is a loss of precision inherent in the process of representing a surface as a grid of points. In order to get accurate results, a large grid ($\sim 10^4 - 10^5$ elements) must be employed. Such large grid sizes result in a large number of computations per time step, which may, of course, lead to unacceptably long computer run times.

2.2.2 The Meridian Method

The meridian method represents an attempt to decrease the loss of precision inherent in simple grid-bases methods. It was first developed by Casten and Gross [6]. Instead of approximating the earth by a set of points, the surface was represented by a set of great circles passing through the poles, or meridians (see Figure 2-2). The latitude range for each meridian for which there is a satellite in view is stored. This information is assembled to provide the percent coverage for each meridian. At this point, it is simple to integrate and average in longitude to determine the overall coverage.

The advantage of this method is that the latitude range of a given meridian for which a given satellite is visible may be calculated analytically. We can calculate the colatitude of the intersection of a satellite footprint and a meridian by using the law of cosines for spherical trigonometry[1]:

$$\cos\lambda = \cos\theta_{sat}\cos\theta + \sin\theta_{sat}\sin\theta\cos\Delta L \tag{2.2}$$

[1]The analysis in this work relies heavily on an understanding of spherical trigonometry. Green [13] is a good source for more information on this subject.

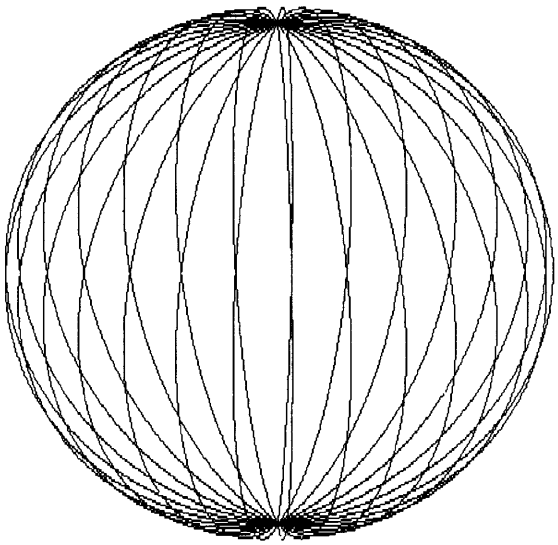

Figure 2-2: Longitude lines in meridian method

where λ is the central angle of the satellite footprint (as discussed further in the following chapter), θ_{sat} is the colatitude of its subsatellite point, and ΔL is the longitude difference between the subsatellite point and the meridian in question. We note that this equation is of the form

$$K = A\cos\theta + B\sin\theta$$

which can be solved by dividing both sides by the radical $\sqrt{A^2 + B^2}$. We proceed, defining the angle ψ by

$$\cos\psi = \frac{\cos\theta_{sat}}{\sqrt{\cos^2\theta_{sat} + \sin^2\theta_{sat}\cos^2\Delta L}} \tag{2.3}$$

$$\sin\psi = \frac{\sin\theta_{sat}\cos\Delta L}{\sqrt{\cos^2\theta_{sat} + \sin^2\theta_{sat}\cos^2\Delta L}} \tag{2.4}$$

deriving that

$$\frac{\cos\lambda}{\sqrt{\cos^2\theta_{sat} + \sin^2\theta_{sat}\cos^2\Delta L}} = \cos\theta\cos\psi + \sin\theta\sin\psi = \cos(\theta - \psi)$$

Since the inverse cosine has both positive and negative roots, the colatitudes of the two intersection points are given by

$$\theta = \psi \pm \arccos\left(\frac{\cos\lambda}{\sqrt{\cos^2\theta_{sat} + \sin^2\theta_{sat}\cos^2\Delta L}}\right) \tag{2.5}$$

where ψ can be determined from either of Equation 2.3 or Equation 2.4.

The advantage of this method over the grid-based methods is that you lose less precision, as there is only one approximation(longitude) rather than two. It also decreases the number of calculations that are necessary for similar reasons. This improvement in precision and speed is accomplished at the price of some loss of information. The grid-based methods provide both latitude and longitude dependence for the coverage. In the meridian method, coverage is stored for each individual meridian, resulting in the loss of latitude dependence (unless, of course, you wish to store latitude information for each meridian for each time step, in which case there is a steep price in memory usage). The improvement in speed and precision often makes the loss of latitude dependence worthwhile. It is still, however, an approximate method and is still slow computationally for high density meshes.

2.2.3 Hayes Method

The approach to calculating coverage detailed in the next chapter is not the first analytical approach to determining coverage. Elizabeth Hayes developed a simple approach to determining this area [14]. Her approach was to divide an n-sided overlap region into an n-sided spherical polygon and n chord regions. The example shown in Figure 2-3 consists of a spherical triangle and three chord regions. The area of a spherical polygon is given by

$$A_{polygon} = \sum_{i=1}^{n} \alpha_i - (n-2)\pi$$

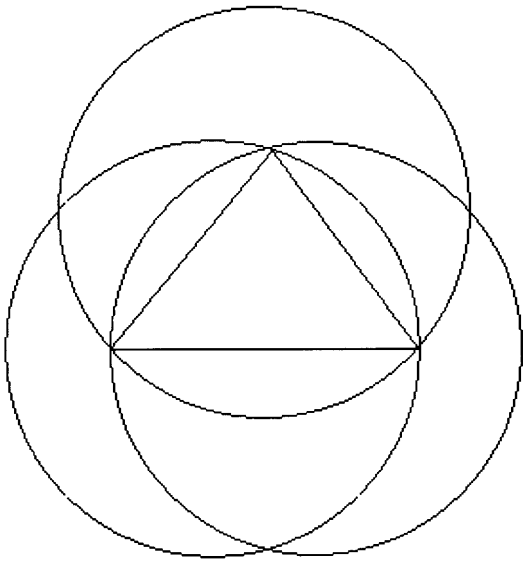

Figure 2-3: Overlap region for Hayes method

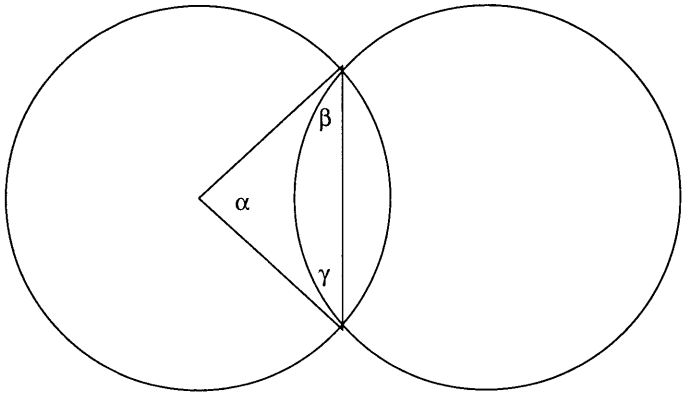

Figure 2-4: Chord area

where n is the number of sides and the α_i are the corner angles of the polygon. The chord area is given by the difference between the corresponding wedge of the circle and the appropriate spherical triangle, as shown in Figure 2-4. The chord area is therefore given by

$$\begin{aligned} A_{chord} &= \alpha\,(1-\cos\lambda) - (\alpha+\beta+\gamma-\pi) \\ &= \pi - \alpha\cos\lambda - \beta - \gamma \end{aligned}$$

The overlap area is then given by the sum of the area of the polygon and the chord areas. The method developed by this author is equivalent in execution time to the Hayes method. In addition, because it relies on classical analytic geometry rather than direct integration for area determination, the Hayes method does not provide an approach to extending the theory, computationally or analytically, to include such effects as the ellipticity of the earth or non-nadir pointing satellites.

Chapter 3

Coverage Theory

This chapter develops the basics for evaluating the coverage of a constellation of satellites. First, some preliminary topics are addressed. After that, an analytic approach to evaluating earth coverage is developed. The analytic theory is applied to a single plane of satellites, and some results of the theory are developed.

3.1 Preliminary Topics

In the last chapter, we defined coverage, but it was defined in terms of the percent of the surface which is "visible" to the constellation. The concept of visibility requires a more precise definition. The simplest definition of visibility is based on whether the satellite is above the horizon of the surface point in question, assuming the surface is a perfect sphere. This, of course, fails to take into consideration the possibility of interference from buildings, mountains, etc. It is, of course, impractical to completely detail the position of all possible interfering bodies precisely; some middle ground is necessary. What is typically done is to define the visibility at some elevation angle. This measures whether the satellite is above the horizon by some fixed angle. This compensates for the existence of shadowing without needlessly complicating calculations. This results in some circular footprint, centered on the sub-satellite

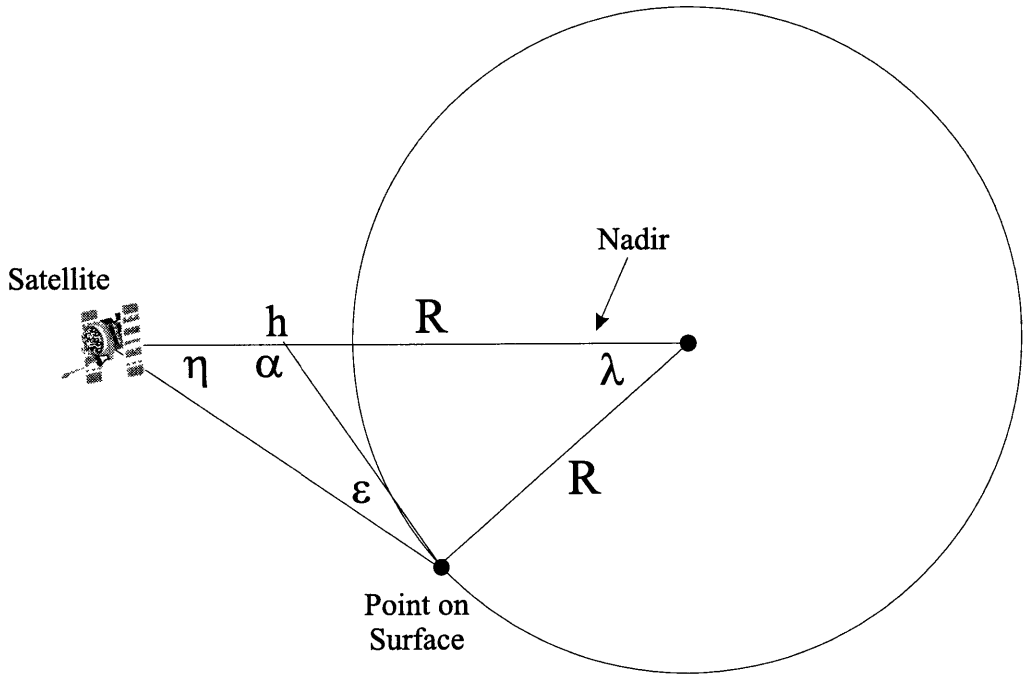

Figure 3-1: Earth-viewing geometry

point, which defines the region of visibility. The angular radius of this region is the earth central angle λ.

In order to derive the equation for visibility, we examine the geometry of a typical earth-viewing satellite, as shown in Figure 3-1. There are three angles of interest. The elevation angle ϵ is the angle the satellite is above the horizon. The nadir angle η is the angle connecting the line connecting the satellite and the point of interest on the surface and the nadir, the line between the satellite and the center of the earth. This angle is often of interest for sensors or communications systems whose beam footprints typically target only part of the available field-of-view. The last angle λ, the central angle of the satellite footprint, is the angle we wish to solve for.

It is clear from basic principles that the angle α is given by

$$\alpha = \frac{\pi}{2} + \lambda$$

and that

$$\alpha + \epsilon + \eta = \pi$$

which implies that

$$\lambda = \frac{\pi}{2} - \epsilon - \eta \tag{3.1}$$

The next step is to eliminate the dependence on η. From the law of sines, we note that

$$\frac{\sin \eta}{R} = \frac{\sin\left(\frac{\pi}{2} + \epsilon\right)}{R + h}$$

where R is the radius of the central body and h is the altitude of the satellite above the surface. Solving for η, we find that

$$\eta = \arcsin\left(\frac{R}{R + h}\cos\epsilon\right)$$

Substituting this result back into Equation 3.1, we derive that

$$\lambda = \frac{\pi}{2} - \epsilon - \arcsin\left(\frac{R}{R + h}\cos\epsilon\right) \tag{3.2}$$

which relates the central angle of the satellite footprint to the satellite altitude and the minimum elevation angle.

In order to determine whether a given point is visible to a particular satellite, all that is required is that the angle between the vectors pointing to the satellite and the surface point, θ, be less than the λ calculated from Equation 3.2 for the satellite. The angle θ can be determined easily from the dot product of the two vectors. This derivation implies that, for the purpose of calculating coverage, a constellation is completely described by the latitude and longitude of the subsatellite point and the central angle of the footprint for each satellite in the constellation.

This method as described relies on evaluating two inverse trigonometric functions. While these evaluations can be slow numerically, they may be accelerated either by creating a look-up table for the inverse cosine or by recognizing that the cosine function is monotonically decreasing for angles between zero and pi. This suggests that the requirement for visibility may be expressed in terms of the cosines of the

angles θ and λ. Some simple trigonometric substitutions yield the requirement for visibility given in Equation 3.3.

$$\frac{\boldsymbol{r}_{point} \cdot \boldsymbol{r}_{sat}}{r_{point} r_{sat}} \geq \frac{R}{R+h} \cos^2 \epsilon + \sin \epsilon \sqrt{1 - \frac{R^2}{(R+h)^2} \cos^2 \epsilon} \tag{3.3}$$

While this form of the visibility condition is more complicated, it is faster numerically and may be used when speed is important.

3.2 Analytic Approach

This section develops a general theory for the integration of regions defined by the overlap of circular sections on the surface of a sphere. This question is addressed by examining the problem of integrating the area of a circular section not centered at the pole from one longitude line to another. Once a solution to this problem is found, it is simple to assemble the area of the overlap region.

3.2.1 Footprint Area

The first question which must be examined is the area contained in the footprint of a single satellite, or the surface area of a region of a sphere bounded by a circle. This area can be derived simply from

$$A_{footprint} = R^2 \int_0^{\lambda} \sin \theta d\theta \int_0^{2\pi} d\phi \tag{3.4}$$

where λ is the central angle of the satellite footprint, as defined in Equation 3.2. This may be easily integrated to yield

$$A_{footprint} = 2\pi (1 - \cos \lambda) \tag{3.5}$$

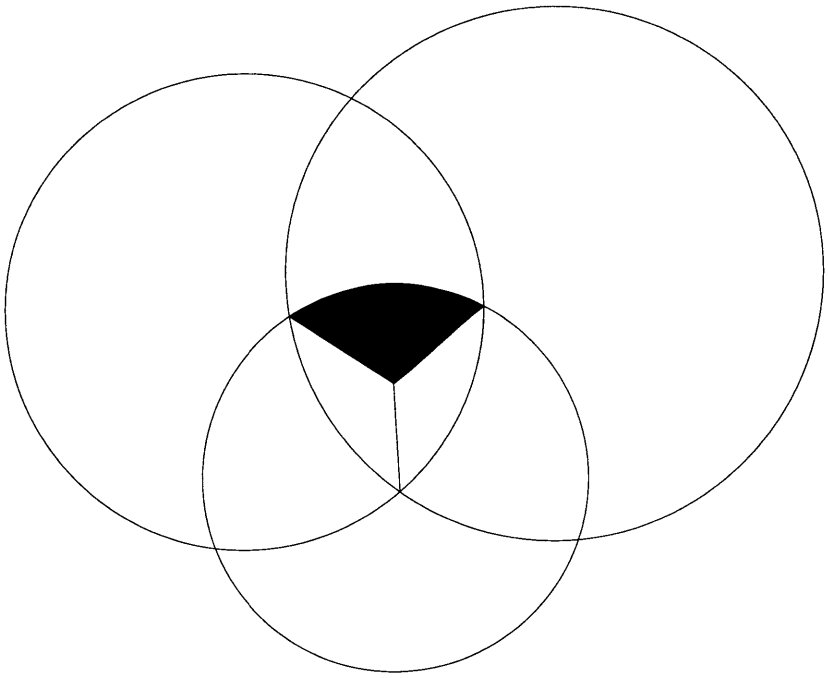

Figure 3-2: "Wedges" of an overlap region

where, here and hereafter, we have set the radius of the earth to unity, as, in the coverage calculations, the radius dependence is eliminated by the ratio.

Here we have made two assumptions. The first is that the earth is spherical. This assumption allows free rotation of the reference frame, in this case such that the center of the circle is located at the pole. The second assumption is that the satellite is nadir-pointing. These two assumptions ensure that the satellite footprint is circular. These are the only assumptions which are required for the analytic method to produce an exact result.

3.2.2 Overlap Area

The next step in the coverage analysis is to determine the area in a general n-way overlap. First, note that, in general, an n-way overlap region can be divided into n or fewer wedge-shaped regions, as shown in Figure 3-2. Each "wedge" is a section of a single satellite footprint, and its area can be determined by integrating that footprint over the appropriate boundary. In general, the central point of the wedges is contained by all of the satellite footprints involved in the overlap region but is not necessarily at the center of any of them. The problem of integrating the overlap

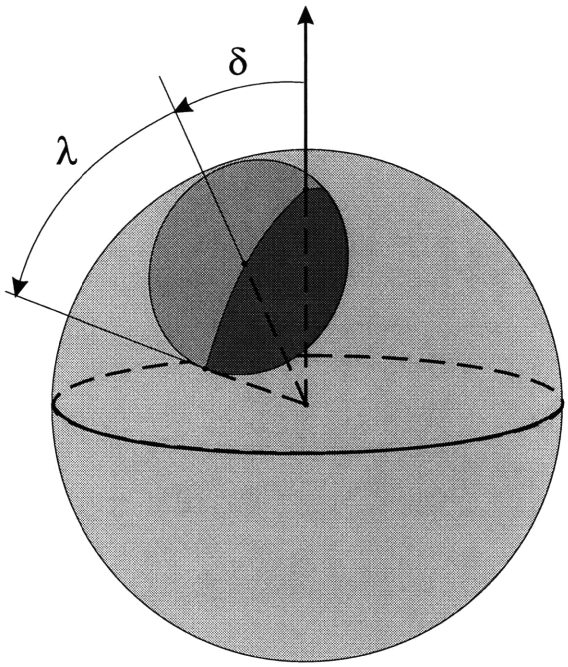

Figure 3-3: Depiction of the wedge area problem

region, then, reduces to integrating the area of a wedge of a circular region where the originating point of the wedge is displaced from the center by some angle δ. The area to be integrated is shown in Figure 3-3.

The surface integral of a region on a sphere with unit radius is given by

$$A = \int_0^{2\pi} d\phi \int_0^{\theta(\phi)} \sin\theta d\theta \tag{3.6}$$

where ϕ is the longitude and θ the colatitude. Integrating in theta, we find

$$\begin{aligned} A &= \int_{\phi_0}^{\phi_1} (1 - \cos\theta(\phi))\, d\phi \\ &= \phi_1 - \phi_0 - \int_{\phi_0}^{\phi_1} \cos\theta(\phi) d\phi \end{aligned} \tag{3.7}$$

Clearly, a relationship between θ and ϕ is required.

We begin with the equation for a circle centered at the pole. If we take the central

angle of the circle to be λ, the equation for this circle, parameterized in terms of the longitude q, is given by

$$r(q) = \begin{pmatrix} \sin\lambda\cos q \\ \sin\lambda\sin q \\ \cos\lambda \end{pmatrix} \tag{3.8}$$

The equation for a similar circle offset from the pole by an angle δ is found by multiplying by an appropriate rotation matrix:

$$r(q) = \begin{pmatrix} 1 & 0 & 0 \\ 0 & \cos\delta & -\sin\delta \\ 0 & \sin\delta & \cos\delta \end{pmatrix} \begin{pmatrix} \sin\lambda\cos q \\ \sin\lambda\sin q \\ \cos\lambda \end{pmatrix} = \begin{pmatrix} \sin\lambda\cos q \\ \sin\lambda\cos\delta\sin q - \cos\lambda\sin\delta \\ \sin\lambda\sin\delta\sin q + \cos\lambda\cos\delta \end{pmatrix}$$

Note that this rotation places the center of the circle in the transformed frame of reference at $(\delta, -\frac{\pi}{2})$. Transforming back to spherical coordinates, we find that

$$\cos\theta(q) = \sin\lambda\sin\delta\sin q + \cos\delta\cos\lambda \tag{3.9}$$

$$\tan\phi(q) = \frac{1}{\sin\lambda\cos q}\left(\sin\lambda\cos\delta\sin q - \cos\lambda\sin\delta\right) \tag{3.10}$$

In these equations, both θ and ϕ are parameterized in terms of the longitude of the unrotated circle. It is desirable to eliminate this extra parameter. By squaring both sides of equation 3.10 and combining terms, we find that

$$\left(\cos^2\delta + \tan^2\phi\right)\sin^2 q - 2\cot\lambda\sin\delta\cos\delta\sin q + \left(\cot^2\lambda\sin^2\delta - \tan^2\phi\right) = 0$$

Using the quadratic formula to solve for $\sin q$, we derive

$$\sin q = \frac{1}{\cos^2\delta + \tan^2\phi}\left(\cot\lambda\sin\delta\cos\delta \pm \tan\phi\sqrt{1 - \csc^2\lambda\sin^2\delta + \tan^2\phi}\right) \tag{3.11}$$

When the rotation angle δ is zero, equation 3.11 reduces to

$$\sin q = \pm\frac{1}{1+\tan^2\phi}\tan\phi\sqrt{1+\tan^2\phi} = \pm\frac{\tan\phi}{\sqrt{1+\tan^2\phi}} = \pm\sin\phi$$

Since, in this case, nothing has been done in the rotation, the initial longitude q should be the same as the final longitude ϕ. We conclude that the positive root is the correct solution. Substituting equation 3.11 back into equation 3.9, we derive the rather complex result:

$$\begin{aligned}\cos\theta(\phi) &= \cos\delta\cos\lambda + \frac{\cos\lambda\sin^2\delta\cos\delta}{\cos^2\delta+\tan^2\phi} \\ &\quad + \frac{\sin\lambda\sin\delta\tan\phi}{\cos^2\delta+\tan^2\phi}\sqrt{1-\csc^2\lambda\sin^2\delta+\tan^2\phi}\end{aligned} \tag{3.12}$$

Integrating the Area Equation

We wish to determine the integral of Equation 3.12 to solve Equation 3.7, and we will set the interval of the integration to be $[-\frac{\pi}{2}, \phi]$. The first term clearly integrates simply to

$$(\phi_1 - \phi_0)\cos\delta\cos\lambda$$

but the other two terms are more complex. They both do become integrable with appropriate substitutions. First, we define the constant $a = \cos\delta$. Using this definition and the substitution $x = \tan\phi$, the integral of the second term becomes

$$\cos\lambda\sin^2\delta\cos\delta\int_{-\frac{\pi}{2}}^{\phi}\frac{d\phi}{\cos^2\delta+\tan^2\phi} = \cos\lambda\sin^2\delta\cos\delta\int\frac{dx}{(a^2+x^2)(1+x^2)} \tag{3.13}$$

Using partial fractions, the integrand becomes

$$\frac{1}{(a^2+x^2)(1+x^2)} = \frac{1}{a^2+x^2} - \frac{1}{1+x^2} \tag{3.14}$$

which is easily integrable. Combining Equation 3.13 and Equation 3.14 and substituting back in for x and a, we conclude that

$$\begin{aligned}\cos\lambda\sin^2\delta\cos\delta\int_{-\frac{\pi}{2}}^{\phi}\frac{d\phi}{\cos^2\delta+\tan^2\phi} &= \frac{\pi}{2}\cos\lambda-\frac{\pi}{2}\cos\lambda\cos\delta \\ &\quad+\cos\lambda\tan^{-1}\left(\frac{\tan\phi}{\cos\delta}\right) \\ &\quad-\phi\cos\lambda\cos\delta \qquad (3.15)\end{aligned}$$

Note the cancellation with the first term.

We now turn our attention to the final term. Using the substitution $x=\tan^2\phi$, and defining $a=\cos\delta$ and $b^2=1-\csc^2\lambda\sin^2\delta$, we find that the third term becomes

$$\frac{1}{2}\sin\lambda\sin\delta\int\frac{\sqrt{b^2+x}}{(a^2+x)(1+x)}\,dx$$

Using partial fractions again,

$$\int_{-\frac{\pi}{2}}^{\phi}\frac{\tan\phi}{\cos^2\delta+\tan^2\phi}\sqrt{1-\csc^2\lambda\sin^2\delta+\tan^2\phi}\,d\phi=\frac{1}{2}\int\sqrt{b^2+x}\left(\frac{1}{a^2+x}-\frac{1}{1+x}\right)dx$$

which integrates to

$$\frac{1}{1-a^2}\left[\sqrt{1-b^2}\tan^{-1}\left(\frac{\sqrt{b^2+x}}{\sqrt{1-b^2}}\right)-\sqrt{a^2-b^2}\tan^{-1}\left(\frac{\sqrt{b^2+x}}{\sqrt{a^2-b^2}}\right)\right]$$

Substituting back in for a, b, and x, we find

$$\sin\lambda\sin\delta\int_{-\frac{\pi}{2}}^{\phi}\frac{\tan\phi}{\cos^2\delta+\tan^2\phi}\sqrt{1-\csc^2\lambda\sin^2\delta+\tan^2\phi}\,d\phi=$$
$$\left[\tan^{-1}\left(\frac{\sqrt{1-\csc^2\lambda\sin^2\delta+\tan^2\phi}}{\csc\lambda\sin\delta}\right)-\cos\lambda\tan^{-1}\left(\frac{\sqrt{1-\csc^2\lambda\sin^2\delta+\tan^2\phi}}{\cot\lambda\sin\delta}\right)\right]_{\phi_0}^{\phi_1}$$

If we define

$$\cos\alpha = \frac{\sin\delta}{\sin\lambda} \tag{3.16}$$

we derive that

$$\begin{aligned}\sin\lambda\sin\delta\int_{-\frac{\pi}{2}}^{\phi}\frac{\tan\phi}{\cos^2\delta+\tan^2\phi}\sqrt{1-\csc^2\lambda\sin^2\delta+\tan^2\phi}\,d\phi = \\ \tan^{-1}\left(\frac{\sqrt{\sin^2\alpha+\tan^2\phi}}{\cos\alpha}\right)-\cos\lambda\tan^{-1}\left(\frac{\sqrt{\sin^2\alpha+\tan^2\phi}}{\cos\lambda\cos\alpha}\right) \\ -\frac{\pi}{2}(1-\cos\lambda)\end{aligned} \tag{3.17}$$

Combining these results, we find that

$$\begin{aligned}A(\phi) &= \pi(1-\cos\lambda)+\phi-\cos\lambda\tan^{-1}\left(\frac{\tan\phi}{\cos\delta}\right)-\tan^{-1}\left(\frac{\sqrt{\sin^2\alpha+\tan^2\phi}}{\cos\alpha}\right) \\ &\quad +\cos\lambda\tan^{-1}\left(\frac{\sqrt{\sin^2\alpha+\tan^2\phi}}{\cos\lambda\cos\alpha}\right)\end{aligned} \tag{3.18}$$

which is the result needed. Equation 3.18 is the basis for integrating the area of overlap regions. Once the overlap region has been divided into wedges, the area of each wedge can be integrated.

Calculating N-way Coverage

The next step is to understand how to develop the total coverage of the constellation from the areas of all of the n-way overlaps. For the overall one-way coverage, the answer, often known as the Inclusion-Exclusion Principle, is simple [4]:

$$\begin{aligned}A(S_1\cup S_2\cup\ldots\cup\S_n) &= \sum_{i=1}^{n}A(S_i)-\sum_{i=1}^{n-1}\sum_{j=i+1}^{n}A(S_i\cap S_j)+\ldots \\ &\quad +(-1)^{n+1}A(S_1\cap S_2\cap\ldots\cap S_n)\end{aligned}$$

which states that the union of n sets consists of each individual set minus all of the intersections of two sets plus all of the intersections of three sets, etc. until the nth way overlap is accounted for.

The values we determine through the method described in this chapter are the values on the right-hand side of this equation, that is the area contained in all the different possible intersections. If we call the total area in n-way intersections A_n, the question is how to determine the n-way coverage, C_n, or the area covered by n or more satellites. The two are not identical, as the area included in the A_i include higher degree intersections many times, while the C_i should account for each region exactly once. Determining the relationship between the two is a combinatorical problem. The answer is asserted without proof to be

$$C_i = \sum_{j=i}^{n} (-1)^{i+j} \begin{pmatrix} j-1 \\ i-1 \end{pmatrix} A_j \tag{3.19}$$

Although it is not obvious from the form of this equation, it states that the C_i are related to the A_i by the Pascal matrix, the matrix equivalent of the well-know Pascal triangle.

3.3 Application to Planar Coverage

Before discussing the implementation of this theory as a coverage tool, it is interesting to apply the theory to a simple case, that of a group of satellites sharing the same orbital plane, separated only in mean anomaly. In this case, two-way overlap is often the maximum depth necessary to describe the problem.

3.3.1 Two–Way Overlap

We begin this analysis by examining the special case of the overlap of two satellite footprints. In this case, the best point in the region to integrate about is clearly

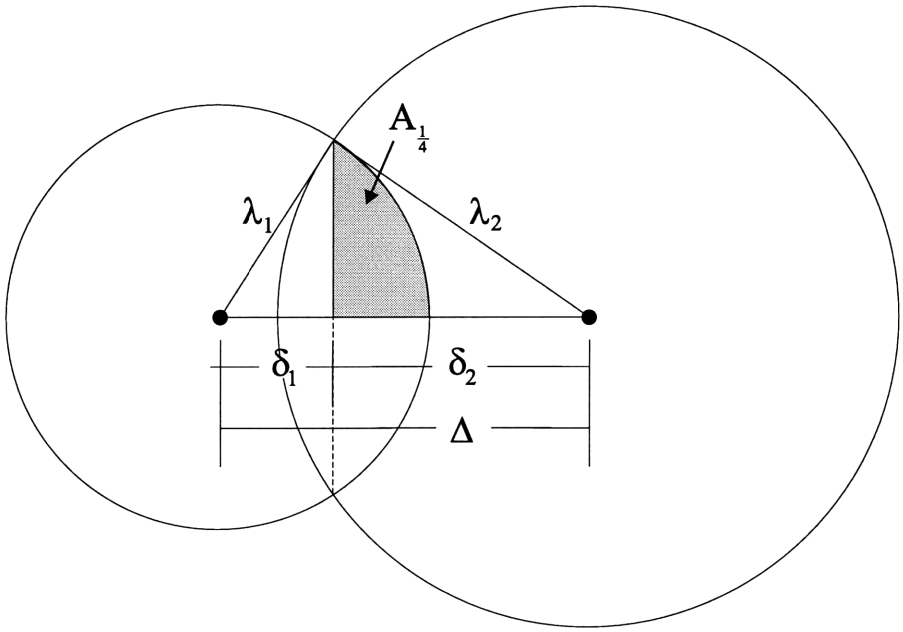

Figure 3-4: A two-way overlap region

the midpoint of the line connecting the two vertices, as shown in Figure 3-4. The satellites need not be at the same altitude, and this is indicated by the difference in the radius of their footprints in Figure 3-4. If the angular distance between the subsatellite points is Δ and the central angles of the two regions are λ_1 and λ_2 respectively, the distance from the central point to the first circle is easily derived to be

$$\tan \delta_1 = \frac{\cos \lambda_2 - \cos \lambda_1 \cos \Delta}{\cos \lambda_1 \sin \Delta} \tag{3.20}$$

Using the fact that the overlap region is symmetric about the line connecting the subsatellite points, we can divide the contributions to the area as follows:

$$A_{overlap} = 2A_{1/4}(\delta_1, \lambda_1) + 2A_{1/4}(\delta_2, \lambda_2) \tag{3.21}$$

where $A_{1/4}$ is

$$\begin{aligned} A_{1/4}(\delta, \lambda) &= A(\delta, \lambda, \frac{\pi}{2}) + A(\delta, \lambda, 0) \\ &= \alpha - \cos\lambda \tan^{-1}\left(\frac{\tan\alpha}{\cos\lambda}\right) \end{aligned} \tag{3.22}$$

where α is defined as in Equation 3.16.

3.3.2 Circular Orbits

Now that we have derived the area in an overlap of two satellite footprints, we derive the equation for the area visible to a plane of satellites. Here we will assume that there are n satellites in a circular orbit. As all the satellites are at the same altitude, their footprints all have the same central angle λ. We will assume the mean anomalies of the satellites M_i are given and that the array elements are increasing monotonically. The δ_i are determined by Equation 3.20, which reduces in this case to

$$\delta_i = \frac{1}{2}\Delta_i = \frac{1}{2}(M_{i+1} - M_i) \tag{3.23}$$

We note that, as $M_1 = M_{n+1}$, the δ_i are related by

$$\sum_{i=1}^{n} \delta_i = \pi \tag{3.24}$$

The contribution to the total area of each individual satellite is the difference of the area of its footprint and the area of an adjoining overlap region. The total area covered by one plane of satellites is therefore

$$A = 2\pi n(1 - \cos\lambda) - 4\sum_{i=1}^{n-1} A_{1/4}(\delta_i) - 4A_{1/4}(\pi - \delta_1 - \ldots - \delta_{n-1}) \tag{3.25}$$

where we have used Equation 3.24 in the last term. One feature of Equation 3.25

is that it depends only on the δ_i, the differences in mean anomalies, not the actual mean anomalies themselves. This indicates that the coverage is unaffected when all of the satellites are rotated within the plane by an equal amount. This suggests that if coverage is the prime consideration, it is unnecessary to correct net rotation of the plane.

The next step is to examine the sensitivity of area to phasing changes. The first term in Equation 3.25 is constant. The derivatives of the other terms are of interest. The effect of changes to δ on the overlap area is given by

$$\frac{dA_{1/4}}{d\delta} = -\sqrt{1 - \frac{\cos^2 \delta}{\cos^2 \lambda}} \tag{3.26}$$

We can now evaluate the sensitivity of the band area to changes in δ.

$$\frac{dA}{d\delta_i} = -4\left(\frac{dA_{1/4,i}}{d\delta_i} - \frac{dA_{1/4,n}}{d\delta_n}\right) \tag{3.27}$$

Setting Equation 3.27 to zero yields the equation for an extremum. Combining Equation 3.26 with Equation 3.27 and solving for δ_i gives that

$$\cos^2 \delta_i = \cos^2 \delta_n \tag{3.28}$$

or that $\delta_i = \delta_n$. This indicates that we have maximal coverage when the satellites are evenly spaced in mean anomaly.

It is also interesting to notice that in the process of maximizing coverage, we have also minimized the two-way coverage of the plane of satellites. This may indicate that, if multiple satellite coverage is required, it would be better to distribute the satellites unevenly within the plane, but further study is required.

3.3.3 Elliptical Orbits

It is possible to derive a similar expression for the area covered by a set of satellites in an elliptical orbit, but the equations are far more complex, although it can be shown analytically that the area visible to a satellite averaged over an orbit, does not depend on anything but the semi-major axis of the orbit (Appendix A). The central angles of the satellites now differ, which results in asymmetric overlap regions. In addition, neither the δ_i nor the λ_i are constant over the orbit, which forces us to time average over the orbit for any meaningful analysis of the coverage. The combination of these two differences from the circular case complicates the equation to the point that it becomes necessary to investigate the question computationally.

It seems likely that the optimal phasing occurs when the satellites are evenly spaced in mean anomaly. Designating the coverage area for that case as nominal, we can determine the area covered for deviations from that phasing. We define a phase factor ϕ_M to be

$$\phi_M = \sum_{i=1}^{n} (M_i - M_{i,ref})^2 \tag{3.29}$$

where we have adjusted the reference mean anomalies to remove the average rotation of the plane, again using the fact that the coverage is not affected by a global rotation in the plane. The coverage, normalized by the nominal coverage, of a large number of possible choices of mean anomaly for a plane of the Ellipso constellation is shown in Figure 3-5. This seems to validate the assumption that evenly distributing the satellites in mean anomaly is also the optimal phasing for an elliptical orbit. It also indicates that the phase factor ϕ_M is an excellent measure of the coverage characteristics of the plane of satellites.

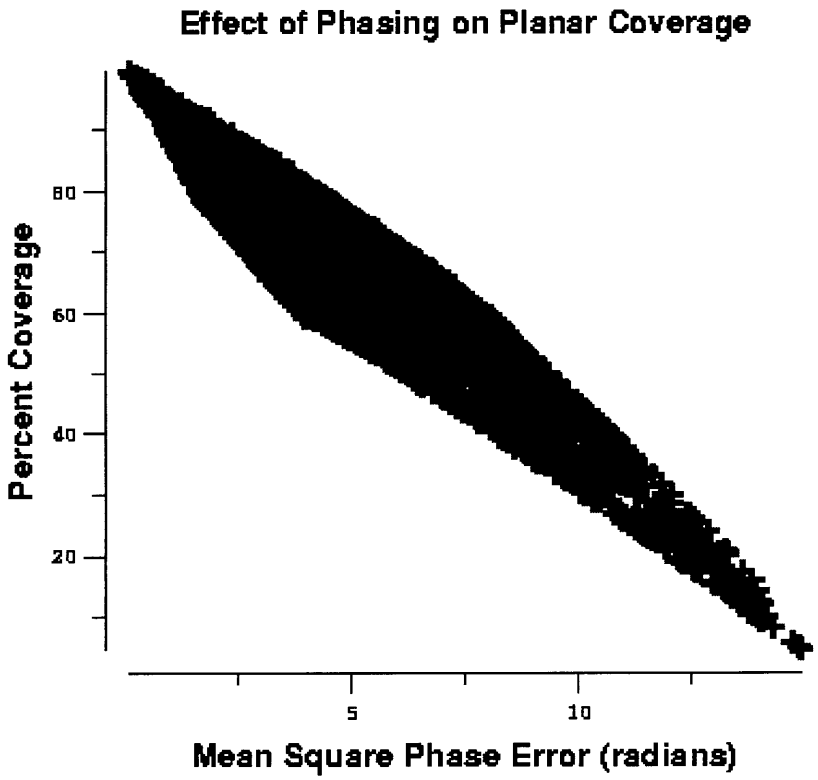

Figure 3-5: Normalized coverage area for an Ellipso plane with phasing varying.

Chapter 4

Description of Coverage Tool

The previous chapter discussed the development of a theory for determining the coverage characteristics of a constellation of satellites. This chapter discusses the issues involved in the actual implementation of this theory. The structure of the coverage tool used in analyzing earth coverage is described, and its performance relative to a typical grid-based numerical approach is evaluated.

4.1 Algorithm

The basic approach of the analytic method, as mentioned briefly in the previous chapter, is to integrate all of the possible overlap regions and to assemble the area covered from set theory. It is easy to see that, for large constellations with high levels of overlap, there is potential for an extremely large number of calculations. With a little care, however, most extraneous calculations can be eliminated.

The algorithm utilized is recursive, searching for n-way overlaps only if the first $n-1$ have a positive overlap. The first step is to scan for "redundant" satellites, whose footprints at the current time make no contribution to the coverage area. These can occur at the overlap of two orbital planes if there is no mean anomaly phasing between the planes or in the case where some satellites are much higher than others. It can

also occur if the optional latitude restrictors are included. The redundant satellites are removed. The program next scans for intersections. For each satellite, a list of the other satellites whose footprints intersect its own is generated and the information stored. This prevents the program from having to scan through all the satellites at every overlap level, greatly reducing the number of calculations. The latitude and longitude of the intersections are also stored for later use. These operations comprise the preliminary analysis.

The program then moves on to the actual area calculations. For each satellite, the area of its footprint is calculated and added to the one-way area total. Then, the two-way overlap of the current satellite and the first satellite in the intersection list is calculated, and the two-way area total is updated. If there are higher levels of overlap, then those are calculated and similarly stored. This continues until all degrees of overlap are accounted for.

The final stage is to extract the coverage information from the area in each level of overlap. This is accomplished by using Equation 3.19. The coverage is then determined by dividing by the total area of interest. This is simply 4π if global coverage is required, but can have a different value if the latitude restrictors are employed. The final n-way coverage values are calculated.

4.1.1 Input

The coverage procedure takes an array of Keplerian orbital elements as input. From these elements a consistent set of latitudes, longitudes, and altitudes / central angles are determined. As the coverage calculated is an instantaneous result, and, in general, it is the coverage over an extended period of time which is of interest, it is necessary to average the coverage over time. For most constellations, averaging the coverage over one orbital period is sufficient to obtain the long-term performance of the constellation, neglecting, of course, orbital drift, which typically occurs on a much longer time scale than the orbital period. The procedure implements a simple Keplerian propagation and averages the instantaneous coverage over one orbital period. The

procedure receives, as input, the number of time steps per orbit required. In practice, twenty to thirty time steps is sufficient for reasonable precision.

4.1.2 Restriction of the Coverage Region

One disadvantage inherent in the analytical approach is the loss of the latitude and longitude dependence of the coverage. While it is difficult to recover this information analytically, it is often unnecessary. Typically, coverage requirements are given as a minimum coverage for a given elevation angle over some latitude range; therefore, what is important is to calculate the coverage in a restricted latitude range.

It is possible to restrict that latitude range for which the analytic method determines the coverage, and this has been implemented in the coverage tool. This is possible because the analytic method views satellite footprints simply as circles on the surface of the earth. It is simple to define latitude restrictors as circles centered on the poles and to subtract away the overlap with these restrictors at each level of overlap.

The coverage tool accepts as input a south and north latitude which becomes the central angle of the restrictor. In addition, it accepts a sun position (latitude and longitude) in order to calculate daytime or night-time coverage. In principle, it is possible to calculate the area in any region which can be defined by circular regions on the sphere. In this implementation, however, only three restrictors, the two at the poles and one representing the sun position, are allowed.

4.2 Preliminary Analysis

Before the actual area calculations occur, some preliminary measures are taken to prevent unnecessary calculations. The first checks for redundant satellites. As will be shown later, not all redundancies may be removed before the area calculations occur, but the effects of these on computational performance are minimal. The next step determines which circles intersect and the coordinates of their intersections. This

information is needed at every level of overlap; it is therefore much more efficient to calculate this data before the recursion begins.

4.2.1 Redundant Satellites

Determining redundant satellites is a nontrivial issue. In this implementation, a simple method was chosen which, while it does not remove all redundancies, removes many of them quickly and simply. The program simply scans for satellites whose footprints are wholly contained by another satellite footprint. If it finds one, that satellite is removed. The mathematical condition for a satellite i to be removed is that

$$\lambda_i + \Delta_{ij} \leq \lambda_j \tag{4.1}$$

for some satellite j, where λ represents the central angle of the appropriate satellite and Δ_{ij} is the angular distance between the two subsatellite points.

This procedure will remove all satellites whose footprints are identical to or wholly contained in the footprint of another satellite. This type of redundancy can occur in two ways. The first is if one satellite is at a much lower altitude than another in the constellation. This occurs in the southern hemisphere and near the equator of the Ellipso constellation, where the Borealis satellites are near their perigee altitude and overlap with the Concordia satellites in much higher circular orbits. This type of redundancy may also occur for constellations with no mean anomaly phasing between orbital planes. For any two planes at the same inclination, there exist two nodes where they overlap. If there is no mean anomaly phasing between the planes, satellites from each plane reach the node at very close to (in theory, exactly at) the same time. When this occurs, the footprints of the satellites are identical. Removing these redundancies can improve the calculation time significantly.

This method removes the redundancies in the constellation which only involve one other satellite. It is possible, however, for a satellite footprint not to be fully contained in the footprint of any one other satellite, but to be contained completely by two or more. One example of this case is shown in Figure 4-1. This case does

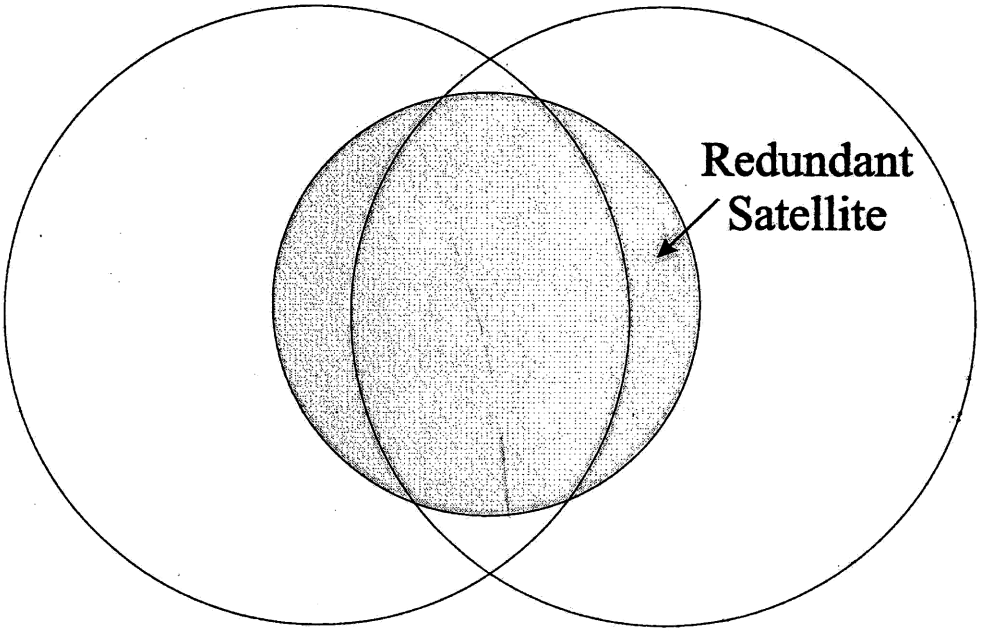

Figure 4-1: Multiple satellite redundancy

not occur frequently. It is handled in the area calculation section.

It should be noted that the removal of the redundant satellites has a large impact if the latitude restrictors are employed. For latitude restrictions of 30 degrees at each pole, at least 12, and sometimes 24, of the 66 Iridium satellites may be removed from the calculation, because the constellation is polar. Because, at the poles, the Iridium constellation can have as many as 18 satellites overlap, the number of calculations is decreased dramatically.

4.2.2 Intersection of Circles

The intersection preliminary consists of determining which satellites overlap and the coordinates of their intersections. Both of these steps can be accomplished with some basic spherical trigonometry. The first part is trivial. Satellites i and j intersect if

$$\lambda_i + \lambda_j > \Delta_{ij} \tag{4.2}$$

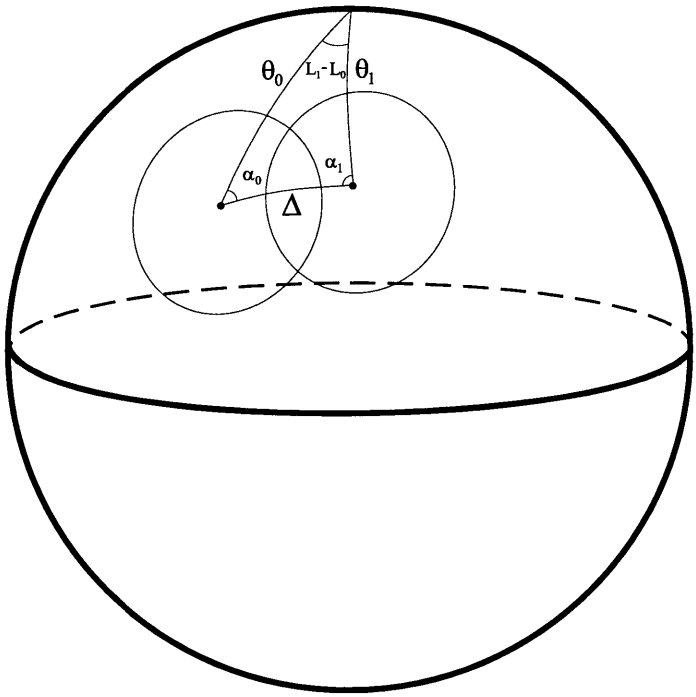

Figure 4-2: Two intersecting circles on a sphere

where, again, λ represents the central angle of the satellite footprint and Δ is the angle between the two subsatellite points. This, of course, is simply the triangle inequality. This requirement is sufficient because the simple redundant cases have already been removed. For each satellite, the satellites whose footprints intersect its own are determined and stored. This allows the program to look for high order (greater than two-way) overlap only among satellites which are known to intersect.

The next step is slightly more complicated. It is necessary to determine the latitude and longitude for each intersection point. We consider the two intersecting circles shown in Figure 4-2. Each circle has central angle λ and colatitude θ, and their longitude difference is $L_1 - L_0$. For simplicity, we take the longitude difference to be positive. We recall the angular distance between the subsatellite points is given by

$$\cos\Delta = \cos\theta_0 \cos\theta_1 + \sin\theta_0 \sin\theta_1 \cos\left(L_1 - L_0\right) \tag{4.3}$$

which is simply the law of cosines in spherical trigonometry. The two other angles of

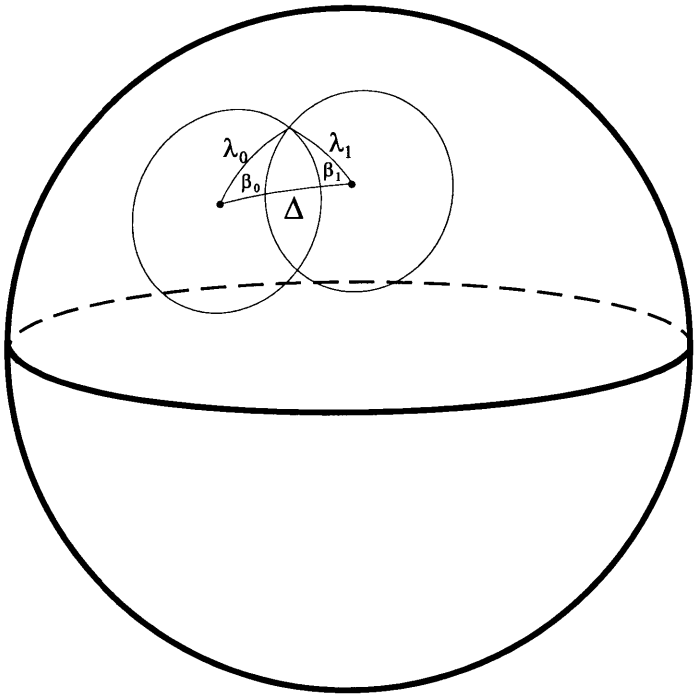

Figure 4-3: Triangle formed by intersection of circles

this triangle, α_0 and α_1 can also be calculated from the law of cosines.

$$\cos\alpha_0 = \frac{\cos\theta_1 - \cos\theta_0\cos\Delta}{\sin\theta_0\sin\Delta} \tag{4.4}$$

where there is a similar equation for α_1. The quadrant of the angles can be determined easily if we also use the law of sines.

$$\frac{\sin\alpha_0}{\sin\theta_1} = \frac{\sin(L_1 - L_0)}{\sin\Delta} \tag{4.5}$$

With Equation 4.4 and Equation 4.5, it is simple to take the inverse tangent to determine α_0 and α_1.

Next we consider the spherical triangle formed by the centers of the circles and one of the intersections, as shown in Figure 4-3. The angle β_0 can be found in the same fashion we determined α_0 above, although the sine does not need to be calculated;

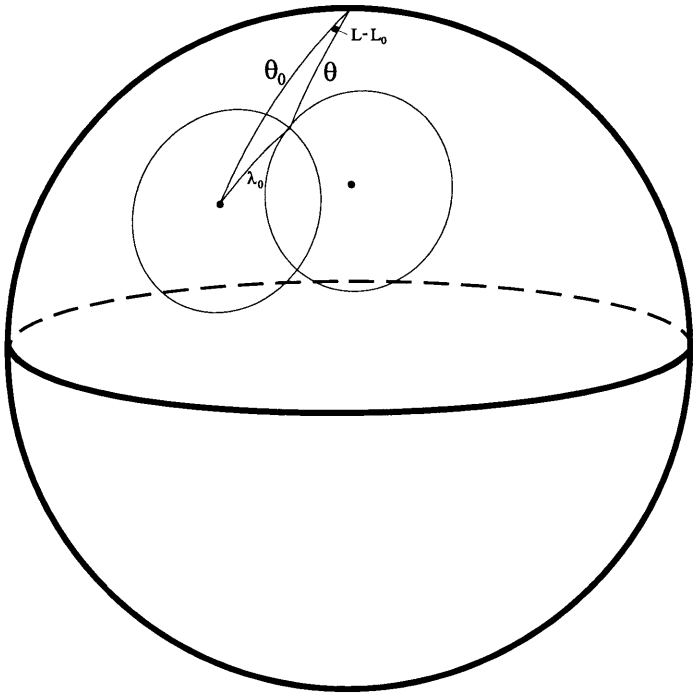

Figure 4-4: Final triangle

as intersections occur for $\pm\beta_0$, all of the necessary information is contained in the cosine. β_0 is given by

$$\cos\beta_0 = \frac{\cos\lambda_1 - \cos\lambda_0\cos\Delta}{\sin\lambda_0\sin\Delta} \tag{4.6}$$

We consider one final triangle to determine the coordinates of the intersections, shown in Figure 4-4. We determine the colatitude of the intersections from

$$\cos\theta = \cos\theta_0\cos\lambda_0 + \sin\theta_0\sin\lambda_0\cos\left(\alpha_0 \pm \beta_0\right) \tag{4.7}$$

The longitude of the intersections are given by

$$\frac{\sin\left(L - L_0\right)}{\sin\lambda_0} = \frac{\sin\left(\alpha_0 \pm \beta_0\right)}{\sin\theta} \tag{4.8}$$

These two equations give the coordinates of the intersections for any two circles on a

sphere. This process is singular if the first satellite is directly over one of the poles. In this case, it is possible to follow exactly the same process using the second satellite instead. At least one of the satellites will be nonsingular, as, if they were both directly over the pole, one would be redundant and would already have been removed.

4.3 Area Calculation

With the list of intersecting satellites determined, the program begins the calculation of the overlap areas. The process is recursive. The first step in the recursion is to calculate the area of the footprint of the current satellite. Then, the area in the two-way intersection between the current satellite and the first satellite in the intersection list is determined. After this, the program determines whether there is a higher order intersection by scanning the next satellites in the intersection list. If satellite i in the list intersects the satellites in the n-way overlap, then a level $n+1$ overlap exists. This continues until all of the overlap areas have been calculated.

The actual area determination is straight forward. The vertices of the overlap region is determined, a point in the region is chosen. The reference frame is rotated such that the point chosen is now at the pole. The area of each wedge is then calculated using Equation 3.18, and the sum of the wedges yield the overlap area.

4.3.1 Determination of Vertices

In order to integrate the overlap area, the vertices of that region must be found, as they define the bounds of integration. The coordinates of each intersection have already been determined, but not all of them will be vertices of the overlap. The vectices are the intersections which are also contained in all of the other circles, i.e. an intersection is a vertex if and only if the distance between it and the center of circle i is less than or equal to that circles central angle for all i. This process yields a set of points which form the vertices of the overlap region.

Once the vertices have been determined, it is necessary to find a point contained

in the overlap region. As nothing is required of this point other than its being in the region, the algorithm is chosen for simplicity. The point determined by the average of the colatitudes and the longitudes of the vertices is chosen. This point is certain to be within the region since all of the bordering curves have negative curvature everywhere, i.e. the line connecting any two points on the boundary is completely contained in the region. The reference frame is then rotated such that this point is at the pole. The new coordinates of the vertices are found from the appropriate rotation matrix.

4.3.2 Integration

The integration proceeds as follows. The vertices are sorted by longitude. The first two vertices are chosen. These vertices must bound a section of one of the circles involved in the intersection. For each vertex, the two circles which intersect at it are stored. The circle which they have in common is the circle which forms this section of the boundary.

The system is rotated such that the center of that circle is placed on the $-\frac{\pi}{2}$ meridian. We are now in position to utilize Equation 3.18 to determine the area of this section. The colatitude of the center of the circle which bounds the current section is δ, and its central angle is λ. The longitudes of the two vertices are ϕ_0 and ϕ_1. The area of the wedge is given by

$$A_{wedge} = A(\delta, \lambda, \phi_1) - A(\delta, \lambda, \phi_0) \tag{4.9}$$

The sum of the area of the wedges is the area of the overlap.

4.3.3 Redundant Case

There is one case which makes this more complicated. For the redundant case pictured in Figure 4-1, it is not immediately obvious computationally which circle forms the boundary of the region. The end points of two sides of the overlap regions are both

formed by the same two circles. In this case, the circle which should be integrated over is the one which is "closer" to the pole. This condition is equivalent to choosing the circle with larger radius of curvature, i.e. the circle with the larger central angle.

4.4 Performance Analysis

In order to examine the performance of this coverage algorithm, it is compared with a typical grid-based method. The grid was chosen to be evenly spaced in latitude and longitude. Although the numerical algorithm was not optimized for speed (using any of the number of numerical tricks available), it was given a sizeable advantage in the comparison. In order to accelerate the numerical approach, only one-way coverage was calculated. This implies that, for a given point, once one satellite is found to be visible, it is not necessary to examine the other satellites. If a point is visible to the constellation, it will be visible to the first half of the constellation about half of the time. Limiting the search to single coverage therefore speeds up the process by about 50 percent. This biases the comparison in favor of the grid-based method.

The results of the computational method for various grid densities are compared to those of the analytical approach. The differences in the results and the time required to obtain them are discussed in the following sections.

4.4.1 Precision

The output produced for various grid sizes are plotted in Figure 4-5. The relative deviation of the computational results from the analytical result is plotted against the number of grid points. As can immediately be seen from the plot, the numerical method converges to the analytical result as the grid density increases. It is also clear that this convergence is exceedingly slow, with performance improving linearly with the number of points on the grid. For a constellation with almost complete coverage, this indicates that, for the numerical method to converge to four places (0.01 % error), the grid must contain on order of 10^5 points. This can be unwieldy,

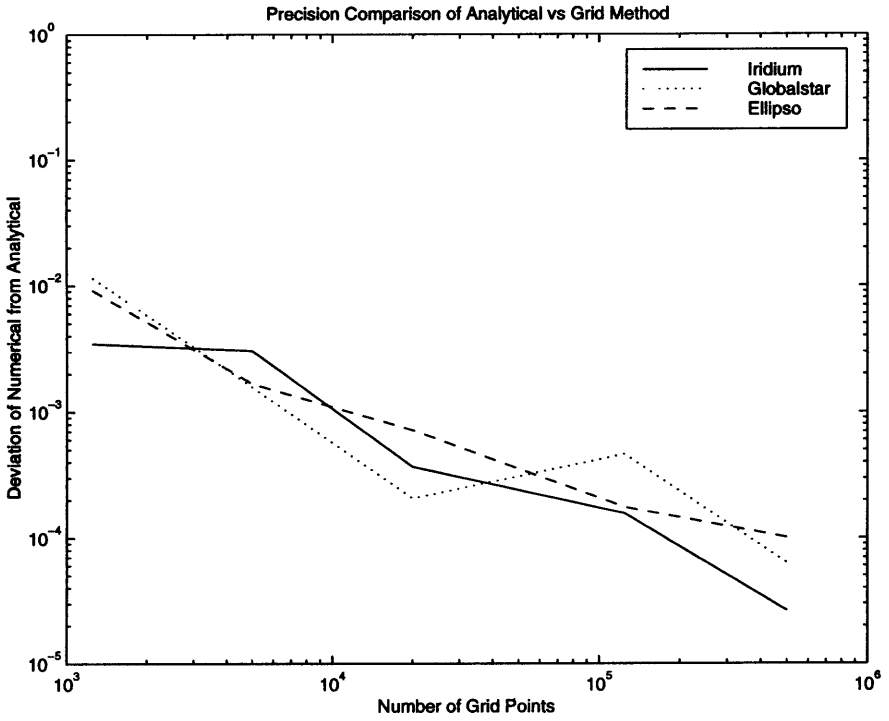

Figure 4-5: Precision comparison : analytical vs. numerical

both in the memory required and the sheer number of calculations required, as will be discussed in the next section.

The other point of interest from Figure 4-5 is that all three constellations show qualitatively the same behavior. They all have approximately the same error from the analytic result for the same grid density. This indicates that the analytical method provides better precision regardless of the size of the constellation.

4.4.2 Calculation Time

The results of the comparison of the execution time for the different approaches are shown in Figure 4-6. The ratio of the execution time for the numerical method to that of the analytical is plotted on the abscissa. In all cases, the time required for the numerical approach increases close to linearly with the grid density. This occurs, of course, because, each grid point requires exactly the same number of calculations; naturally, the time scales linearly with the number of points. The time required for

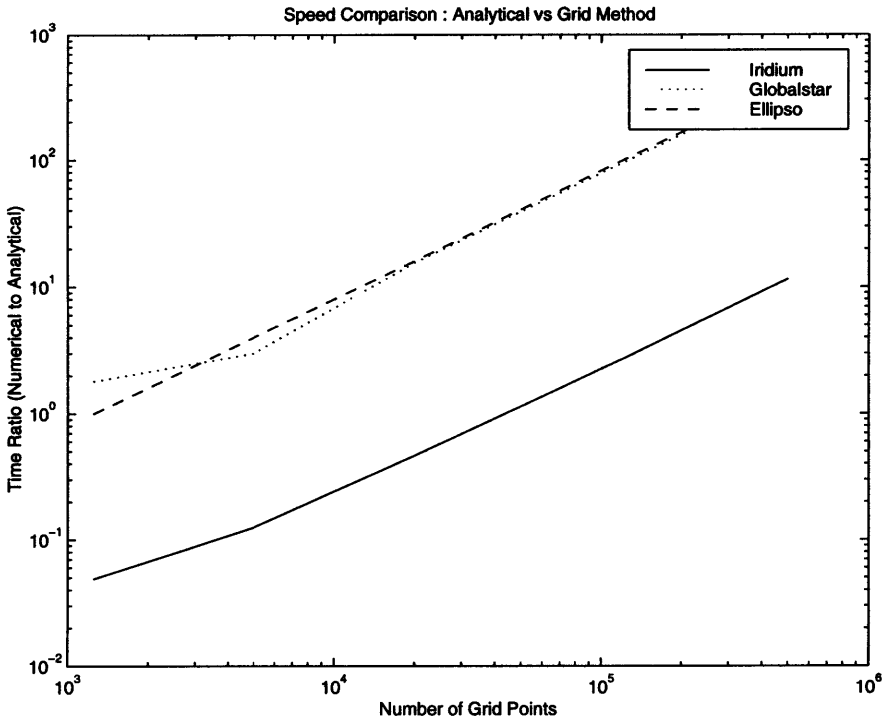

Figure 4-6: Execution times for analytical and numerical methods

the analytical method, of course, was constant.

Also, it is clear that there are two different sorts of behavior. The analytical coverage method performs substantially better for Ellipso and Globalstar than for Iridium. It would be easy to attribute the performance difference to the large number of satellites in the Iridium constellation, but that would be a mistake. There is almost no difference in performance between Ellipso and Globalstar, although the latter has almost three times as many satellites as the former. Clearly, the longer execution time for Iridium is not simply a result of the number of satellites.

The most significant difference between Iridium and the other two constellations is that Iridium is polar, while the Globalstar is a Walker pattern and Ellipso is an elliptical hybrid of a Walker pattern. In a polar constellation, all of the orbital planes share common nodes, i.e. they all intersect in the same place, in this case at the north and south poles. This leads to a large number of satellite footprints intersecting near the poles. This does not occur for Walker patterns. Because there are no nodes

common to all of the orbital planes, the maximum level of overlap tends to be much lower.

While this is a problem if coverage near the poles is an important issue, that is rarely the case. There is little market for telecommunication services near the poles. Thus, for example, when sufficiently large latitude restrictors are added, the performance of the analytical method for Iridium quickly improves.

That being noted, the performance speed for the analytical method is still quite good. For convergence to four places, the analytical approach for Iridium breaks even with the numerical and, for the other two constellations, is far superior. In fact, for Globalstar and Ellipso, the analytical method runs more quickly even for very small grids. While there are a number of numerical tricks which may be applied to accelerate the grid-based method, many of these (such as a lookup table for trigonometric functions) could be equally well applied to the analytical algorithm. Despite the substantial advantage which was provided to the numerical approach (limiting analysis to single coverage), it is clear that the analytical coverage algorithm is superior to the most common numerical approach where high precision is required, and at least competitive for low precision applications.

4.4.3 Ellipticity of the Central Body

The results of the precision analysis described above need to be qualified slightly. The analytical result produces an exact coverage for a spherical planet. The earth, however, is not exactly spherical, and deviation from a perfect sphere could adversely effect the accuracy of the result. The largest deviation of the earth from a perfect sphere is the flattening of the poles, which results from the rotation of the earth, and the measure of this effect is the ellipticity of the earth, which is the ratio of the polar radius to the equatorial radius. For the earth, this equatorial excess is only 1/300. This is a small effect and may not influence the coverage significantly at all, but further study is necessary to be certain of this.

Ellipticity, and, in fact, arbitrary deviations from a perfect sphere, can be acco-

modated by grid-based methods, although some care is necessary. The grid can be chosen to fit an arbitrary surface. The challenge lies in determining the proper area element. For an oblate spheroid, the denominator of Equation 2.1 will not simply be $\cos\theta$, but something slightly more complex. It is possible that the effects of ellipticity may be compensated for in the analytic method, possibly by a Taylor series expansion of the area equation in terms of ellipticity. Such an analysis has not yet been attempted. Additional work in this area is required.

Chapter 5

Control Requirements

One of the difficulties in engineering any system lies in finding a systematic approach for determining the requirements and specifications of the components of the systems from the requirements of the system as a whole. This is one of the basic problems of system engineering. In this chapter, system engineering techniques are applied to control of a constellation of satellites. An approach for budgeting control specifications for individual satellites from a top-level requirement (in this case, coverage) is developed. This approach is then applied to several of the constellations discussed previously.

5.1 Approach

The approach to deriving the control requirements for individual satellites in the constellation depends on understanding in what fashion the performance of constellations degrade. There are two primary modes in which the coverage of a constellation may decrease, as shown in Figure 5-1. The first is a global decrease in the semi-major axis of the satellite orbits. The lower altitudes associated with this mode decrease the size of the satellite footprints, which, in turn, adversely effects the coverage. The second mode through which coverage may degrade occurs when the phasing of the

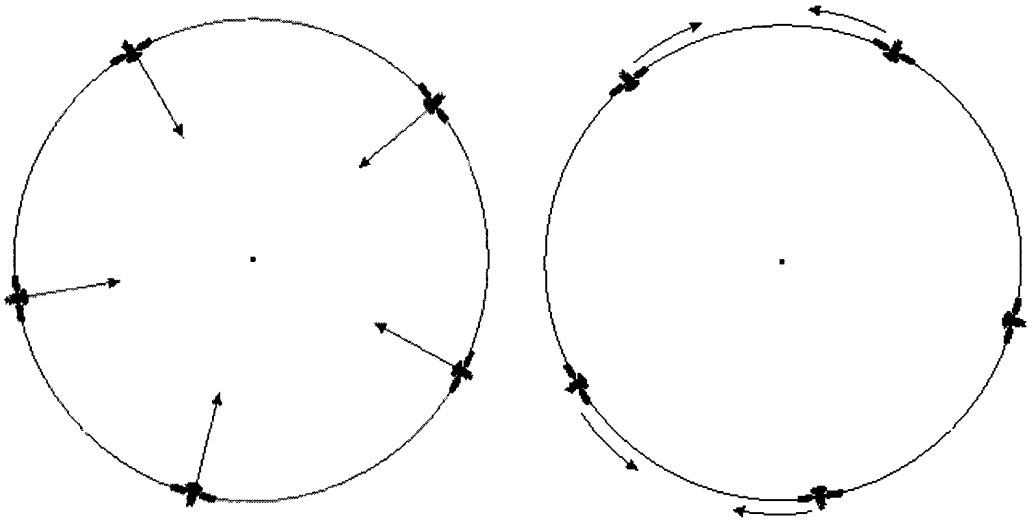

Figure 5-1: Modes of coverage degradation of a constellation: (a) semi-major axis decrease and (b) incorrect phasing.

constellation suffers, i.e. when satellites in a plane or entire orbital planes bunch together. The poor phasing of the constellation may create gaps in the coverage.

The mode by which a constellation fails varies, of course, with the orbital elements of the constellation, the characteristics of the individual satellites, and the time epoch of the analysis. Determining which failure mode actually occurs therefore requires a dynamical simulation of the perturbations to which the constellation is actually exposed. Once the failure mode is determined, the requirements on the individual satellites may be determined from varying the constellation elements in the appropriate mode to determine the coverage characteristics. The point at which the coverage violates the requirement is the maximum allowable variation in the orbital parameter.

This sort of analysis is simple for the first mode of failure. One simply decreases the semi-major axis of the entire constellation until the coverage fails. Analysis of the second mode is more complicated. One must choose a pattern for the dephasing of a constellation. In addition, the ascending node must be varied as well as the mean anomaly for this case. Contour plots of coverage are developed. For a given coverage requirement, these provide a curve relating the control requirement on mean anomaly with that for ascending node. If a control strategy for these two parameters

is assumed, the Δv required to correct a given configuration can be determined for any parameter set chosen. The point on a given coverage contour for which the Δv requirement is minimized represents the optimal choice of station-keeping requirements for this control strategy. Once requirements for both modes of failure are determined, it is simple to return to the results of the simulation and determine which mode is correct. The requirements associated with that mode become the orbital element limitations of choice.

This approach can be generalized for missions with other types of configurations. In the general case, coverage will no longer be the metric of choice, but, as long as a metric can be developed, the analysis will proceed similarly. The sensitivity of the metric to changes in various orbital parameters is examined to determine the most important parameters to control. Given a control strategy, it is possible to determine the best choice of control requirements for a given value of the metric. Further work in this area is necessary.

5.1.1 Constellation Sensitivity Analysis

The rate of change of the orbital elements of a satellite is typically small enough that the element rates may be approximated as constant over the time interval between successive corrections. Under this approximation, the semi-major axis, eccentricity, and inclination all vary linearly with time. The other mean element rates depend upon all of these three; their variations are therefore more complex.

The simplest of these occurs for mean anomaly. The mean anomaly rate, also known as the mean motion n, is determined from Kepler's Third Law,

$$n^2 a^3 = \mu \tag{5.1}$$

where a is the semi-major axis of the orbit, and μ is the product of the gravitational constant and the mass of the central body. Taking the time derivative of both sides

and rearranging slightly, we find that

$$\dot{n} = -\frac{3}{2}\frac{n}{a}\dot{a} \tag{5.2}$$

For slow variations about a given orbit, the fractional variation in mean motion is proportional to the fractional variation in semi-major axis. In the linear regime, therefore, the mean motion rate is proportional to the semi-major axis rate. As the mean motion rate is the second derivative of the mean anomaly, the mean anomaly error will grow as a quadratic in time.

A similar result can be found for the longitude of the ascending node, although the equations are slightly more complex. We begin with the equation for the regression of the node of an orbit in a gravitational potential including only the central force and J_2 effects [3].

$$\dot{\Omega} = -\frac{3}{2}nJ_2\left(\frac{R_e}{p}\right)^2\cos i \tag{5.3}$$

where R_e is the equatorial radius of the central body, i is the inclination of the orbit, p is its parameter, and J_2 is the measure of the oblateness of the central body. For most nonpolar orbits about the earth, this effect dominates the evolution of the longitude of the ascending node.

If we assume a given reference orbit, with fixed inclination i_0 and fixed node rate $\dot{\Omega}_0$ given by Equation 5.3, and a linear perturbation of the inclination, the node rate of the satellite is given by

$$\dot{\Omega} = k\cos\left(i + \frac{di}{dt}t\right) \tag{5.4}$$

where k is the constant multiplying the cosine term in Equation 5.3, and with apologies for the $\dot{\text{i}}$ nomenclature. If we assume that the change in inclination is small relative to the inclination, Equation 5.4 can be expanded as

$$\dot{\Omega} = \dot{\Omega}_0 - k\frac{di}{dt}t\sin i \tag{5.5}$$

The node rate, under these assumptions, varies linearly in time, which implies that, like the mean anomaly, the error in the ascending node is a quadratic in time. This sort of behavior is also observed for the argument of perigee, but its variation tends to be less important, at least for the constellations examined here. For Ellipso, the orbit is critically inclined, causing the J_2 contribution, again by far the dominant effect, to be small. Also, argument of perigee control for Ellipso is effectively free, as it tends to vary in the same fashion as longitude of the ascending node. For the other constellations, the eccentricities are all very small. For these near circular orbits, variations in argument of perigee have no significant impact on the coverage of the constellation.

5.1.2 Formation Flying

Although the number of parameters describing the constellation has been reduced by a factor three, there are still far too many to be convenient for analysis. The next step is to determine parameters which summarize the error in the mean anomaly and ascending node for the entire constellation. One parameter which suggests itself is the mean error. The mean error of some set of points x_i from their reference values r_i is given by

$$\sigma = \sum_{i=1}^{n} |x_i - r_i| \tag{5.6}$$

In general, this would be expected to be a good measure of the vector x_i from its nominal state. For the orbital elements of interest, as has been pointed out before, the performance of the constellation is not effected by global rotation of a plane of satellites or all of the orbital planes.

To account for this symmetry, the average displacement of the satellites must be removed. For a plane of satellites, the average rotation of the satellites is given by

$$\overline{\delta M} = \frac{1}{n_s} \sum_{i=1}^{n_s} M_i - M_{ref,i} \tag{5.7}$$

where n_s is the number of satellites in the plane. Typically, it is desired, for reasons explored in Chapter 3, that the satellites be spaced evenly in mean anomaly. If the elements of M_i are in increasing order, Equation 5.7 may be rewritten as

$$\overline{\delta M} = \frac{1}{n_s} \sum_{i=1}^{n_s} M_i - \frac{2\pi i}{n_s} \tag{5.8}$$

The reference positions of the satellites in the plane are then rotated to remove the average rotation. The new mean anomalies are defined by

$$M_i' = M_i - \overline{\delta M} \tag{5.9}$$

The mean variation in mean anomaly for the plane is therefore given by

$$\sigma_M = \sum_{i=1}^{n_s} \left| M_i' - \frac{2\pi i}{n_s} \right| \tag{5.10}$$

The coverage of a plane of satellites was discussed in a previous chapter. The planar coverage for one plane of the Ellipso Borealis constellation was plotted against σ_M in Figure 3-5. It is clear that there is a strong correlation between the two parameters. This correlation is weaker for constellations which contain more satellites in each plane. This results from the larger number of degrees of freedom in possible variations of the in-plane phasing. When the satellites are near even distribution in the plane, however, the coverage is a quadratic in the mean anomaly variation vector. This parameter is therefore a good measure of the coverage of the plane of satellites for small deviations from nominal even for large constellations.

A similar parameter may be derived to describe the deviation from nominal of the longitude of the ascending node of the planes in the constellation. In this case, as there are more than one satellite in each plane, the ascending node for that plane must be determined from the average of the ascending nodes for each satellite in the plane. In general, the ascending nodes of the satellites in a given orbital plane are

almost identical. Strong resonances over a long period of time are required to cause differential changes in the orbits of satellites which start in the same orbital plane. The equation for the mean deviation of the ascending node is

$$\sigma_\Omega = \sum_{i=1}^{n_p} \left| \Omega_i' - \frac{2\pi i}{n_p} \right| \tag{5.11}$$

where n_p is the number of planes in the constellation and the Ω_i' are determined from the average ascending node of each plane of satellites in a manner precisely analogous to the derivation of Equation 5.9.

This parameter is well defined for simple Walker pattern and polar constellations, but is not clear how best to apply it to a hybrid constellation such as Ellipso. Ellipso, as has been discussed before, consists of two inclined, elliptical orbital planes augmented by an equatorial plane of satellites. For the purposes of the coverage analysis, Ellipso could be considered a polar constellation rotated 90 degrees, but this would needlessly complicate the orbital propagation. For Ellipso, in particular, it is doubly irrelevant, as the variation in the node is fixed not only by coverage requirements but by sun-synchronicity, and because the slow orbital drift rate of the Concordia orbit [28] makes it possible to ignore variations in it for the derivation of control requirements. These issues will be discussed in more detail in later sections.

One nice feature of the parameters which have been defined in this section is that they separate the determination of control requirements into control of the planes of satellites and control of satellites within the plane. This is an appropriate approach, as, with the exception of mean anomaly, the orbital elements of satellites in a similar plane tend to change at the same rate. This may simplify mission operations, as it immediately distinguishes between planar and plane change orbit maneuvers, which are required with differing frequencies and should be handled separately.

The coverage of each constellation is explored for a range of these two parameters, σ_M and σ_Ω. As, for a given value of one of these parameters, there are many possible configurations, it is necessary to choose a pattern for the deviations from nominal. The choice made in this coverage analysis is the case in which all of the satellites are

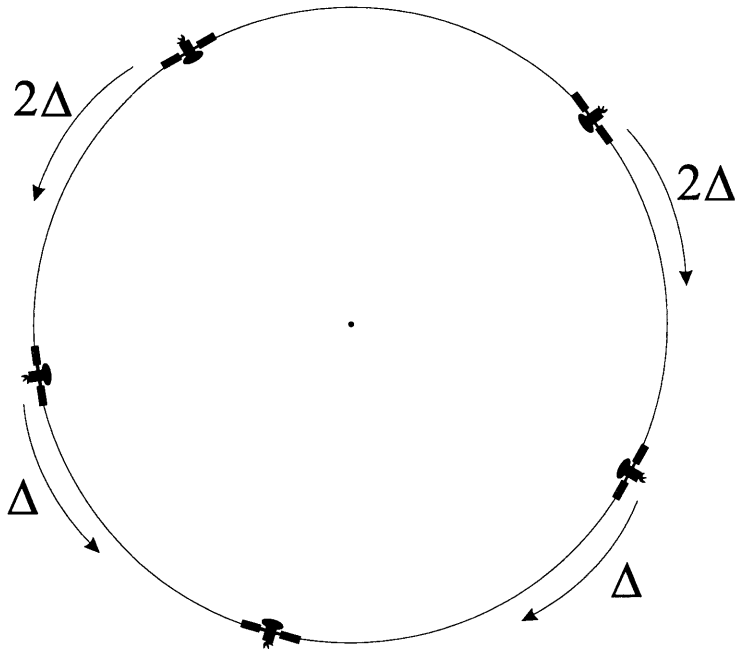

Figure 5-2: Phasing pattern for coverage analyses

superimposed at a point for 100 percent dephasing, as shown in Figure 5-2. The equations for this form of dephasing are different for an odd number of satellites in a plane than for an even number. If we assume the satellites to be ordered by increasing mean anomaly, the dephasing equations for an odd number of satellites is

$$\delta M_i = \begin{cases} 0 & \text{if } i = 0 \\ -\frac{2\pi i}{n_s}\alpha & \text{if } 1 \leq i \leq \frac{n_s-1}{2} \\ \frac{2\pi i}{n_s}\alpha & \text{if } i > \frac{n_s-1}{2} \end{cases} \tag{5.12}$$

and, for an even number of satellites, is

$$\delta M_i = \begin{cases} -\frac{(2i+1)\pi}{n_s}\alpha & \text{if } i < \frac{n_s}{2} \\ \frac{(2i+1)\pi}{n_s}\alpha & \text{if } i \geq \frac{n_s}{2} \end{cases} \tag{5.13}$$

where δM is the mean anomaly alteration resulting from the dephasing, and n_s is the

number of satellites in the plane. The coverage analyses for the constellations can now be performed, and the coverage contours in the parameter space determined.

5.1.3 Control Philosophy

The coverage analysis provides contours (or, for 100 percent coverage, a region) for a given level of coverage. Since each point on the contour corresponds to requirements on mean anomaly and ascending node, any point on the curve could be chosen as the control requirement for the satellites. It is better, however, to take into account a control strategy to determine which configuration is best.

There are many different methodologies for correcting a satellite orbit, and, in general, the choice of approach must be determined separately for each constellation, after taking into account the type of orbit and the dominant perturbations to which it is subjected. Once this strategy is determined, the amount of Δv , and, therefore, the quantity of fuel, required for a given correction can be determined. This provides a metric for the comparison of points on a given coverage contour to determine which is the optimal choice of requirements for a given control methodology.

General LEO Case

In the absence of a strong resonance, the behavior of satellites in circular, low altitude orbits is dominated by the effects of drag. The primary secular effects of drag on a satellite is to reduce the its altitude and to circularize its orbit. The second effect tends to eliminate the necessity to control eccentricity, but the first leads to frequent semi-major axis corrections. The changes in semi-major axis influence both the node rate and the mean motion of the satellite. Typically, the effects of drag affect all satellites in a constellation with similar semi-major axis and eccentricity in the same fashion, which causes the node rate and mean motion to remain approximately equal for all of the satellites in the constellation. This corresponds to the first failure mode discussed above. In this case, the control is simple. The semi-major axes of all of the satellites in the constellation are raised at once, in order to avoid the mean anomaly

phasing errors which result from differing semi-major axes. The amount the orbit is raised is not limited by coverage concerns and may be chosen for a preferred frequency of reboost operations. In practice, the maximum semi-major axis may be limited by such factors as the maximum slant range for which the link may be made (for a communications satellite), by maximum resolution (for a surveillance or surveying mission), or by other factors altogether.

Resonance-Driven Case

The general LEO case described above is a very desirable situation. In some cases, however, requirements dictate that the satellite orbits be in a regime where resonance effects, whether tesseral harmonics, third body, or radiation pressure, have differential effects on orbital planes or on satellites within a given plane. In these cases, the phasing of the constellation suffers, and the complexities of the second failure mode described above must be dealt with.

For this case, the mean anomaly and the ascending node of the satellite must be controlled separately. Mean anomaly is most efficiently controlled through the semi-major axis of the orbit, and the node rate will be controlled through the inclination. In this case, the elements must be controlled much more tightly than in the prior case. Also, variations in both the positive and negative directions must be removed; having too slow or too fast a mean motion or node rate causes the constellation to dephase equally quickly. The control strategy is chosen to maintain the orbital elements within the chosen boundaries with a minimum number of corrections. We begin by determining the proper semi-major axis correction for a given violation of mean anomaly.

The vector z, defined as the difference of the orbital elements $[aei\Omega\omega M]^T$ of the satellite from those of the reference, measures the deviation of the satellite from its nominal. We begin by assuming that the inclination of the orbit remains constant as the semi-major axis varies linearly in time. Also, we assume that the satellite has just reached the limit imposed on the mean anomaly. For this situation, we wish to derive the Δa necessary to correct the mean anomaly.

The mean motion of the satellite is determined from Equation 5.1. Assuming that we have just boosted the semi-major axis, the satellite mean motion may be written as

$$n_{sat} = \sqrt{\mu}\left(a_0 + \Delta a + \dot{a}t\right)^{-\frac{3}{2}} \tag{5.14}$$

where a_0 is the reference semi-major axis, Δa is the amount above nominal chosen for the correction, and $\dot{a}$ is the semi-major axis rate. Expanding around the nominal value, the mean motion is approximately

$$n_{sat} \approx \sqrt{\mu} a_0^{-\frac{3}{2}} \left(1 - \frac{3}{2}\frac{\Delta a + \dot{a}t}{a_0}\right) \tag{5.15}$$

The mean motion of the reference is given by

$$n_{ref} = \sqrt{\mu} a_0^{-\frac{3}{2}} + \frac{1}{n_s}\dot{z}_6 \tag{5.16}$$

where n_s is the number of satellites in the plane, and the second term takes into account the variation of the reference due to formation flying. The rate of the mean anomaly error is the difference of the actual and the reference, which may be solved to yield

$$\dot{z}_6 = -\frac{3}{2}\frac{\sqrt{\mu}}{1+\frac{1}{n_s}} a_0^{-\frac{5}{2}} \left(\Delta a + \dot{a}t\right) \tag{5.17}$$

Integrating Equation 5.17 yields the mean anomaly error.

$$z_6 = z_{6i} - \frac{3}{2}\frac{\sqrt{\mu}}{1+\frac{1}{n_s}} a_0^{-\frac{5}{2}} \left(\Delta a t + \frac{1}{2}\dot{a}t^2\right) \tag{5.18}$$

where z_{6i} is the mean anomaly at the time of correction and is therefore equivalent to the allowed variation in mean anomaly. A typical phase space curve for the mean anomaly and semi-major axis errors is shown in Figure 5-3. The motion in the figure is counter-clockwise along the phase-space curve.

We wish to choose Δa such that we maximize the time between corrections. As

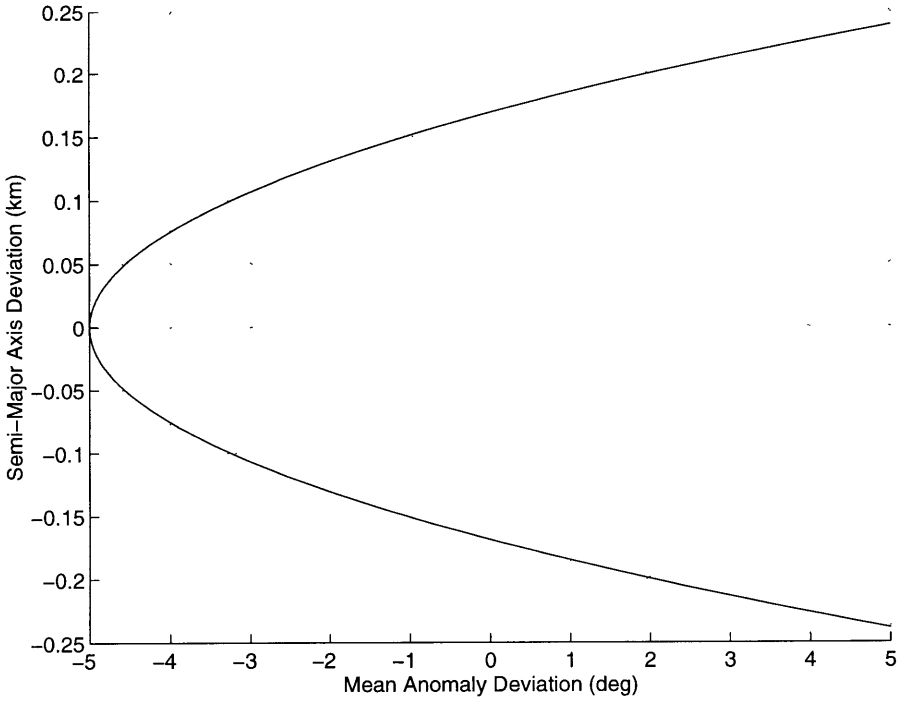

Figure 5-3: Qualitative behavior of mean anomaly error after a correction

the behavior of z_6 is parabolic, it is clear that it will reach an extremal value. This extremal value of the mean anomaly error occurs, of course, when its rate is zero, which, from Equation 5.17, is clearly when

$$t_{ext} = -\frac{\Delta a}{\dot{a}} \tag{5.19}$$

If we increase Δa, we clearly increase the time between violations on the same side of nominal as the original violation. If, however, the value of Δa is made too large, the mean anomaly will violate on the opposite side of nominal. The maximum time between corrections clearly occurs when the vertex of the extremal value of z_6 is set to be $-z_{6i}$. This family of mean anomaly histories with a mean anomaly limit of five degrees is shown in Figure 5-4.

In order to correct mean anomaly in this manner we require that the mean anomaly error be $-z_{6i}$ at $2t_{ext}$. Making this substitutions into Equation 5.18 and solving for

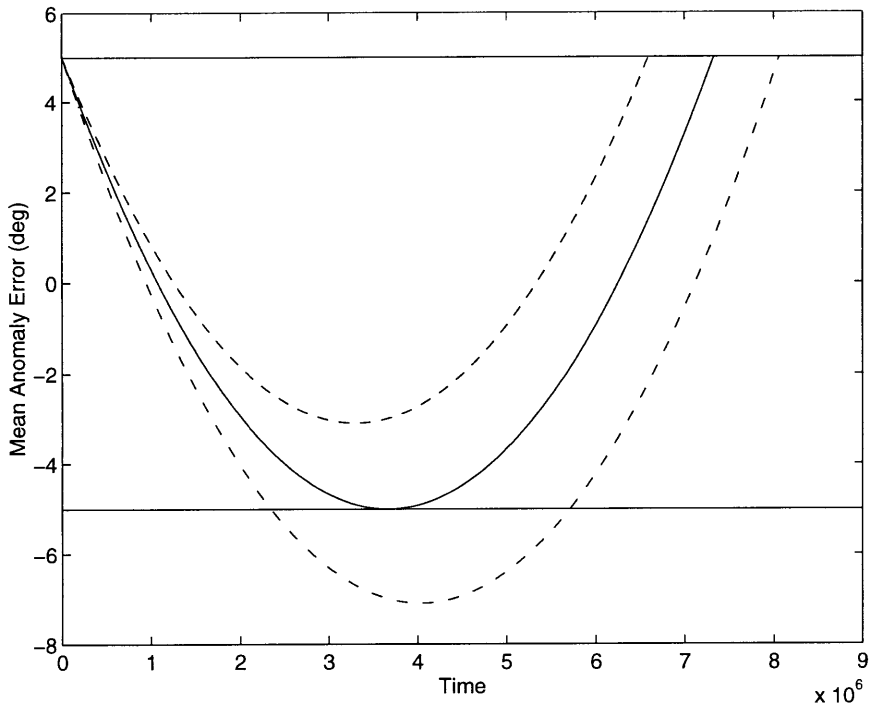

Figure 5-4: Mean anomaly error histories for varying semi-major axis changes

Δa, we find that

$$\Delta a = \sqrt{-\frac{8}{3}\left(1+\frac{1}{n_s}\right)\frac{a_0^{\frac{5}{2}}}{\sqrt{\mu}}\dot{a}z_{6i}} \tag{5.20}$$

The total correction is clearly the sum of Δa and z_{1i}, the initial value of the semi-major axis error.

Δa is clearly undefined if z_{6i} and $\dot{a}$ have the same sign. This restricts corrections to occurring only in quadrant four of Figure 5-3. In this case, at least one of z_1 and z_4 are moving toward their nominal value, and the correction should wait until it is moving away from nominal again. In order to prevent violations in this case, it may be appropriate to create an interior limit on the node more stringent than the actual requirement to prevent having to tolerate violations of the true limit while in the wrong quadrant.

This interior limit is also valuable to protect against variations in the effects of drag. This analysis assumed that the semi-major axis rate is constant over the

corrections cycle. Variations in the solar cycle, however, may change the semi-major axis rate significantly, which will alter the behavior of the satellite. Maintaining an interior limit provides a margin for error to help absorb some of these effects. If more precision is required, this approach may be easily modified to determine numerically the optimal choice of Δa for a given drag model, although this is unnecessary for this analysis.

A similar analysis may be undertaken for the error in the ascending node. In this case, the errors are corrected by slight changes in the inclination. The analysis is completely analogous to the derivation of 5.20 and will therefore be omitted. The resulting inclination deviation after the burn is given by

$$\Delta i = \sqrt{4\frac{z_{4i}}{\alpha \sin i_0}\left(1+\frac{1}{n_p}\right)\dot{z}_3} \tag{5.21}$$

where z_{4i} is the node error at violation, i_0 is the nominal inclination, n_p is the number of planes, $\dot{z}_3$ is the rate of the inclination deviation, and α is the proportionality constant in Equation 5.3, or

$$\alpha = \frac{3}{2} n J_2 \left(\frac{R_e}{p}\right)^2 \tag{5.22}$$

There are again limitations on where corrections may take place in order for the radicand of Equation 5.21 to be positive, as in the case of the mean anomaly correction, and similar caveats apply.

Fuel Usage

In the analysis of the Δv usage, there are clearly two different types of corrections required. The first requires a change in the semi-major axis. The most efficient method for changing the semi-major axis of the orbit without affecting the other orbital elements is the elliptic Hohmann transfer[1]. The Δv used in this maneuver is

[1]For cases in which the ratio of the semi-major axis of the final orbit to that of the initial orbit is large, the bielliptic transfer can be more efficient, but, for small orbital corrections, the Hohmann transfer is clearly both more practical and more efficient.

given by

$$\Delta v = \sqrt{\frac{\mu}{r_{p0}}}\left(\sqrt{1+e_t} - \sqrt{1+e}\right) + \sqrt{\frac{\mu}{r_{a1}}}\left(\sqrt{1-e} - \sqrt{1-e_t}\right) \tag{5.23}$$

where r_{p0} is the perigee height of the lower orbit, r_{a1} is apogee height of the second orbit, and the eccentricity of the transfer orbit is given by

$$e_t = \frac{r_{a1} - r_{p0}}{r_{a1} + r_{p0}} \tag{5.24}$$

The second maneuver is an inclination change. The Δv used in this maneuver is given by

$$\Delta v = \frac{2\mu}{h} \sin\frac{\Delta i}{2}\left(1 \pm e\cos\omega\right) \tag{5.25}$$

where h is the angular momentum of the orbit, ω is its argument of perigee, e is eccentricity, and Δi is the change in inclination required.

Between Equation 5.23 and Equation 5.25, it is possible to determine the amount of Δv used in the corrections determined for a given set of element limits. In addition to coverage contours, there are also Δv contours, and the best choice of requirements is determined from the intersection of the coverage contour corresponding to the coverage requirement and the minimal Δv contour to intersect it.

5.2 Sample Requirements

The numerical simulations of the orbital evolution of these constellations was carried out with the Draper Semi-Analytic Satellite Theory (DSST). These simulations include, among other perturbations, zonal harmonics, tesseral resonance up to 21x21, third-body effects, drag, and radiation pressure. Planes of satellites were simulated to determine whether the individual satellites in each plane were perturbed differently. The results were then assembled to understand the relative evolution of the orbital

planes. As has been discussed before, if the satellites are all perturbed equally, then no dephasing of the constellation occurs, and semi-major axis decay is the primary mode of coverage degradation. For this case, the orbital element limits are developed simply by determining at what altitude does coverage decay below the allowed value. For the case where dephasing is important, the coverage and Δv contours are developed, as described above, and the optimal choice of requirements is developed.

5.2.1 Globalstar

For Globalstar, a LEO constellation which is not in a repeating ground-track, there is no reason to expect any contribution from resonance effects. In addition, at such a low altitude, the contributions of drag are expected to dominate the perturbations on the satellite orbits. It is therefore expected that the constellation fail due to semi-major axis degradation, and this result was born out by the numerical simulations.

The mean anomaly difference from reference (in a formation-flying scenario) is plotted in Figure 5-5[2]. This plot represents a five year history of the mean anomaly deviation for the orbital plane with an initial ascending node of 0 at an epoch of Jan 1, 1997. As can easily be seen from the scale of the mean anomaly variations, the satellite phasing remains intact over the time scale of the simulation. In fact, the variations in mean anomaly are so small as to suggest that they are merely the artifacts of numerical noise rather than any real physical effect. This behavior is typical for all of the planes in the Globalstar constellation.

A similar result is obtained for the ascending node of the orbital planes. In Figure 5-6, the time evolution of a single satellite (0 mean anomaly at epoch) from each orbital plane is plotted. Only comparing one satellite from each plane is a valid approach, as it has already been shown that all of the satellites in a given plane evolve similarly. The deviations in the ascending node clearly grow at the same rate, indicating that the constellation stays perfectly in phase as it evolves. This behavior

[2]The orbital elements plotted in all of the history plots in this work are sampled every 50 iterations, or "frames." The iteration time is constrained to be less than the orbital period; consequently, the unit of time in these plots varies for different constellations.

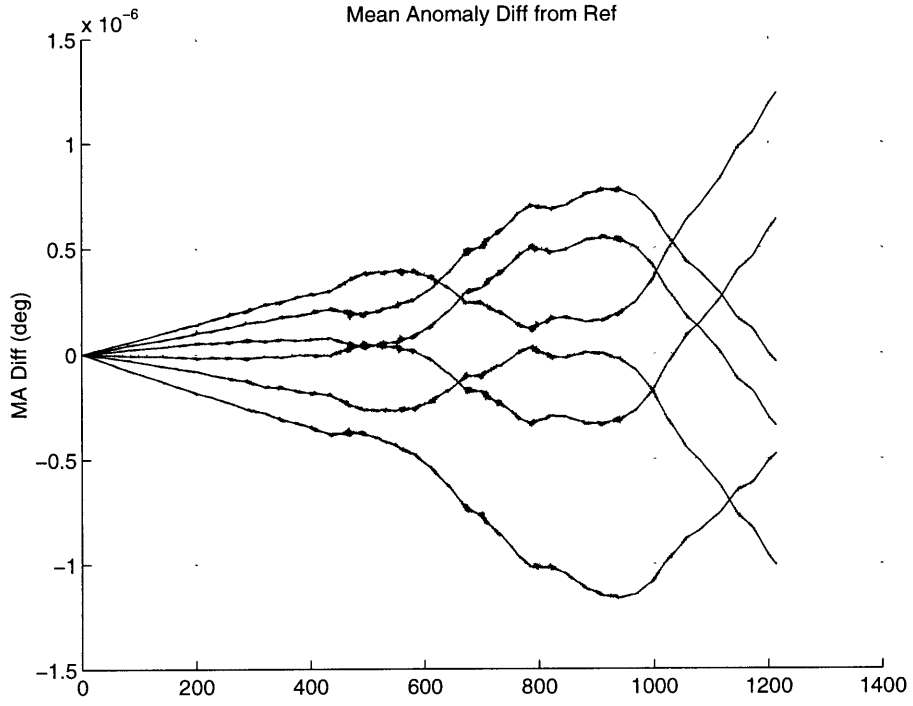

Figure 5-5: Five year history of mean anomaly deviation for a Globalstar plane

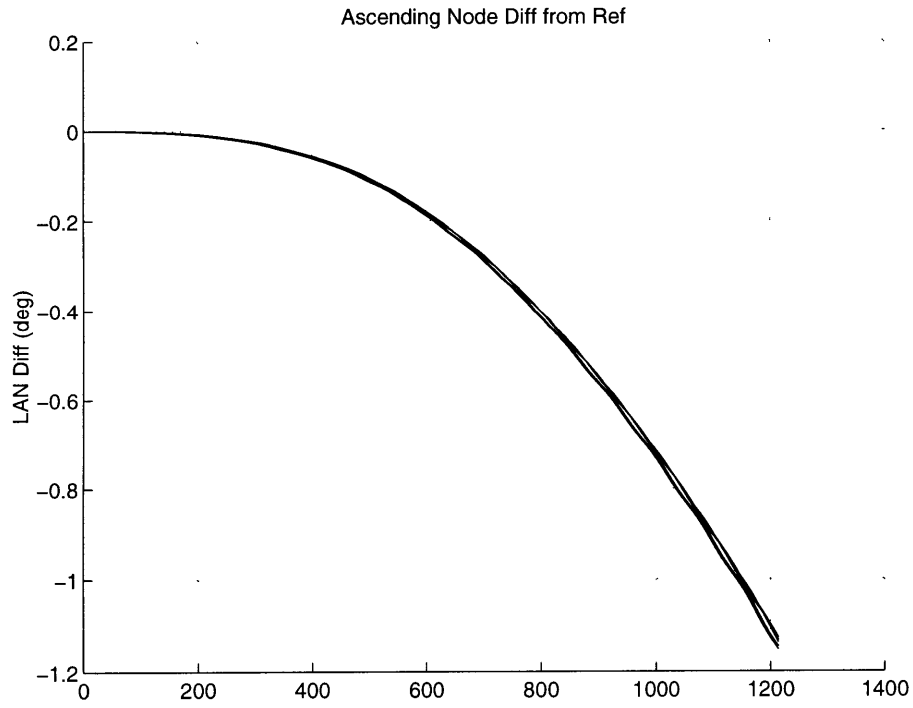

Figure 5-6: Five year history of node deviation for the Globalstar constellation

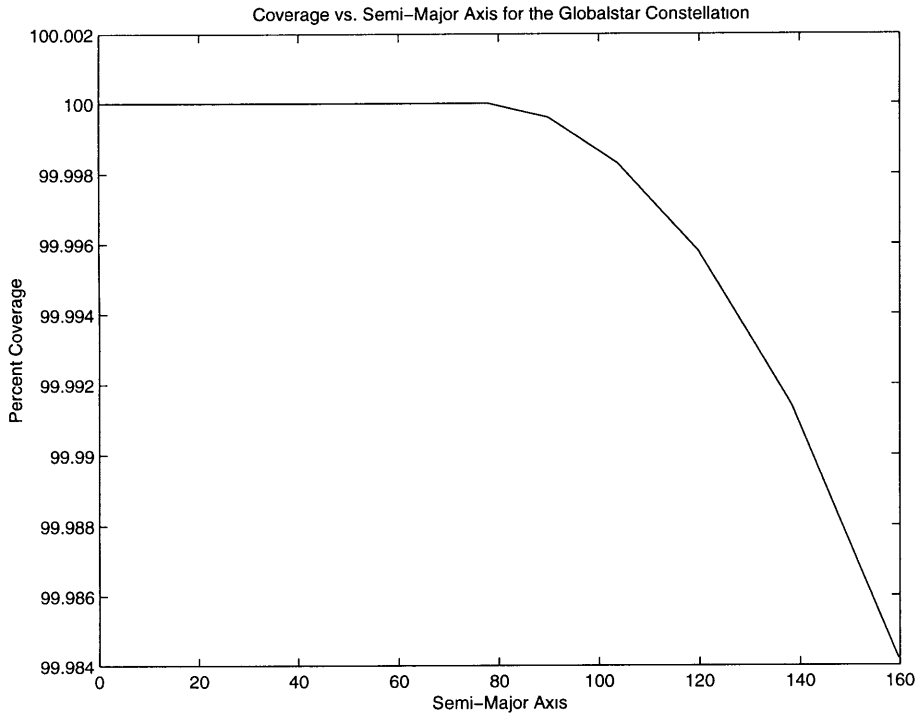

Figure 5-7: Semi-major axis requirement determination for Globalstar

is again typical of circular LEO constellations for which the dominant perturbation is atmospheric drag.

As the coverage degradation clearly results only from the lowering of the semi-major axis of the constellation, the requirement analysis proceeds along the first path. The coverage for Globalstar was analyzed as the semi-major axis varies for the latitude range from 70° N to 70° S for an elevation angle of 10°. The results are plotted in Figure 5-7. As can be seen from the plot, the coverage gaps do not begin to appear until the semi-major axis has been lowered by more than 70 km, a huge variation from an astrodynamics standpoint and one which does not occur during the lifetime of the constellation.

While the parameters chosen for the coverage analysis are variable (such as extending the coverage region to ±75° latitude or using an elevation angle of 10°, and such changes would have an effect on the semi-major axis variation allowable, the magnitude of the variation required to have a negative effect on the overall coverage

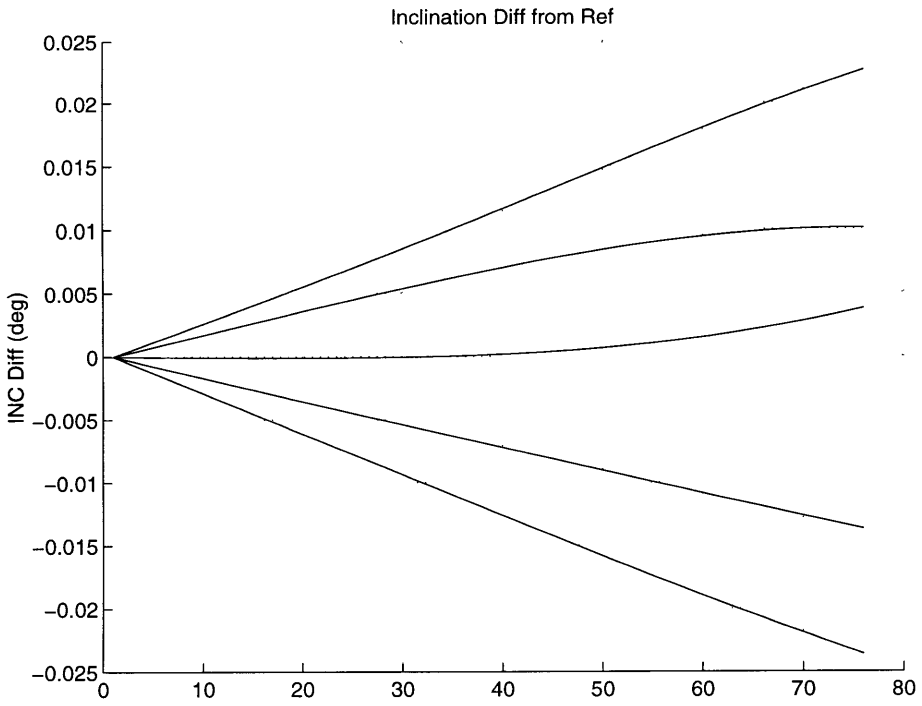

Figure 5-8: Inclination evolution of an Ellipso Borealis plane over six months

is so large that the essential conclusion remains the same. The coverage of the Globalstar constellation does not decay significantly for long periods of time. Therefore, if coverage is the metric for station-keeping, no control is required for the constellation over a reasonable lifetime ($\sim$ 10 yr).

5.2.2 Ellipso

Ellipso, unlike Globalstar, is at a much higher semi-major axis and is, as a result, less likely to be dominated by drag effects. The Borealis constellation is, in addition, in an 8:1 repeat ground-track. The combination of repeat ground-track and sun-synchronicity with high apogee heights suggests that resonance plays a large role in the orbital evolution, and this, in fact, has already been observed [26]. These effects are easily verified.

The inclination history for one plane of the Ellipso Borealis constellation is plotted for a six month period in Figure 5-8. The inclination evolves approximately linearly

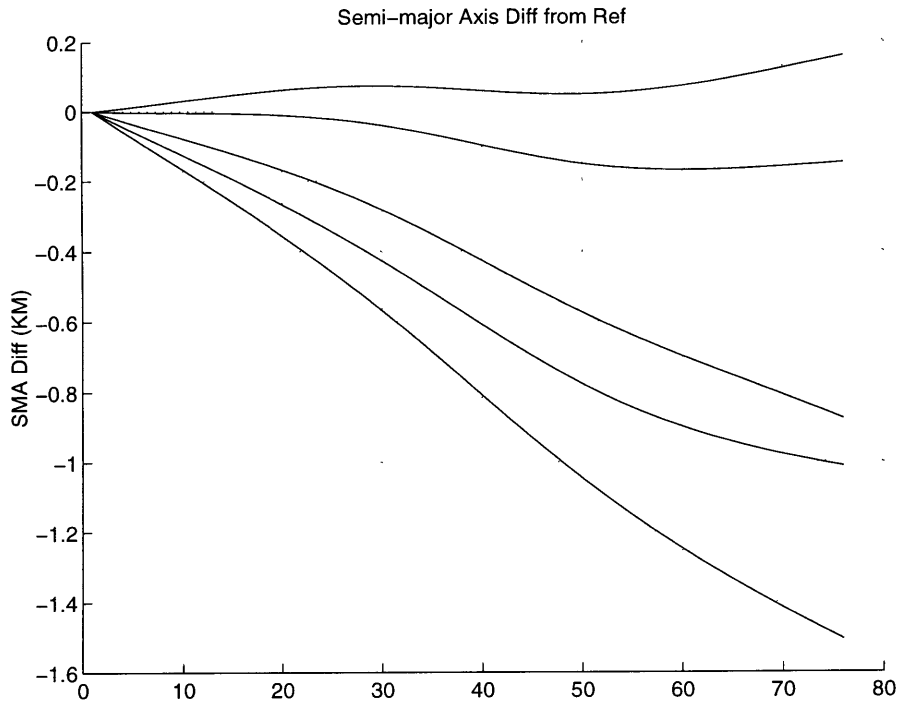

Figure 5-9: Semi-major axis evolution of an Ellipso Borealis plane over six months

over the time frame of the simulation, but the inclination rate varies among the satellites in the plane. This behavior is not unexpected for a sun-synchronous orbit with a repeat ground-track. This combination causes the satellite to be in the same position in the orbit relative to the sun over some repeat cycle. The satellite is therefore in resonance for solar third-body effects as well as for radiation pressure. This suggests that maintaining the proper phasing for the constellation may well be an issue.

The semi-major axis deviation for the same plane and time frame is shown in Figure 5-9. Again there is clear evidence of the impact of radiation pressure resonance. The satellites evolve quite differently; one even receives a net increase in semi-major axis. These variations in the semi-major axes of satellites in a given plane also suggest some difficulty in maintaining proper intersatellite-phasing.

These suspicions are borne out by the evolution of the mean anomaly deviations. In Figure 5-10, variations in mean anomaly (from a formation-flying reference) are

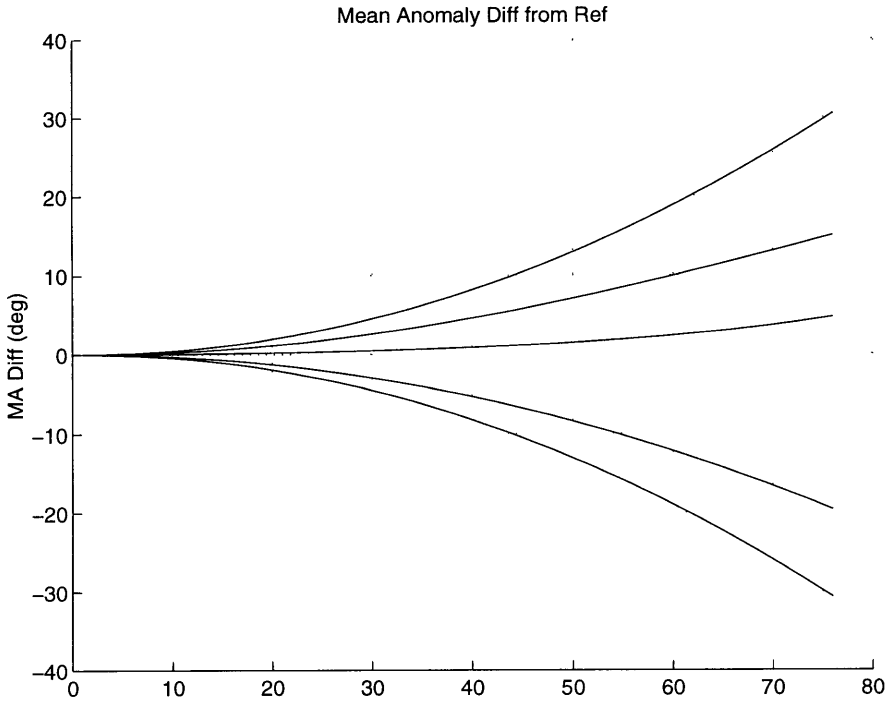

Figure 5-10: Mean anomaly deviation of an Ellipso Borealis plane over six months

plotted for a six month period. The mean anomaly deviations reach 30° within six months, which contrasts sharply with the benign behavior of the Globalstar constellation. Clearly, a large gap in the planar coverage is being created. Ascending node varies in a similar, if not quite as dramatic, pattern.

Unlike the two Borealis planes, the variations in the Concordia plane are much more benign. This is illustrated in Figure 5-11. This result is hardly unexpected, as the Concordia plane is not sun-synchronous and is at such a high altitude that non-spherical earth effects will be small. In the coverage analysis, therefore, the phasing of the Concordia plane will not be perturbed.

The analysis of the Ellipso constellation proceeds as described above. The coverage contours generated are shown in Figure 5-12. The contours, especially as they approach 100 percent, show signs of numerical noise, a consequence of the interpolation routine MATLAB utilizes to produce them. It is interesting that such a wide variation in both node and mean anomaly may occur without violating global

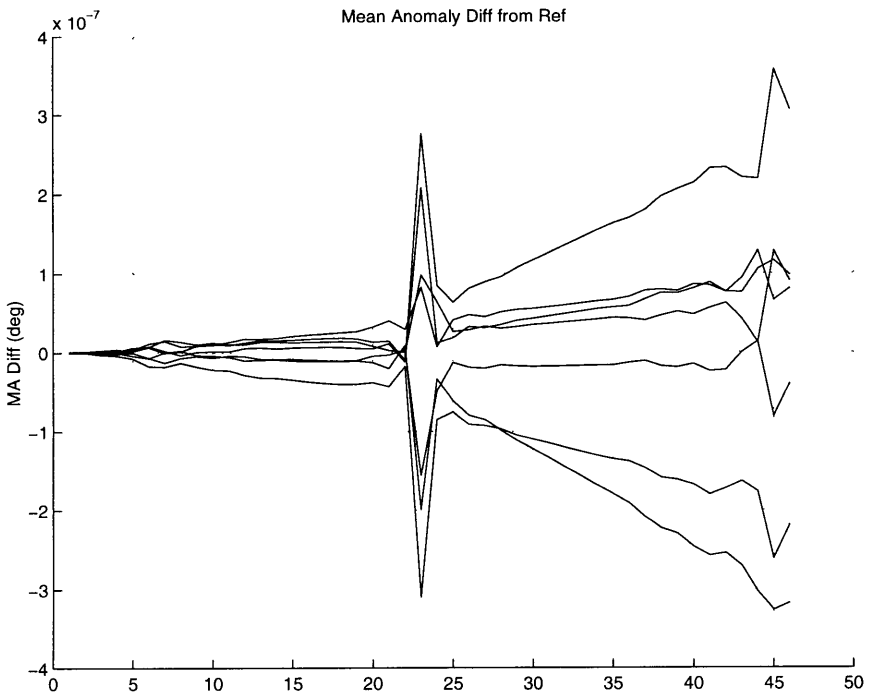

Figure 5-11: Five year history of mean anomaly for the Concordia plane

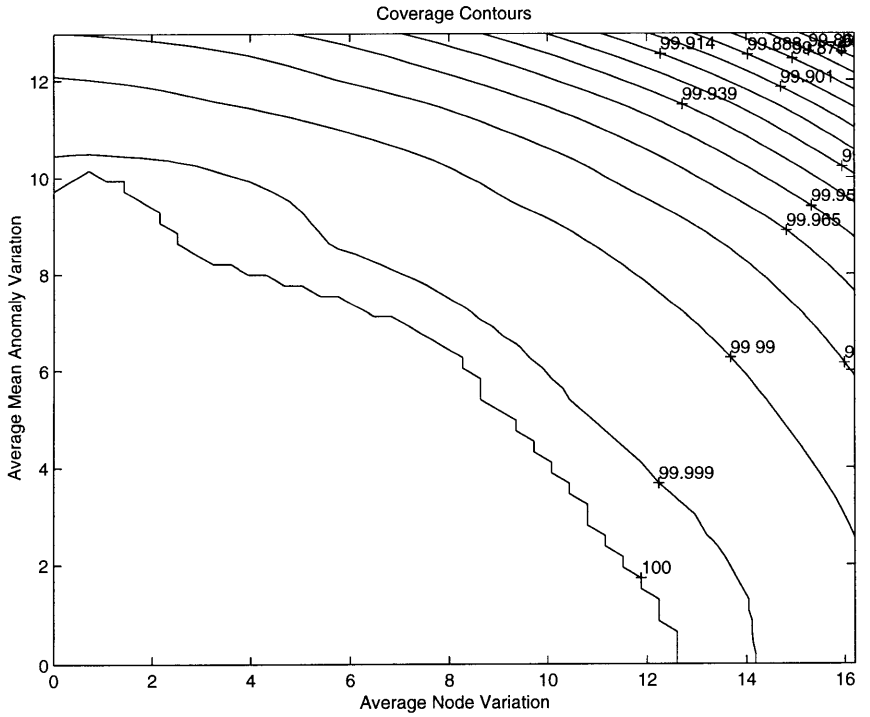

Figure 5-12: Coverage contours for the Ellipso constellation

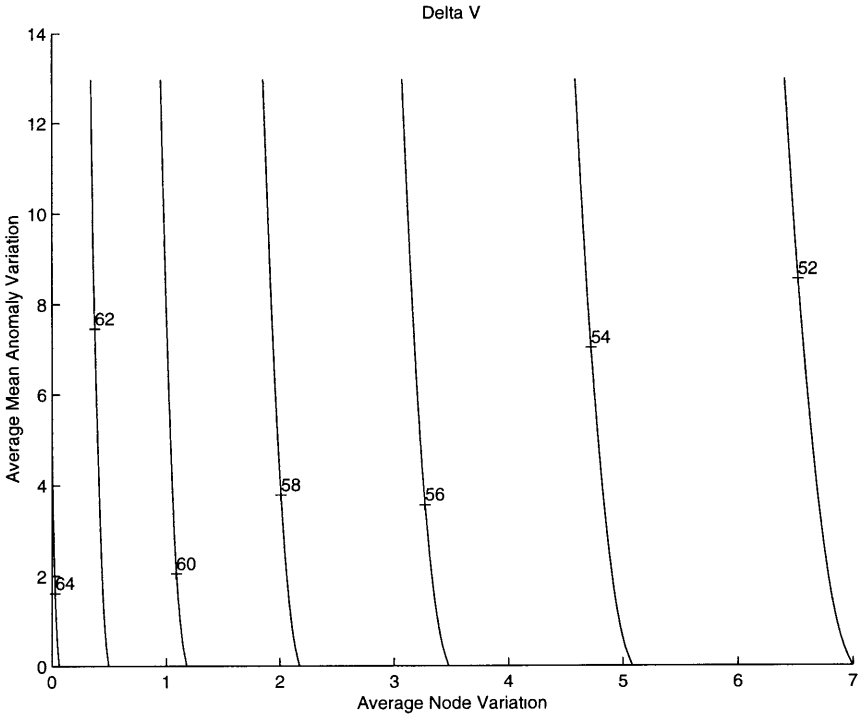

Figure 5-13: Δv contours for the Ellipso constellation

coverage (at 25 degree elevation angle). This is primarily a result of how effective Concordia is at covering the low to mid latitudes. With the Concordia constellation in proper phase, the only requirement on the Borealis planes is that a few of its satellites be near the north pole to supplement Concordia at the high latitudes. This is not a terribly difficult requirement to meet, and this is reflected in Figure 5-12.

The Δv contours for the Ellipso constellation are shown in Figure 5-13. The interesting facet of this figure is that the contours are almost vertical. This is typical of this form of control and is a result of two factors. The first is that inclination burns are so much more expensive than in-plane maneuvers. The second is that the mean anomaly corrections are much more frequent than the node corrections. The node rate drift is so much smaller than the drift in mean motion that it is possible to eliminate node corrections if the restriction on the node is made large enough. The requirement for which no node corrections are required over the five year lifetime used in this analysis may be seen in Figure 5-13 as the value for which the Δv contours

are no longer linear.

The Δv behavior indicates that the proper approach to controlling the Ellipso constellation is to control mean anomaly as precisely as possible and to let the node essentially drift where it will. If it were possible to maintain mean anomaly perfectly, the maximum node variation allowed for Ellipso is slightly larger than 12 degrees. In practice, of course, maintaining mean anomaly so precisely would require maneuvering too frequently. But maintaining mean anomaly within 0.5 degrees only requires burns every couple of weeks, a reasonable frequency. What a reasonable frequency is is mostly a matter of operational philosophy (and operational complexity and the maximum thrust available from the propulsion system, etc.), but the algorithm remains the same.

The best choice of requirements for maintaining 100 percent coverage at 25 degree elevation angle can be read right off of Figure 5-12 to be 0.5 degree in mean anomaly and 12 degrees in node. The Ellipso satellites, however, are being designed under the assumption of maintaining sun-synchronicity, and the limit on node variations MCHI has chosen is only 0.2 degrees [8]. For this choice of node limit, the allowable mean anomaly variation is 9.5 degrees. In the following chapter, the results of these two choices for station-keeping requirements will be compared.

5.2.3 GPS

The coverage analysis for GPS presents a slightly different challenge. The goal of the GPS constellation is to provide navigation data to the entire surface of the earth. Since at least four satellites are required for a position fix, three for the spatial coordinates and one to correct the clock on the GPS receiver, it makes little sense to design or control the GPS constellation for one-way coverage, and, in fact, the constellation definition for GPS required continuous 5-way global coverage [30].

The performance of the GPS receiver is affected by two factors which may be controlled through constellation design. The first is the number of satellites in view. The second is the geometric dilution of precision (GDOP). The optimal metric for

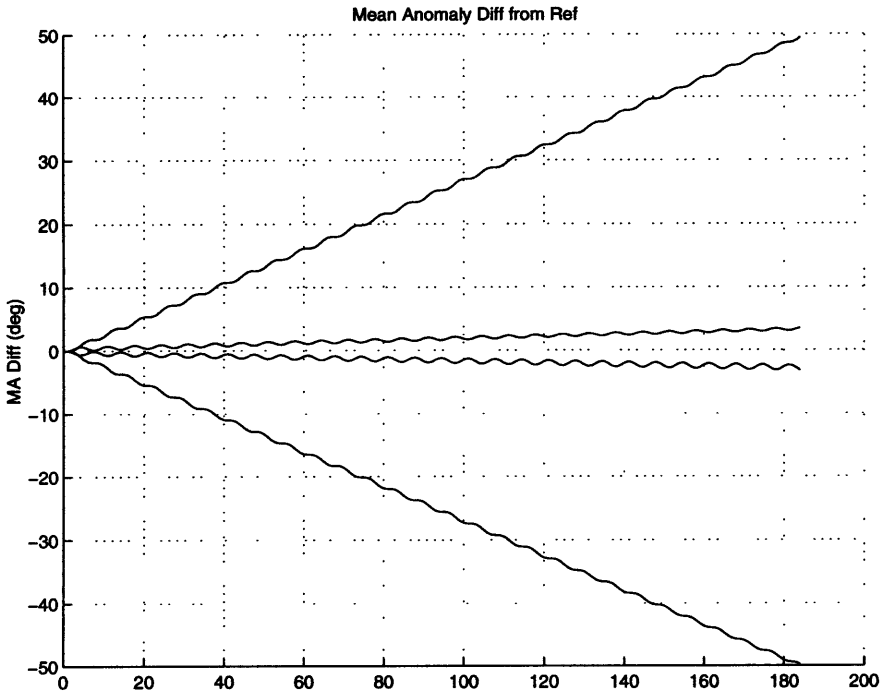

Figure 5-14: Five year history of mean anomaly for a GPS plane

evaluating GPS constellation performance would include some combination of the effects of both of these parameters and would probably vary with the filtering routine used to determine position. For this analysis, however, multiple satellite coverage will be the sole metric.

The GPS satellites, like Ellipso, are in fixed ground-track orbits. It is not surprising, therefore, that the coverage of the GPS constellation also decays through dephasing. Figure 5-14 shows the five year history of the mean anomaly variations for a GPS plane. The node variations among planes shows similar signs of drifting out of phase. The analysis of the requirements therefore proceeds similarly to that for Ellipso.

An interesting fact was discovered in the process of determining phase contours for GPS. Optimal 5-way and 6-way coverage does not occur for satellites evenly spaced within the orbital planes. Instead, displacing pairs of satellites together actually increases the coverage performance of the GPS constellation. This behavior is dis-

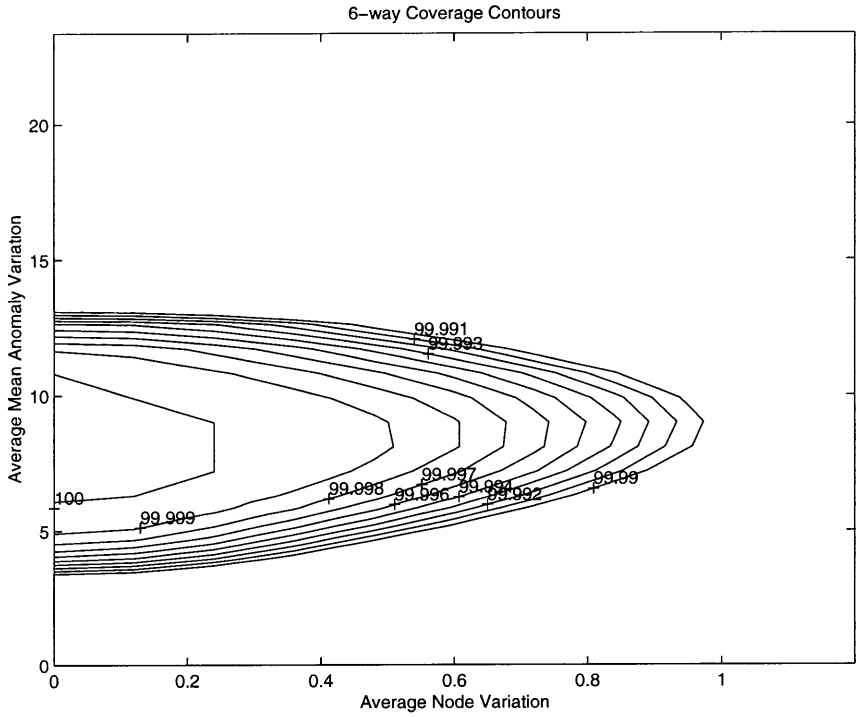

Figure 5-15: 6-way coverage contours for GPS configuration choice

played in Figure 5-15. The coverage contours for 5-way coverage are topologically similar, although the 100 percent coverage region is much larger, encompassing the complete 6-way coverage region. From Figure 5-15, two conclusions may be drawn. First, variations in ascending node decrease the performance of the GPS constellation. Second, variations in mean anomaly may improve the performance of GPS. The optimal choice of mean anomaly "pairing" of satellites in the plane is approximately 8.5 degrees. This choice maximizes 6-way coverage of GPS; this configuration will be used as nominal for the analysis of GPS station-keeping requirements. It should be noted that this analysis neglected the effects of variations in inter-plane phasing (the F factor in Walker's terminology). In addition, the effect of these changes on the GDOP performance of the constellation remains unknown.

The coverage analysis may now proceed as before. The results of the coverage analysis for 6-way coverage are shown in Figure 5-16. The Δv contours are again approximately vertical; the optimal choice of station-keeping requirements again de-

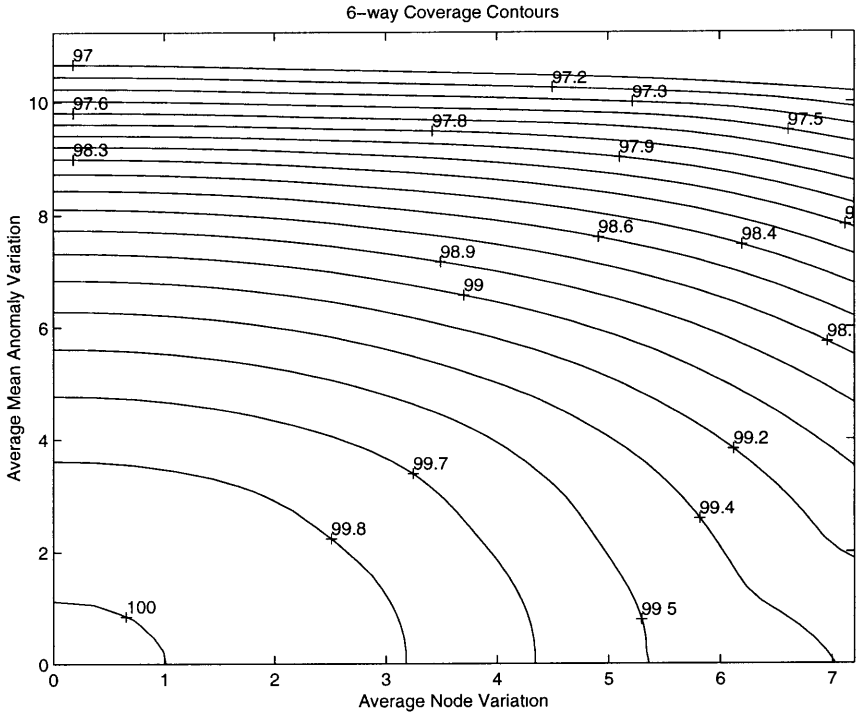

Figure 5-16: 6-way coverage contours for GPS

pends on the maximum reasonable frequency for satellite maneuvers. Again choosing 1 degree as the maximum variation in mean anomaly, the corresponding station-keeping requirement for the ascending node is 0.5 degrees. The maintenance of the GPS constellation will be further examined in the following chapter.

Chapter 6

Verification

In the previous chapter, station-keeping requirements for several constellations were determined. In this chapter, the performance of these constellations is tested for these requirements. The Δv necessary to maintain the constellation is determined through the Automated Station-Keeping Simulator, developed at Draper Laboratory by Naresh Shah [27]. The coverage of the constellations is calculated with the coverage algorithm described in Chapter 4.

6.1 ASKS

ASKS is a complex, parallel system which performs station-keeping maneuvers for a number of satellites simultaneously, utilizing MPI (Message Passing Interface) to implement parallel processing. A process is created for each satellite which requires station-keeping. Each process propagates both a reference and an actual trajectory, determines if the satellite is going to violate the orbital element limits, and calculates an appropriate burn to correct the violations. The processes are coordinated and controlled from a single main program, which also outputs element histories and coverage data as well as redefining the reference trajectories appropriately. The orbit propagation is implemented by means of DSST. The target element sets in case

of a violation are determined from the equations in Chapter 5. The optimal burn sequences are calculated through a numerical scheme based on primer vector theory.

6.1.1 DSST

The Draper Semi-Analytic Satellite Theory (DSST) is a mean-element orbital propagator derived from the much larger Goddard Trajectory Determination System, developed at Draper Laboratory. In a comparison of DSST to several other orbital propagators, the authors conclude that DSST provided the best combination of accuracy and computation time [5].

Mean Elements

An orbital propagator is a software system which solves the equation of motion for an object near a large central body (such as the earth). For it to be generally useful, it must take into account the perturbations to the simple Keplerian motion which result from disturbances such as a non-spherical central body, other gravitating bodies, drag, etc. The equation of motion for such a system can be written as

$$\frac{d^2\boldsymbol{r}}{dt^2} + \frac{\mu}{r^3}\boldsymbol{r} = \boldsymbol{a}_d \tag{6.1}$$

where $\boldsymbol{r}$ is the position vector of the satellite relative to the center of mass of the central body, and $\boldsymbol{a}_d$ is the combined acceleration from all perturbative forces. The solution to this equation gives the state of the orbiting object, the vector consisting of position and velocity, as a unique function of time and the initial state of the system. This approach is referred to as special perturbations. Most propagators solve this system of equations, and, indeed, this approach is the most straight-forward.

It is possible, however, to improve the computational behavior of the system as well as gaining valuable physical insight into the problem by transforming the problem to a different set of variables, the classical orbital elements. This approach is beneficial because most of the elements vary slowly when compared to the state variables $\boldsymbol{r}$ and

$\boldsymbol{v}$; this allows larger step sizes to be used. In addition, as orbits are typically designed in terms of the classical elements, the response of a system to various perturbations often becomes clearer when presented in its alternate form. The disadvantage of this approach is the loss of the simplicity in the implementation.

While it is not intended to include here a full development of mean element propagation theory (the interested reader may find more complete analysis in the references [10, 25]), it is important to understand the basis of the theory. We begin by noting that Equation 6.1 may be divided into two separate equations.

$$\frac{d\boldsymbol{r}}{dt} = \boldsymbol{v} \tag{6.2}$$

$$\frac{d\boldsymbol{v}}{dt} = -\frac{\mu}{r^3}\boldsymbol{r} + \boldsymbol{a}_d \tag{6.3}$$

The perturbative forces are typically much smaller than the inverse square force of the central body. It is therefore reasonable to model the perturbations as slowly modifying the basic two-body trajectory. If, following Battin [3], we take the six orbital elements $\boldsymbol{\alpha}$ as the constants of integration, the unperturbed trajectory can be written as

$$\boldsymbol{r} = \boldsymbol{r}\left(t, \boldsymbol{\alpha}\right) \tag{6.4}$$

$$\boldsymbol{v} = \boldsymbol{v}\left(t, \boldsymbol{\alpha}\right) \tag{6.5}$$

The derivative of the position vector along the disturbed trajectory is, by the chain rule,

$$\frac{d\boldsymbol{r}}{dt} = \frac{\partial \boldsymbol{r}}{\partial t} + \frac{\partial \boldsymbol{r}}{\partial \boldsymbol{\alpha}}\frac{d\boldsymbol{\alpha}}{dt} \tag{6.6}$$

If we require the velocity vector of the undisturbed motion, $\frac{\partial r}{\partial t}$ to be the same as the velocity of the disturbed motion, it is clear from Equation 6.6 that

$$\frac{\partial \boldsymbol{r}}{\partial \boldsymbol{\alpha}}\frac{d\boldsymbol{\alpha}}{dt} = \mathbf{o} \tag{6.7}$$

Similarly, we may conclude that

$$\frac{\partial \boldsymbol{v}}{\partial \boldsymbol{\alpha}} \frac{d\boldsymbol{\alpha}}{dt} = \boldsymbol{a}_d \tag{6.8}$$

These two equations may be combined into a simpler form. If we pre-multiply Equation 6.7 by $[\partial \boldsymbol{v}/\partial \boldsymbol{\alpha}]^T$ and Equation 6.8 by $[\partial \boldsymbol{r}/\partial \boldsymbol{\alpha}]^T$ and take the difference, we get that

$$\left(\left[\frac{\partial \boldsymbol{r}}{\partial \boldsymbol{\alpha}}\right]^T \frac{\partial \boldsymbol{v}}{\partial \boldsymbol{\alpha}} - \left[\frac{\partial \boldsymbol{v}}{\partial \boldsymbol{\alpha}}\right]^T \frac{\partial \boldsymbol{r}}{\partial \boldsymbol{\alpha}} \right) \frac{d\boldsymbol{\alpha}}{dt} = \left[\frac{\partial \boldsymbol{r}}{\partial \boldsymbol{\alpha}}\right]^T \boldsymbol{a}_d \tag{6.9}$$

where the multiplier on the left-hand side is called the Lagrange matrix. The inverse is of the Lagrange matrix is the much more commonly known Poisson matrix, whose elements are found from the Poisson bracket.

$$P_{ij} = (\alpha_i, \alpha_j) = \frac{\partial \boldsymbol{\alpha}}{\partial \boldsymbol{r}} \left[\frac{\partial \boldsymbol{\alpha}}{\partial \boldsymbol{v}}\right]^T - \frac{\partial \boldsymbol{\alpha}}{\partial \boldsymbol{v}} \left[\frac{\partial \boldsymbol{\alpha}}{\partial \boldsymbol{r}}\right]^T \tag{6.10}$$

Using the Poisson matrix, we may rewrite Equation 6.9 as

$$\frac{d\boldsymbol{\alpha}}{dt} = \boldsymbol{P}^T \left[\frac{\partial \boldsymbol{r}}{\partial \boldsymbol{\alpha}}\right]^T \boldsymbol{a}_d \tag{6.11}$$

Substituting in the transpose of Equation 6.10, we find that

$$\frac{d\boldsymbol{\alpha}}{dt} = \left(\frac{\partial \boldsymbol{\alpha}}{\partial \boldsymbol{v}} \left[\frac{\partial \boldsymbol{r}}{\partial \boldsymbol{r}}\right]^T - \frac{\partial \boldsymbol{\alpha}}{\partial \boldsymbol{r}} \left[\frac{\partial \boldsymbol{r}}{\partial \boldsymbol{v}}\right]^T \right) \boldsymbol{a}_d \tag{6.12}$$

which clearly reduces to

$$\frac{d\boldsymbol{\alpha}}{dt} = \frac{\partial \boldsymbol{\alpha}}{\partial \boldsymbol{v}} \boldsymbol{a}_d \tag{6.13}$$

Equation 6.13 provides a basis for determining the equations which describe the evolution of the orbital elements of the system. All that is needed is to calculate the partial derivatives of the orbital elements with respect to the velocity vector, a

straight-forward if tedious process. The resulting variational equations are known as Gauss' equations and are summarized below:

$$\begin{aligned}
\frac{da}{dt} &= \frac{2a^2}{h}\left(e\sin f a_{dr} + \frac{p}{r}a_{d\theta}\right) \\
\frac{de}{dt} &= \frac{1}{h}\left\{p\sin f a_{dr} + \left[(p+r)\cos f + re\right]a_{d\theta}\right\} \\
\frac{di}{dt} &= \frac{r\cos\theta}{h}a_{dh} \\
\frac{d\Omega}{dt} &= \frac{r\cos\theta}{h\sin i}a_{dh} \\
\frac{d\omega}{dt} &= \frac{1}{he}\left[-p\cos f a_{dr} + (p+r)\sin f a_{d\theta}\right] - \frac{r\sin\theta\cos i}{h\sin i}a_{dh} \\
\frac{dM}{dt} &= n + \frac{b}{ahe}\left[(p\cos f - 2re)\,a_{dr} - (p+r)\sin f a_{d\theta}\right]
\end{aligned} \tag{6.14}$$

These equations may be averaged over some time interval. This removes the high-frequency variations in the elements, which are often uninteresting in comparison to long-term variations. Typically, the first five mean elements vary slowly (i.e. on a time scale significantly larger than the orbital period), while the mean anomaly varies quickly. This can be seen in the presence of the mean motion n in the variational equation for mean anomaly. These equations form the basis for mean element propagators, although, in practice, these equations are typically transformed further to eliminate the singularities of the classical orbital elements for zero eccentricity or inclination.

Semi-Analytic Theory

For many perturbations, it is possible to solve these equations analytically. The solutions to various perturbations are then superimposed to produce the actual trajectory for the satellite. Propagators which follow this route are said to use general perturbations. The advantage of this approach is that, since all results are analytical, the entire trajectory is determined at once and no numerical integration is required. This means that the calculation time required to produce a trajectory is independent of the duration of that trajectory. This approach can produce high accuracy if enough

perturbations at high enough orders are included but at the expense of computation time. In practice, for reasonable computation times, the accuracy suffers.

Semi-analytic theory is an attempt to find a middle ground between special and general perturbations, including the physical insight of the latter with the speed and accuracy of the former. Gauss' equations are averaged over some time interval in order to remove high frequency components. These high frequency effects are often uninteresting, especially if it is the long-term behavior that is desired. As the iteration time step is limited by the period of the shortest frequency effect to be studied, this approach allows much larger steps sizes than those required in special perturbative methods. The high frequency terms, or short-periodics, may be recovered, if desired, as Fourier expansions in the fast variable.

Capabilities

The standalone DSST propagator is a powerful tool for orbital analysis. The perturbations to the mean elements which are available in DSST for earth orbits are [10]:

- Nonspherical central body gravitational potential, including zonal and tesseral harmonics to 21 by 21.
- Third body point mass effects for the sun and moon.
- Atmospheric drag, assuming a spherical cross-section, using either Jacchia-Roberts or Harris-Priester atmosphere models.
- Solar radiation pressure with cylindrical shadowing, also assuming a spherical cross-section.
- J_2^2 second order effects, expanded to first order in eccentricity.

Short periodic variations resulting from several of these perturbations are also available, but for station-keeping purposes, only the mean element variations were of interest.

The propagator calculates mean and osculating equinoctial elements, mean element rates, and position and velocity vectors at each time step. These parameters are

available either in the true of reference or mean of 1950 reference frames. The true of date reference frame is, of course, preferable, and, while this capability is being added to DSST, it was not available for this analysis.

6.1.2 Primer Vector Theory

Primer vector theory was developed by Lawden [20] as a method for determining if a trajectory defined by impulsive burns is optimal. It assumes that all burns are impulsive and that linearization of the equations of motion about the initial trajectory is reasonable. Consider another form of the equations of motion

$$\begin{aligned} \frac{d\boldsymbol{r}}{dt} &= \boldsymbol{v} \\ \frac{d\boldsymbol{v}}{dt} &= \boldsymbol{g} \end{aligned} \tag{6.15}$$

If we now examine small variations about this coasting trajectory, we find that the equations of motion for the perturbations is given by

$$\begin{bmatrix} \delta\dot{\boldsymbol{r}} \\ \delta\dot{\boldsymbol{v}} \end{bmatrix} = \boldsymbol{F} \begin{bmatrix} \delta\boldsymbol{r} \\ \delta\boldsymbol{v} \end{bmatrix} \tag{6.16}$$

where the matrix $\boldsymbol{F}$ is defined by

$$\boldsymbol{F} = \begin{bmatrix} \mathbf{o} & \boldsymbol{I} \\ \frac{\partial \boldsymbol{g}}{\partial \boldsymbol{r}} & \mathbf{o} \end{bmatrix} \tag{6.17}$$

The vectors $[\boldsymbol{\phi}\ \boldsymbol{\lambda}]^T$ are defined as the adjoint to the perturbation state $[\delta\boldsymbol{r}\ \delta\boldsymbol{v}]^T$. The evolution of λ is described by

$$\frac{d^2\boldsymbol{\lambda}}{dt^2} = \left(\frac{\partial \boldsymbol{g}}{\partial \boldsymbol{r}}\right)^T \boldsymbol{\lambda} = \frac{\partial \boldsymbol{g}}{\partial \boldsymbol{r}} \boldsymbol{\lambda} \tag{6.18}$$

where we have used the fact that the gravity gradient matrix must be symmetric. The adjoint to the velocity perturbation $\boldsymbol{\lambda}$ is known as the primer vector, and it clearly must satisfy the same differential equations as $\boldsymbol{\delta r}$.

The primer vector also represents a Lagrange multiplier in the Hamiltonian representation of the impulsive rendezvous problem. Lawden analyzed this problem in terms of the primer vector and developed four conditions which are necessary for a trajectory to be optimal. The Lawden's conditions on the primer vector are:

- The primer vector and its derivative must be continuous.
- At any time an impulse occurs, the primer vector must be aligned with the impulse and have unit magnitude.
- The magnitude of the primer vector must always be less than one on a coasting arc (any time not at a burn).
- The primer vector must be at a maximum at each burn.

Lawden's conditions provide a test of the optimality of a solution to the impulsive rendezvous problem and also indicate approximately where an additional burn could be applied to improve the solution. Shah [28] derives an explicit equation for the time of impulse and burn velocity which most effectively reduce the cost of the maneuver, but concludes that it is more practical to explore numerical methods. A complete optimization would require the exploration of a four-dimensional parameter space (time and the three velocity components), but, as we have already assumed that the impulsive maneuvers cause only small perturbations to the coasting trajectory, Shah recognizes that these four parameters may be reduced to one, the time at which the interior burn occurs.

He then formulates a numerical approach which provides near-optimal solutions. The time interval for which an interior burn is desired is discretized. At each time, the interior burn which reduces the total cost of the maneuver most is determined. The magnitude and direction of the perturbation at the time of the interior burn can be derived from primer vector theory. When this is known, the determining the

new burn sequence is equivalent to solving several Lambert boundary value problems. Gauss' solution to the two body Lambert problem described in Battin [3] is used as an initial guess for the proper trajectories and is refined in the presence of disturbing accelerations through comparison with DSST predictions. This provides the best burn sequence for each grid point within the time interval. The burn sequence which requires the least Δv is the optimal solution. Interior burns are added until Lawden's conditions are met everywhere. This yields a good approximation to the optimal trajectory.

6.1.3 Interface

The ASKS reads in constellation data from an input deck. The deck contains the initial Keplerian element sets of both the reference and actual orbits for each satellite in the constellation. It also contains orbital element limits for each plane of satellites. All of the perturbations to the mean elements which DSST provides can be controlled independently for both reference and actual trajectory for each individual satellite. Finally, several targeting strategies for station-keeping are available, although only the approach described previously, which is method 5 with formation flying on, is used in this analysis. A sample input deck is shown in Appendix B.

The main process outputs the orbital elements and the element rates of both the reference and actual trajectories for all of the satellites, as well as the errors and error rates at fixed intervals into several text files. Coverage data may also be outputted. In addition, each satellite process outputs information particular to itself, including the number of each type of burn required, the average burn magnitude, and the total Δv used by that satellite.

6.2 Simulations

Simulations were performed for the Ellipso constellation. Ideally, simulations would be attempted for all of the constellations analyzed previously, but, unfortunately, the

Simulation	Node Limit (deg)	Mean Anomaly Limit (deg)
1	0.2	0.5
2	0.2	9.5
3	0.5	12.0

Table 6.1: Station-Keeping Requirements for the Ellipso Simulations

parallel nature of ASKS as well as the enormous CPU usage each process requires, it was impractical to study large constellations. The simulations were run on an eight processor SGI machine, and, on this particular computer, Ellipso was the largest constellation which could be handled in reasonable time frames. Therefore, the Ellipso constellation was used in order to validate the algorithm for station-keeping requirements.

Two simulations were run for Ellipso, the first using the orbital element limits currently chosen by MCHI, and the second with the ones derived previously. The ASKS results demonstrate that much less stringent requirements than those currently proposed for Ellipso will maintain equally good coverage. Simulations of the station-keeping of the Ellipso constellation were run for the three sets of requirements developed in the previous chapter: the baseline MCHI set, the set derived for maintaining sun-synchronicity, and the set derived while ignoring the sun-synchronous requirement. The node and mean anomaly limits for these simulations are shown in Table 6.1. For each constellation, ASKS was run for a one year period in order to determine the coverage performance for the given station-keeping requirements. Coverage calculations were made using a 25 degree elevation angle for the northern hemisphere only. Since the Borealis satellites are always close to perigee when in the southern hemisphere, the Concordia plane bears the responsibility of covering the southern hemisphere; as Concordia does not get out of phase over the lifetime of the constellation, coverage of the southern hemisphere remains at nominal without control. In addition, each Borealis plane was simulated independently over a two year period in order to get a more accurate estimate of the Δv usage.

The complete element histories and coverage performance for these simulations

Satellite Number	Case 1	Case 2	Case 3
1	13.142	15.409	10.841
2	15.537	17.810	11.145
3	14.372	14.874	13.680
4	15.729	19.116	13.508
5	13.596	15.248	11.913
6	11.058	10.732	10.340
7	12.007	48.257	12.061
8	6.178	8.783	9.128
9	29.924	20.691	16.958
10	25.978	16.885	11.821
Average	16.168	15.505	12.148

Table 6.2: Average yearly delta v (m/s) requirement for simulations

can be found in the appendices; only a cross-section of the results will be included here. The average yearly Δv usage which resulted from these simulations is shown in Table 6.2. In this table, the anomalously large Δv requirement for Satellite 7 in the second simulation results from an error in ASKS in which the targeting mechanism forces the variations from nominal rather than damping them. The cause for this will be discussed in a later section.

With this in mind, the average Δv usage for the satellites was calculated omitting Satellite 7. The results agree qualitatively with the expectations from the analysis in Chapter 5. Simulation 1 had the most stringent requirements and, consequently, the highest Δv usage. Simulation 2 was only slightly better, as increasing the allowed mean anomaly variation only slightly decreases the Δv necessary. Simulation 3 required the least maintenance, which is not surprising, as no node corrections were required over the time period of the simulation. All three configurations maintained 100 percent coverage of the northern hemisphere at 25 degree elevation angle (see Figures C-1, D-1, and E-1).

What is more interesting is to examine the two–way coverage in more detail. The two-way coverage contours produced by the coverage analysis are shown in Figure 6-1. From these contours, we may determine the expected two-way coverage performance for each simulation. For Simulation 2, for example, the predicted minimum two–way

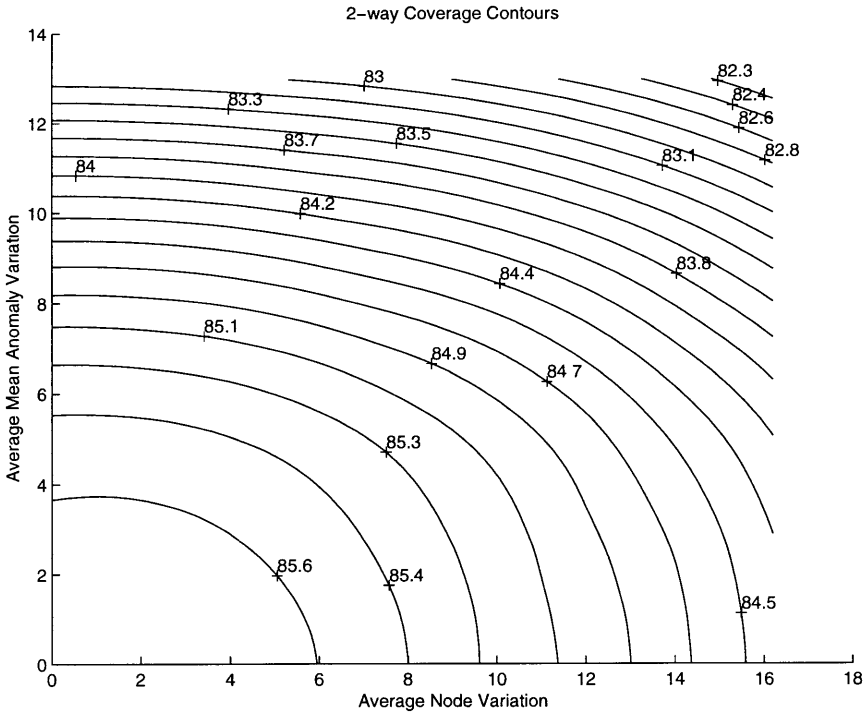

Figure 6-1: Two-way coverage contours for the Ellipso constellation

coverage is 84.5 percent. The actual two–way coverage for Simulation 2 is shown in Figure 6-2. The observed minimum value of the two–way coverage is 84.7 percent. For the other two cases, the correspondence of the predictions and simulations is not as good, but they still parallel each other closely.

The two primary sources of error of the predicted value of two-way coverage from what is actually observed in the simulations are variations in eccentricity and argument of perigee. The coverage analysis in Chapter 5 may be extended, however, to include these effects. The argument of perigee varies in phase with the longitude of the ascending node, as similar equations govern their evolution in the presence of J_2.

The eccentricity variation is more complex, both in cause and effect. Virtually every perturbation included in the simulation changes the evolution of the eccentricity in some fashion, and the exact characteristics change over time. Variations in eccentricity cause the node rate and perigee rate to change. As eccentricity is being controlled when semi-major axis changes are made, the frequency of mean anomaly

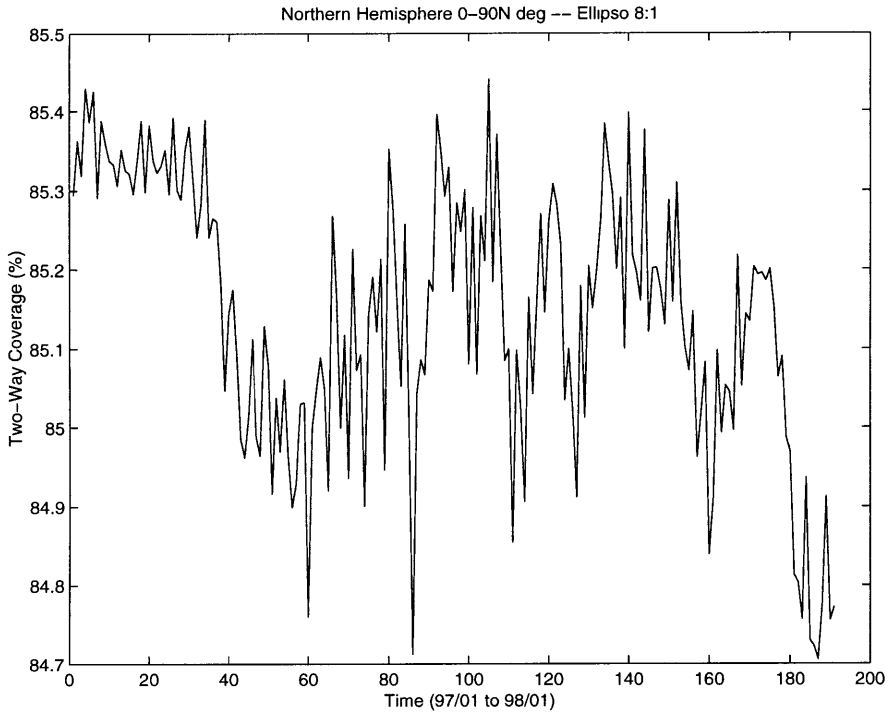

Figure 6-2: One year history of the two–way coverage in Simulation 2

corrections will have an impact on the frequency and magnitude of ascending node corrections.

There are two approaches to extending the coverage analysis to include the effects of eccentricity variations. A worst–case eccentricity rate may be determined from the uncontrolled run which proceeds the coverage analysis. This rate would be used in the coverage analysis. The analysis would require two changes. The node (and perigee) rate would vary as the eccentricity evolved from nominal. Also, the equation for the Δv required to correct the mean anomaly variations would change slightly to account for the initial and final orbits having different eccentricities. Both of these alterations are easily accomplished.

The other approach to including eccentricity effects would require more restructuring of the algorithm. Instead of determining worst–case element rates, the coverage program would utilize the orbital propagator to determine in exactly what fashion all of the elements vary. The coverage at each step would be calculated, and coverage

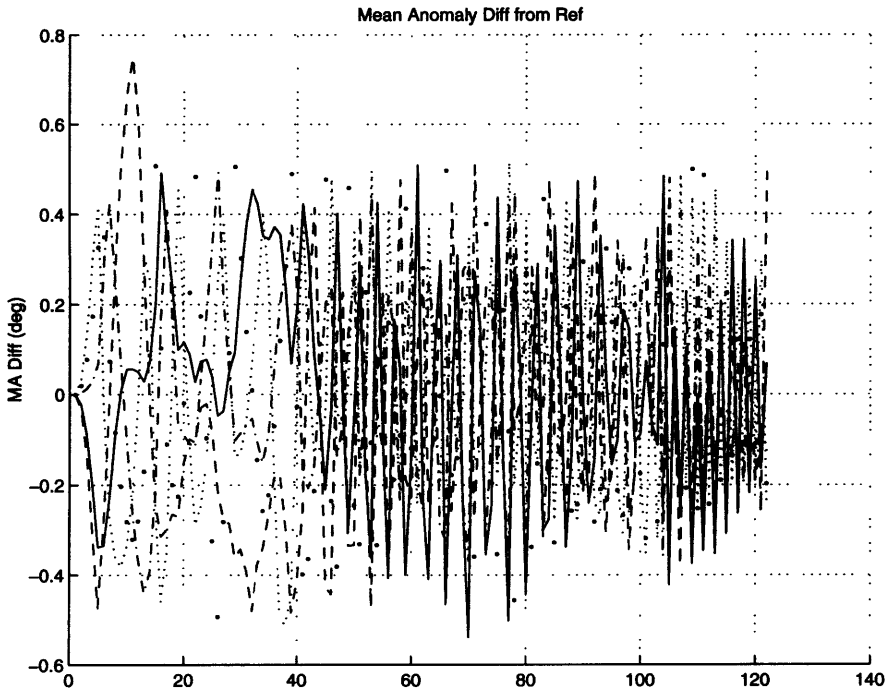

Figure 6-3: Two year mean anomaly error history for a Borealis plane

contours would be plotted against the largest mean anomaly and node errors which actually occurred at that time step. This would give more accurate results, but the analysis would be much more time intensive. Both methods, however, allow for the extension of the theory to include eccentricty and argument of perigee variations.

Another important question to answer is how well the linear targeting strategy developed in Chapter 5 worked in the simulations. Figure 6-3 shows the mean anomaly history of the node–at–noon plane in Simulation 1. The mean anomaly remains well bounded within the specified range. The occasional excursion from the defined control requirement is the result of the program choosing not to make the correction until the semi-major axis rate is positive. All of the element rates are composed of three terms: a secular (linear) drift over time, oscillations about the secular rate, and short-periodics, which were not included in the simulation. The program waits until the semi-major axis rate is no longer working to correct the deviation. In some cases, the satellite will drift back to nominal, and, for others, it decreases the size of the

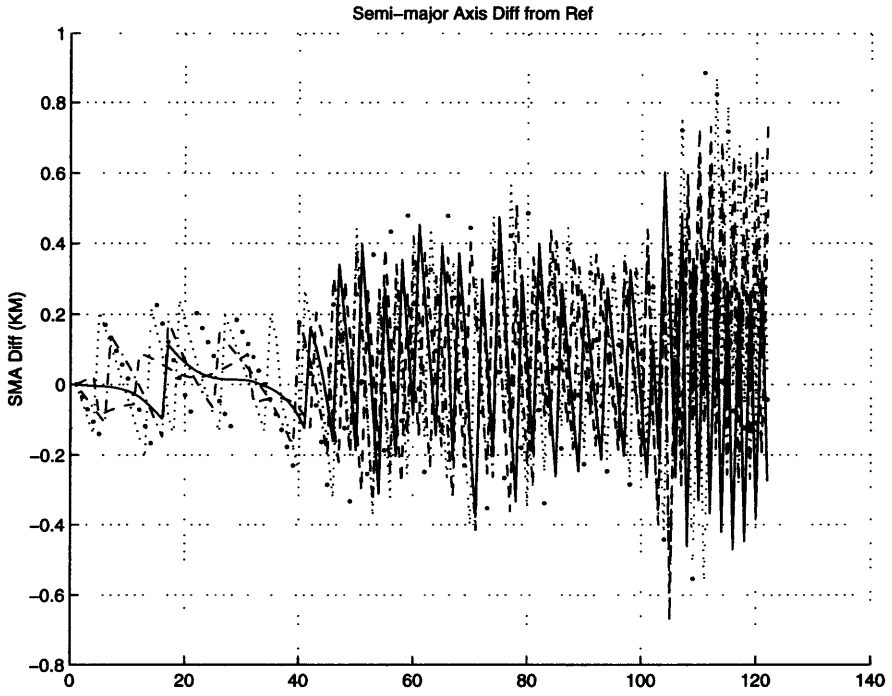

Figure 6-4: Two year semi-major axis error history for a Borealis plane

burn required. If such rare excursions are unacceptable, it is a simple correction to force ASKS to respond more rapidly. It should be noted, however, that this violation clearly was acceptable, as the coverage of the constellation did not suffer for it.

Another feature of Figure 6-3 is that the linearized targeting scheme, while adequate, was clearly not a perfect model. The semi-major axis corrections cause the satellite to drift back past nominal, but do not consistently force it to reach an extremal mean anomaly at the opposite coverage limit. This results from variations in the semi-major axis drift rate which, in this case, is dominated by the gradual increase of atmospheric drag. The density of the upper atmosphere varies with the solar cycle, and, at the epoch chosen for the simulations, is increasing for the first two years. This, of course, causes the semi-major axis to decay more quickly.

This effect can also be seen in Figure 6-4, which shows the semi-major axis deviation for this same case. Increasing the drag also increases the frequency of corrections required to maintain the satellite within the same mean anomaly limits, and this can

be seen in the compression of the peaks in Figure 6-4. At the end of the simulation, mean anomaly corrections are required approximately weekly. Another result of the changing element rate is that the size of the semi-major axis correction necessary varies with time. These features are all present in the inclination and node deviation plots but, due to the much longer time scale of the motion, are not as obvious.

Chapter 7

Future Work

The analysis described in previous chapters applies systems engineering methodology to the problem of determining station-keeping requirements for satellites in a specific type of constellation, namely one for which coverage is the only criterion. This analysis was undertaken through the use of the analytic coverage theory developed in Chapter 3 and the ASKS described in the preceding chapter. This work, while interesting in its own right, opens up a number of interesting theoretical avenues for constellation analysis. This chapter discusses what the next steps in this area should be and what further elements are necessary in order to take them.

7.1 Coverage Theory

The analytical coverage theory developed previously provides for fast, accurate calculation of the n-way percent coverage of a sphere by a constellation of satellites as a function of time. In addition, it may be used to determine the coverage of any subset of a spherical surface which may be defined by some combination of circles projected onto that surface. In this analysis, that capability was utilized to determine coverage within a given latitude range, as well as to distinguish between daytime and nighttime coverage. But the generalization of this concept leads to some other intriguing

applications.

7.1.1 Applications

One example of a case for which the use of additional restrictor circles would be appropriate is for the analysis of synthetic aperture radar (SAR) satellite constellations. Synthetic aperture radar is a method of improving the resolution and performance of a radar system without increasing the size of the antenna, which is typically the limiting factor in these systems. Essentially, a moving radar antenna can be made, with the aid of proper analysis techniques, to simulate a larger stationary antenna. For this technique to work properly, however, the object to be imaged must be a certain distance away from the nadir track.

For a satellite, this implies that the footprint of a given satellite is the projection of an annulus onto a sphere rather than a circle, as we assumed in the analysis of the telecommunications systems. This situation can be handle easily within the coverage theory already developed. Instead of a single array, consisting of subsatellite points and central angles, there would now be two arrays, one for the outer circle and one for the inner circle. The second array, the inner circle data, would be treated as restrictors, in exactly the same fashion as latitude restrictors were used before.

Another example of a problem for which this approach would be useful is the issue of satellite system geometric interference. With the number of proposed satellite telecommunications constellations, there are going to be more satellites in orbit at various altitudes than ever before. When two satellites align with a ground station, the interference of the two signals may prevent proper communication between the satellite and the ground segment. This could, if not considered and handled properly, interrupt service for a large region, presumably full of (unhappy) customers. Some preliminary work concerning interference between LEO constellations and geostationary satellites has already been done by Lang [18].

The analysis would proceed similarly to that of the SAR systems. In this case, however, rather than excluding the region of overlap between primary and restrictor

arrays, only that overlap would be of interest. In addition, as interference would occur only for close to perfect alignments, the effective elevation angles would be very high (close to 90 degrees). For this problem, the number of overlaps would be very small, the highest level of overlap would never be much larger than two satellites. The combination of these two factors indicate that the analytical method would greatly outperform numerical analysis techniques for this problem.

One final example of a problem for which the analytical technique is appropriate is that of above-the-horizon (ATH) coverage. This is a military term and refers to the ability to detect incoming objects at various altitudes. The ATH coverage could represent the probability of missile detection at various altitudes.

Such detection often depends on instrumentation sensitive to infrared radiation, but sensitive infrared receivers often cannot point directly at the earth, for fear of saturating or burning out the sensors. They therefore are typically pointed almost tangentially to the earth's surface. The coverage problem is therefore similar to the one for SAR systems, the overlap of multiple annuli, although, in this case, the annuli are much thinner. In addition, here the coverage depends not only on the altitude of the satellites, but the minimum altitude available for detection, which depends on how close to the horizon the sensors may be pointed.

Also, the analytic approach may be applied to systems which look outward rather than toward some nearby central body. An example of this type of system is an orbital interferometer, in which several satellites arranged in some fixed pattern are used to simulate an antenna much larger than any that can actually be built. This approach could, for example, allow imaging of planets around distant stars. In this case, it is interesting to examine the overlap of the fields-of-view for all of the satellites, as it is only in concert that they can provide worthwhile observations. For this problem, the important parameter for each satellite is the beam width of the antenna rather than some fixed elevation angle, but this does not require any alteration of the analytic coverage theory.

It is interesting and exciting that one single methodology may handle such a wide range of applications efficiently and accurately. As more satellite constellations are

designed and deployed, the analytical coverage method will certainly provide a useful analysis tool.

7.1.2 Extensions

As was discussed in Chapter 3, two assumptions were made in the course of the coverage analysis: that the coverage surface is spherical and that the satellites are nadir-pointing. The next step in extending this theory is to attempt to relax these requirements. The easier of the two to relax is the requirement of a spherical surface. The surface of the earth is well described as an oblate spheroid, and the deviation of the appropriate oblate spheroid from a perfect sphere is, as has been noted previously, quite small. This suggests two approaches to handling the discrepancy.

The first approach is optimistic. It may well be that the ellipticity of the earth is sufficiently small that it has no significant impact on coverage calculations. If this were the case, of course, the first assumption is valid. The error produced by ellipticity effects may be calculated numerically and compared to the result of the analytical method. We may predict that such effects will be largest at the poles and the equator, where the actual altitude of the satellite is higher (or lower) than expected. This may be important in the formation and dissolution of coverage gaps, but should not change the actual coverage percentage significantly.

The second avenue of analysis is to attempt to extend the analytic theory to include ellipticity effects selectively. The spherical earth assumption has two important results. The first is that the satellite footprints are circular, and the second that, as all orientations are equivalent, the reference frame may be rotated freely. The second is clearly a far more important restriction than the first. For analysis purposes, it is appropriate to include ellipticity in the derivation of the area equation, perhaps exactly, perhaps as a power series expansion about the spherical case, but still to allow the reference frame to be rotated freely. I believe this approach may yield useful results if ellipticity effects are found to be significant.

The second requirement, that of nadir-pointing satellites, is a much more dif-

ficult one to remove, but the rewards are much greater. Satellites are often not nadir-pointing, but instead are skewed off nadir throughout their orbit. Even in telecommunications satellites, this may be the case. The Odyssey system satellites are designed to alter their attitude to focus coverage area on land masses. Also, if off-nadir pointing could be incorporated, it would allow analysis of beam patterns, which are often intersections of cones with common vertex (an antenna).

Analytical analysis of this problem is much more difficult. Instead of simple circles, the satellite footprints are now a complex egg-shaped regions. Therefore, rather than describing the region simply by a central angle, multiple parameters, possibly an average central angle, a measure of something like an "eccentricity," and an angle indicating the direction of the long axis, would be required. An added complication lies in the fact that the horizon of the earth may now be in the viewing region, further altering the satellite footprint. Nevertheless, it may be that an area equation may be determined, although the best that may reasonably be hoped for is to reduce the problem to a dimensionless quadrature which may be evaluated numerically or stored in a look-up table. Whether the result of such an extension maintain the speed advantage over numerical techniques can not be predicted at this time.

7.2 ASKS

ASKS has proven to be a useful tool in analyzing station-keeping of satellite constellations. There are a number of extensions which might be made to greatly improve its functionality. Several of these relate to the orbital propagator which ASKS is built around, such as the addition of a proper true-of-date reference frame, but the improvement of DSST is already being addressed at Draper Laboratory [16]. These changes will cause only small changes to the results of ASKS runs.

More important issues must be addressed in the methodology ASKS uses to maintain the satellite orbits. One change which would greatly improve the applicability of ASKS results would be to allow for multiple-period orbital corrections. Currently, the

maximum time over which a burn sequence may occur is the period of the orbit. This results from the use of Lambert solutions to the two-body boundary value problem as the initial guess in the numerical scheme for determining the proper burn magnitudes and directions; solutions of the Lambert problem result in multiple solutions for multi-period transfers.

This problem could be solved by instead using typical maneuver methodologies as the initial guess for the numerical scheme. Typically, for example, semi-major axis alterations are done by a combination of perigee and apogee burns, and inclination changes are accomplished by impulsive burns at the ascending or descending node of the orbit. Certain stock maneuvers could be incorporated to provide an initial estimate of the burn vectors required for a given type of maneuver, and these could easily incorporate multiple-orbit transfers. As the maneuvers would more closely approximate operational approaches, the Δv calculated by the program could be compared to actual cases, resulting in greater confidence in the results.

Another context in which ASKS might be improved is in targeting long-term trajectories to maximize time between maneuvers. In Chapter 5, a linearized model of the orbital element drift was developed, but, as was seen in the preceding chapter, this model is not always appropriate. Instead of the linearized equations, DSST could be used to predict the actual time between violations, and a simple numerical scheme could easily be developed to maximize that interval. This would greatly improve the station-keeping performance of ASKS, in terms of both deviation from the nominal trajectory and Δv expenditure, as well as reducing the burden on the user, by eliminating the need to design an appropriate control strategy for the particular constellation. This would provide a valuable extension to ASKS functionality.

7.3 Requirement Determination

In previous chapters, a systematic approach to determining station-keeping requirements for one class of missions has been developed and validated. As constellations

become more common, it will become valuable to determine these requirements with greater accuracy and for a larger variety of mission types. This will require improvements to the approach developed here. Some possible extensions were discussed in the previous chapter. Several more are considered here.

7.3.1 Multiple Iterations

The methodology for determining station-keeping requirements, as applied thus far, provides a "good" set of orbital element limitations. The results of this analysis cannot yet be said to be optimal. Optimality can, in principal, be obtained through successive iterations of the process described previously. After determining a set of requirements, ASKS may be run to determine performance. The orbital element histories may then be used to determine a better model for the actual pattern in which the satellite and planar phasing decays. This pattern would then be used to run through the requirement analysis again, and the process would be repeated until the requirements did not change significantly. Several iterations would yield a set of requirements close to optimal. As the financial support for space systems decreases, any reduction in satellite mass becomes important, and the fuel mass reduction possible with proper choice of station-keeping requirements becomes increasingly valuable.

7.3.2 Additional Metrics

The most exciting aspect of this work lies in that it demonstrates that system engineering techniques may be effectively applied to satellite constellations. System engineering, in the early stages of design, includes developing a measure of performance, a metric, and examining a trade space to provide the best possible performance. This approach was applied to a very specific class of satellite constellations.

Now that the method has been validated, however, it seems likely that it may be extended to include other mission types by developing an appropriate metric. For military reconnaissance, perhaps the appropriate metric is minimum revisit time

between passes. For other systems, perhaps maintaining cross-links or keeping a certain set of ground-tracks is the important issue. This approach may even prove appropriate for other multiple-spacecraft configurations. For a cluster of satellites, one might imagine a correlation coefficient or even something as simple as the lifetime of the cluster as an appropriate choice of metric. In any case, if metrics can be developed and evaluated, it is likely that appropriate parameter spaces for analysis will present themselves, and near-optimal requirements may be developed.

7.4 Conclusion

In this work, a systematic approach for determining station-keeping requirements for earth-viewing satellite constellations was developed. For this class of satellites, earth coverage, within a latitude range and above a certain elevation angle, is an appropriate measure of the performance of the constellation. In order to aid in the analysis of these constellations, a flexible analytical approach to calculating satellite coverage of a given latitude and longitude range was developed, and this approach was shown to have substantial accuracy and speed advantages over traditional numerical methods, with applications which include many exciting problems beyond those for which it was applied to in this work. The algorithm for determining station-keeping requirements was shown to determine the best choice of element limits for maintaining a given level of coverage. This combination of fast coverage calculations and systematic analysis of their performance opens up new possibilities in constellation design and optimization.

Appendix A

Miscellaneous Astrodynamics

This section contains several simple astrodynamic derivations. The proof that the average coverage area a satellite sees over an orbit depends only on the semi-major axis of the orbit is developed. Also, the Δv requirements for the two types of orbital corrections discussed in Chapter 5 is determined.

A.1 Coverage Area for Elliptic Orbits

We begin with Equation 3.5, which gives the total area of a satellite footprint as a function of its central angle.

$$A_{footprint} = 2\pi \left(1 - \cos \lambda\right) \tag{A.1}$$

The average of a function over a period is given by

$$\langle f \rangle = \frac{2}{\tau} \int_0^{\tau/2} f\left(t\right)\ dt \tag{A.2}$$

The average of the first term is clearly trivial; we need to determine the average of $\cos \lambda$ over an orbit.

We also recall that the total area of a satellite footprint is given by Equation 3.2, which defines the central angle λ of a satellite footprint as a function of the elevation angle ϵ, satellite radius r, and the radius of the earrth R.

$$\lambda = \frac{\pi}{2} - \epsilon - \arcsin\left(\frac{R}{R+h}\cos\epsilon\right) \tag{A.3}$$

The time average of $\cos\lambda$ is therefore given by

$$\langle\cos\lambda\rangle = \frac{2}{\tau}\int_0^{\tau/2} \sin\epsilon\sqrt{1 - \frac{R^2}{r^2}\cos^2\epsilon} + \frac{R}{r}\cos^2\epsilon \; dt \tag{A.4}$$

where we have used some basic trigonometric identities to simplify the expression.

This expression is still quite complex. The general solution can not be obtained in a closed form, but we may make some more headway if we require the elevation angle to be zero. In this case, Equation A.4 becomes

$$\langle\cos\lambda\rangle = \frac{2}{\tau}\int_0^{\tau/2} \frac{R}{r}\; dt \tag{A.5}$$

Kepler's second law states that a satellite traverses equal angle in equal time, i.e. that

$$r^2\frac{df}{dt} = h \tag{A.6}$$

where h is the angular momentum of the orbit, which is, of course, conserved over the orbit. We may use Kepler's law to rewrite Equation A.5 as

$$\langle\cos\lambda\rangle = \frac{2}{\tau}\frac{p}{h}R\int_0^{\tau/2} \frac{df}{1 + e\cos f} \tag{A.7}$$

where we have also used the equation of orbit for r. This expression can be integrated

analytically to show that

$$\langle \cos \lambda \rangle = \frac{2\pi}{\tau} \frac{p}{h\sqrt{1-e^2}} R = \frac{R}{a} \tag{A.8}$$

The average area visible to a satellite is therefore

$$\langle A_{footprint} \rangle = 2\pi \left(1 - \frac{R}{a}\right) \tag{A.9}$$

which, indeed, depends only on the semi-major axis of the orbit.

A.2 Elliptic Hohmann Transfer

In this section, we consider a Hohmann transfer between two coaxial elliptical orbits. We begin with the equations for position and velocity at the apses of an eccentric orbit:

$$\begin{aligned} r_p &= a\,(1-e) \quad r_a = a\,(1+e) \\ v_p &= \tfrac{\mu}{h}\,(1+e) \quad v_a = \tfrac{\mu}{h}\,(1-e) \end{aligned} \tag{A.10}$$

The velocity equations may be rewritten in terms of the perigee and apogee heights using the definition of the parameter p.

$$\begin{aligned} v_p &= \sqrt{\frac{\mu}{r_p}}\sqrt{1+e} \\ v_a &= \sqrt{\frac{\mu}{r_a}}\sqrt{1-e} \end{aligned} \tag{A.11}$$

This form of the velocities at the apses is more clear intuitively. The first equation, for example, states that a satellite at apogee of an elliptical orbit is moving more slowly than one in a circular orbit at the same height. Similarly, a satellite at perigee of an elliptical orbit is moving more quickly than one in a circular orbit at that height.

Now we consider a two-burn transfer from an orbit with semi-major axis a_0 to a

higher one with a semi-major axis of a_1. The first burn will be at perigee of the initial orbit, and the second will be at the apogee of the final orbit. This plan is optimal for raising the orbit. The transfer orbit clearly has semi-major axis of

$$a_t = \frac{1}{2}(r_{a1} + r_{p0}) \tag{A.12}$$

Since the position of the satellite must be the same before and after the first burn, the perigee heights of the transfer orbit and the initial orbit must be the same. This implies that the eccentricity of the transfer orbit is given by

$$e_t = \frac{r_{a1} - r_{p0}}{r_{a1} + r_{p0}} \tag{A.13}$$

Using Equation A.11 for both the initial and transfer orbit, it is easy to show that the velocity increment required to place the satellite into the transfer orbit is

$$\Delta v_1 = \sqrt{\frac{\mu}{r_p}}\left(\sqrt{1+e_t} - \sqrt{1+e}\right) \tag{A.14}$$

since the two orbits have the perigee. Similarly, the impulsive burn neceesary to place the satellite in the final orbit is

$$\Delta v_2 = \sqrt{\frac{\mu}{r_a}}\left(\sqrt{1-e} - \sqrt{1-e_t}\right) \tag{A.15}$$

The total burn is clearly the sum of Equation A.14 and Equation A.15.

A.3 Inclination Change for an Elliptic Orbit

The final problem is to determine the Δv for an inclination change maneuver with a single burn. We begin with the equation for the velocity in terms of the orbital

elements [3, 125]:

$$\boldsymbol{v} = -\frac{\mu}{h}\begin{bmatrix} \cos\Omega\left(\sin\theta + e\sin\omega\right) + \sin\Omega\cos i\left(\cos\theta + e\cos\omega\right) \\ \sin\Omega\left(\sin\theta + e\sin\omega\right) + \cos\Omega\cos i\left(\cos\theta + e\cos\omega\right) \\ -\sin i\left(\cos\theta + e\cos\omega\right) \end{bmatrix} \tag{A.16}$$

where θ is defined by $\theta = \omega + f$. For determining the cost of this maneuver, we can take the inclination and node of the initial orbit both to be zero without loss of generality, as the reference frame may be rotated freely. Also, for there to be a single-burn solution, the maneuver must occur at either the ascending or descending node; the argument of latitude must therefore be either zero or π. Substituting in these values to Equation A.16, we find that the initial velocity is

$$\boldsymbol{v}_0 = \frac{\mu}{h}\begin{bmatrix} -e\sin\omega \\ e\cos\omega \pm 1 \\ 0 \end{bmatrix} \tag{A.17}$$

Similarly, the velocity after the burn must be

$$\boldsymbol{v}_1 = \frac{\mu}{h}\begin{bmatrix} -e\sin\omega \\ \cos\Delta i\left(e\cos\omega \pm 1\right) \\ \sin\Delta i\left(e\cos\omega \pm 1\right) \end{bmatrix} \tag{A.18}$$

The difference of these two equations is the Δv required. The magnitude of this vector is easily shown to be

$$\Delta v = \frac{2\mu}{h}\sin\frac{\Delta i}{2}\left(1 \pm e\cos\omega\right) \tag{A.19}$$

Appendix B

Sample ASKS Input

This is an incomplete input deck for ASKS. It contains the header information and one plane for the first Ellipso simulation (see Chapter 6). The orbital elements for the Ellipso 8:1 constellation [26] used in these simulations are tabulated below: This data is in mean-of-1950 coordinates.

	Plane 1	Plane 2	Plane 3
Semi-Major Axis (km)	10559.271	10559.270	14440.137
Eccentricity	0.345705	0.235675	0.00001
Inclination (deg)	116.3074	116.8226	0.0002618
Longitude of the Ascending Node	279.3744	99.4212	89.1038
Argument of Perigee	269.948	270.052	0.294
Mean Anomaly	0, 72, 144, 216, 288	0, 72, 144, 216, 216, 288	0, 51.4, 102.9, 154.3, 205.7, 257.1, 308.6

Table B.1: Ellipso constellation orbital elements

ellipso_full.dat :

```
Number of Planes     :     3
Stat-Keep Method     :     1  (0=box; 1=formation)

Targeting Method     :     5
Power                :  1.00
kmax                 :    50
max_burns            :     4

Epoch Date: 19970101.0  Epoch Time:      0.0000
Final Date: 19990101.0  Final Time:      0.0000
Iteration Time Step  :         0.10300000000000000D+05   sec

****************************************
Plane                :     1
Sats In This Plane   :     5

Maximum Parameter Limits:      1.00000000000000000D+03   km    sma
   Keplerian Elements:         0.00020000000000000D+00         ecc
                               0.00005000000000000D+03   deg   inc
                               0.00020000000000000D+03   deg   lan
                               0.00100000000000000D+03   deg    ap
                               0.00050000000000000D+03   deg    ma
Scale (outer limits) :  0.98
Deadband Parameter Limits:     0.95000000000000000D+00   km    sma
   Keplerian Elements:         0.00095000000000000D+00         ecc
                               0.00004500000000000D+03   deg   inc
                               0.00018000000000000D+03   deg   lan
                               0.00095000000000000D+03   deg    ap
                               0.00470000000000000D+03   deg    ma

Maximum Overshoot Limits :     0.98000000000000000D+00   frac  sma
                               0.98000000000000000D+00   frac  ecc
                               0.98000000000000000D+00   frac  inc
                               0.65000000000000000D+00   frac  lan
                               0.98000000000000000D+00   frac   ap
                               1.25000000000000000D+00   frac   ma

----------------------------------------
Satellite Number     :     1

Actual State:
   Keplerian Elements:         0.10559271000000000D+05   km    sma
                               0.34570500000000000D+00         ecc
                               0.11630740006000000D+03   deg   inc
```

```
                              0.2793744530100000D+03   deg   lan
                              0.2699478224900000D+03   deg    ap
                              0.0000000000000000D+03   deg    ma

CD:                    2.20000000 Rho One:          0.00000000
S/C Mass:            700.00000000 S/C Area:         0.00002500
Integrator Step: 43200.00000000

Retro:       1 Atmos Mdl:    1  Potent Mdl:  4
Nmax:       21 Mmax:        21  Izonal:      1  IJ2J2:   1
Nmaxrs:     21 Mmaxrs:      21  Ithird:      1
Ind Drg:     1 Iszak:        2  Ind Sol:     1

Reference State:
   Keplerian Elements:         0.1055927100000000D+05   km    sma
                               0.3457050000000000D+00         ecc
                               0.1163074000600000D+03   deg   inc
                               0.2793744530100000D+03   deg   lan
                               0.2699478224900000D+03   deg    ap
                               0.0000000000000000D+03   deg    ma
Reference Switch     :     0    ! (0=DSST, 1=Fixed Rates)
Reference State Rates:
   Keplerian Rates:            0.0000000000000000D+00   km/sec  sma
                               0.0000000000000000D+00   1/sec   ecc
                               0.0000000000000000D+00   deg/sec inc
                               1.1407711610000000D-05   deg/sec lan
                               0.0000000000000000D+00   deg/sec  ap
                               3.3338114140000000D-02   deg/sec  ma

CD:                    2.20000000 Rho One:          0.00000000
S/C Mass:            700.00000000 S/C Area:         0.00002500
Integrator Step: 43200.00000000

Retro:       1 Atmos Mdl:    1  Potent Mdl:  4
Nmax:       21 Mmax:         0  Izonal:      1  IJ2J2:   1
Nmaxrs:      2 Mmaxrs:       2  Ithird:      1
Ind Drg:     2 Iszak:        2  Ind Sol:     2
-----------------------------------------
Satellite Number     :     2

Actual State:
   Keplerian Elements:         0.1055927100000000D+05   km    sma
                               0.3457050000000000D+00         ecc
                               0.1163074000600000D+03   deg   inc
                               0.2793744530100000D+03   deg   lan
                               0.2699478224900000D+03   deg    ap
                               0.0720000000000000D+03   deg    ma
```

```
CD:                  2.20000000 Rho One:          0.00000000
S/C Mass:          700.00000000 S/C Area:         0.00002500
Integrator Step: 43200.00000000

Retro:      1 Atmos Mdl:   1  Potent Mdl:  4
Nmax:      21 Mmax:       21  Izonal:      1  IJ2J2:   1
Nmaxrs:    21 Mmaxrs:     21  Ithird:      1
Ind Drg:    1 Iszak:       2  Ind Sol:     1

Reference State:
   Keplerian Elements:          0.1055927100000000D+05   km    sma
                                0.3457050000000000D+00         ecc
                                0.1163074000600000D+03   deg   inc
                                0.2793744530100000D+03   deg   lan
                                0.2699478224900000D+03   deg    ap
                                0.0720000000000000D+03   deg    ma
Reference Switch     :     0    ! (0=DSST, 1=Fixed Rates)
Reference State Rates:
   Keplerian Rates:             0.0000000000000000D+00   km/sec  sma
                                0.0000000000000000D+00   1/sec   ecc
                                0.0000000000000000D+00   deg/sec inc
                                1.1407711610000000D-05   deg/sec lan
                                0.0000000000000000D+00   deg/sec  ap
                                3.3338114140000000D-02   deg/sec  ma

CD:                  2.20000000 Rho One:          0.00000000
S/C Mass:          700.00000000 S/C Area:         0.00002500
Integrator Step: 43200.00000000

Retro:      1 Atmos Mdl:   1  Potent Mdl:  4
Nmax:      21 Mmax:        0  Izonal:      1  IJ2J2:   1
Nmaxrs:     2 Mmaxrs:      2  Ithird:      1
Ind Drg:    2 Iszak:       2  Ind Sol:     2
-----------------------------------------
Satellite Number     :     3

Actual State:
   Keplerian Elements:          0.1055927100000000D+05   km    sma
                                0.3457050000000000D+00         ecc
                                0.1163074000600000D+03   deg   inc
                                0.2793744530100000D+03   deg   lan
                                0.2699478224900000D+03   deg    ap
                                0.1440000000000000D+03   deg    ma

CD:                  2.20000000 Rho One:          0.00000000
S/C Mass:          700.00000000 S/C Area:         0.00002500
```

```
Integrator Step: 43200.00000000

Retro:      1 Atmos Mdl:   1  Potent Mdl:  4
Nmax:      21 Mmax:       21  Izonal:      1  IJ2J2:   1
Nmaxrs:    21 Mmaxrs:     21  Ithird:      1
Ind Drg:    1 Iszak:       2  Ind Sol:     1

Reference State:
   Keplerian Elements:          0.1055927100000000D+05   km    sma
                                0.3457050000000000D+00         ecc
                                0.1163074000600000D+03   deg   inc
                                0.2793744530100000D+03   deg   lan
                                0.2699478224900000D+03   deg    ap
                                0.1440000000000000D+03   deg    ma
Reference Switch     :     0    ! (0=DSST, 1=Fixed Rates)
Reference State Rates:
   Keplerian Rates:             0.0000000000000000D+00   km/sec  sma
                                0.0000000000000000D+00   1/sec   ecc
                                0.0000000000000000D+00   deg/sec inc
                                1.1407711610000000D-05   deg/sec lan
                                0.0000000000000000D+00   deg/sec  ap
                                3.3338114140000000D-02   deg/sec  ma

CD:                   2.20000000 Rho One:          0.00000000
S/C Mass:           700.00000000 S/C Area:         0.00002500
Integrator Step: 43200.00000000

Retro:      1 Atmos Mdl:   1  Potent Mdl:  4
Nmax:      21 Mmax:        0  Izonal:      1  IJ2J2:   1
Nmaxrs:     2 Mmaxrs:      2  Ithird:      1
Ind Drg:    2 Iszak:       2  Ind Sol:     2
-----------------------------------------
Satellite Number     :     4

Actual State:
   Keplerian Elements:          0.1055927100000000D+05   km    sma
                                0.3457050000000000D+00         ecc
                                0.1163074000600000D+03   deg   inc
                                0.2793744530100000D+03   deg   lan
                                0.2699478224900000D+03   deg    ap
                                0.2160000000000000D+03   deg    ma

CD:                   2.20000000 Rho One:          0.00000000
S/C Mass:           700.00000000 S/C Area:         0.00002500
Integrator Step: 43200.00000000

Retro:      1 Atmos Mdl:   1  Potent Mdl:  4
```

```
Nmax:      21 Mmax:       21  Izonal:      1  IJ2J2:   1
Nmaxrs:    21 Mmaxrs:     21  Ithird:      1
Ind Drg:    1 Iszak:       2  Ind Sol:     1

Reference State:
   Keplerian Elements:          0.1055927100000000D+05   km    sma
                                0.3457050000000000D+00         ecc
                                0.1163074000600000D+03   deg   inc
                                0.2793744530100000D+03   deg   lan
                                0.2699478224900000D+03   deg    ap
                                0.2160000000000000D+03   deg    ma
Reference Switch     :     0    ! (0=DSST, 1=Fixed Rates)
Reference State Rates:
   Keplerian Rates:             0.0000000000000000D+00   km/sec  sma
                                0.0000000000000000D+00   1/sec   ecc
                                0.0000000000000000D+00   deg/sec inc
                                1.1407711610000000D-05   deg/sec lan
                                0.0000000000000000D+00   deg/sec  ap
                                3.3338114140000000D-02   deg/sec  ma

CD:                  2.20000000 Rho One:          0.00000000
S/C Mass:          700.00000000 S/C Area:         0.00002500
Integrator Step: 43200.00000000

Retro:       1 Atmos Mdl:    1  Potent Mdl:  4
Nmax:       21 Mmax:         0  Izonal:      1  IJ2J2:   1
Nmaxrs:      2 Mmaxrs:       2  Ithird:      1
Ind Drg:     2 Iszak:        2  Ind Sol:     2
-----------------------------------------
Satellite Number     :     5

Actual State:
   Keplerian Elements:          0.1055927100000000D+05   km    sma
                                0.3457050000000000D+00         ecc
                                0.1163074000600000D+03   deg   inc
                                0.2793744530100000D+03   deg   lan
                                0.2699478224900000D+03   deg    ap
                                0.2880000000000000D+03   deg    ma

CD:                  2.20000000 Rho One:          0.00000000
S/C Mass:          700.00000000 S/C Area:         0.00002500
Integrator Step: 43200.00000000

Retro:       1 Atmos Mdl:    1  Potent Mdl:  4
Nmax:       21 Mmax:        21  Izonal:      1  IJ2J2:   1
Nmaxrs:     21 Mmaxrs:      21  Ithird:      1
Ind Drg:     1 Iszak:        2  Ind Sol:     1
```

```
Reference State:
   Keplerian Elements:          0.1055927100000000D+05   km    sma
                                0.3457050000000000D+00         ecc
                                0.1163074000600000D+03   deg   inc
                                0.2793744530100000D+03   deg   lan
                                0.2699478224900000D+03   deg    ap
                                0.2880000000000000D+03   deg    ma
Reference Switch     :     0    ! (0=DSST, 1=Fixed Rates)
Reference State Rates:
   Keplerian Rates:             0.0000000000000000D+00   km/sec  sma
                                0.0000000000000000D+00   1/sec   ecc
                                0.0000000000000000D+00   deg/sec inc
                                1.1407711610000000D-05   deg/sec lan
                                0.0000000000000000D+00   deg/sec  ap
                                3.3338114140000000D-02   deg/sec  ma

CD:                   2.20000000 Rho One:          0.00000000
S/C Mass:           700.00000000 S/C Area:         0.00002500
Integrator Step: 43200.00000000

Retro:       1 Atmos Mdl:    1  Potent Mdl:  4
Nmax:       21 Mmax:         0  Izonal:      1  IJ2J2:   1
Nmaxrs:      2 Mmaxrs:       2  Ithird:      1
Ind Drg:     2 Iszak:        2  Ind Sol:     2
-----------------------------------------
```

Appendix C

Simulation One

This appendix contains all of the output plots for the first of the three simulations of Chapter 6. It includes coverage and the element histories of the satellites in each plane.

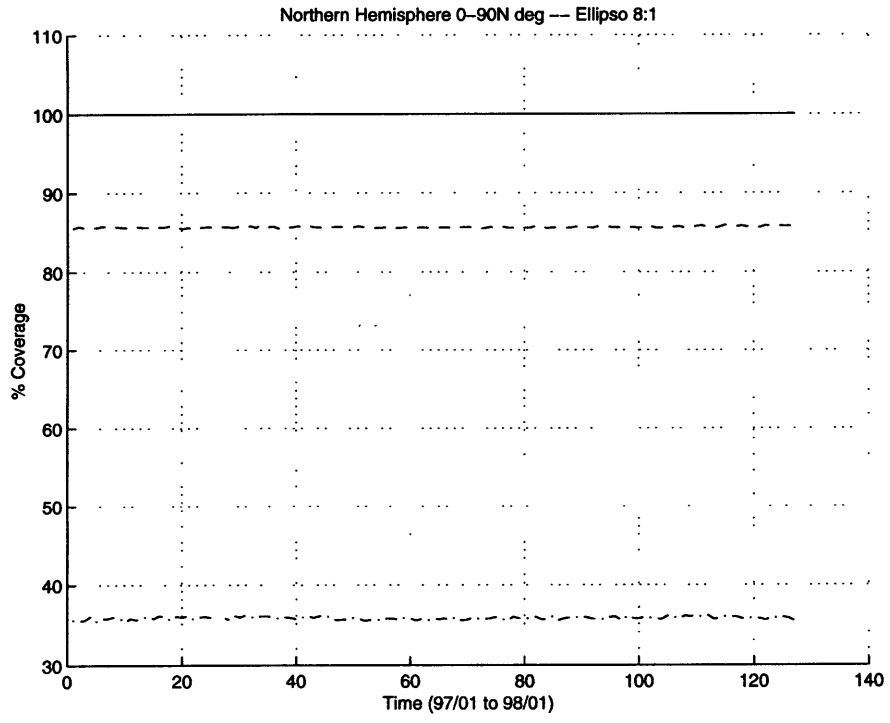

Figure C-1: Coverage history for Ellipso for one year

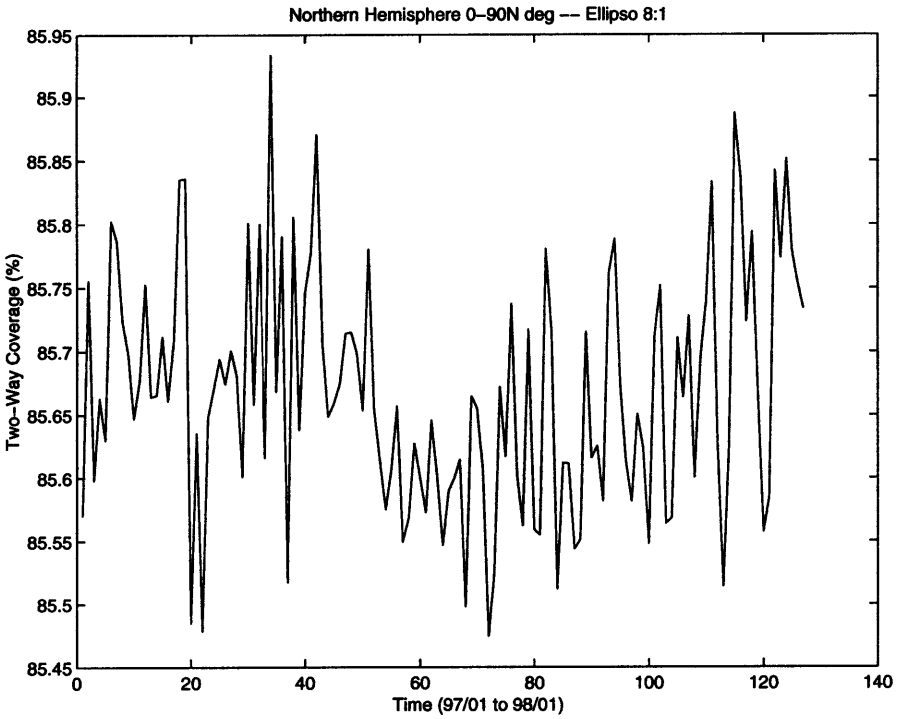

Figure C-2: Two-way coverage history for Ellipso for one year

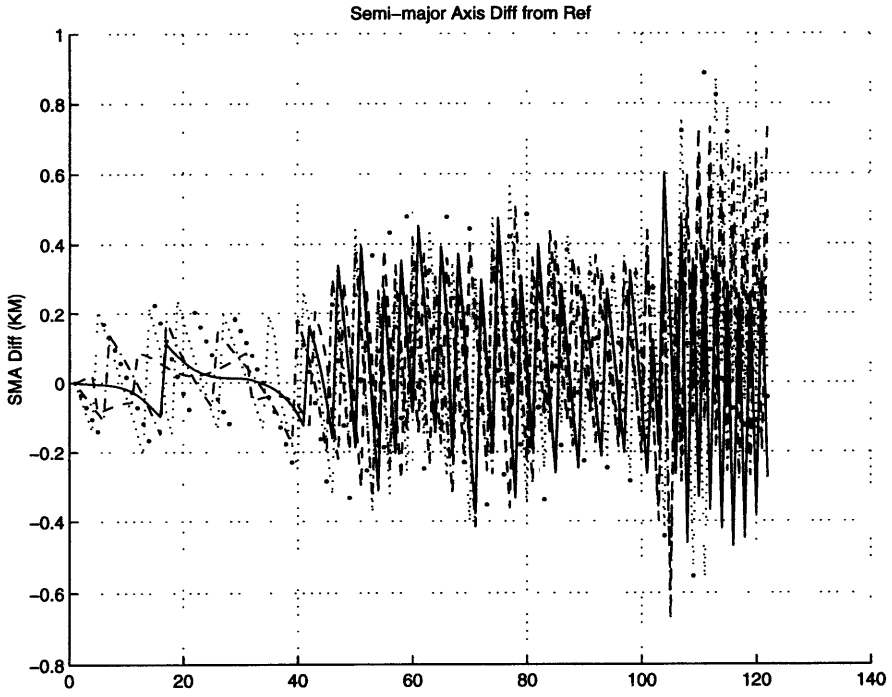

Figure C-3: 2 year semi-major axis error history for Borealis node at noon plane

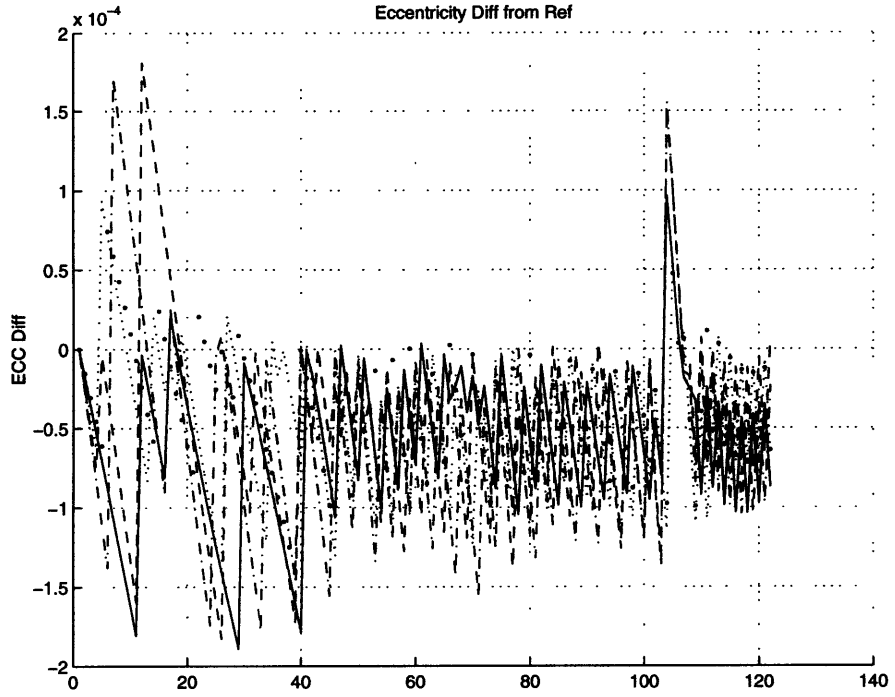

Figure C-4: 2 year eccentricity error history for Borealis node at noon plane

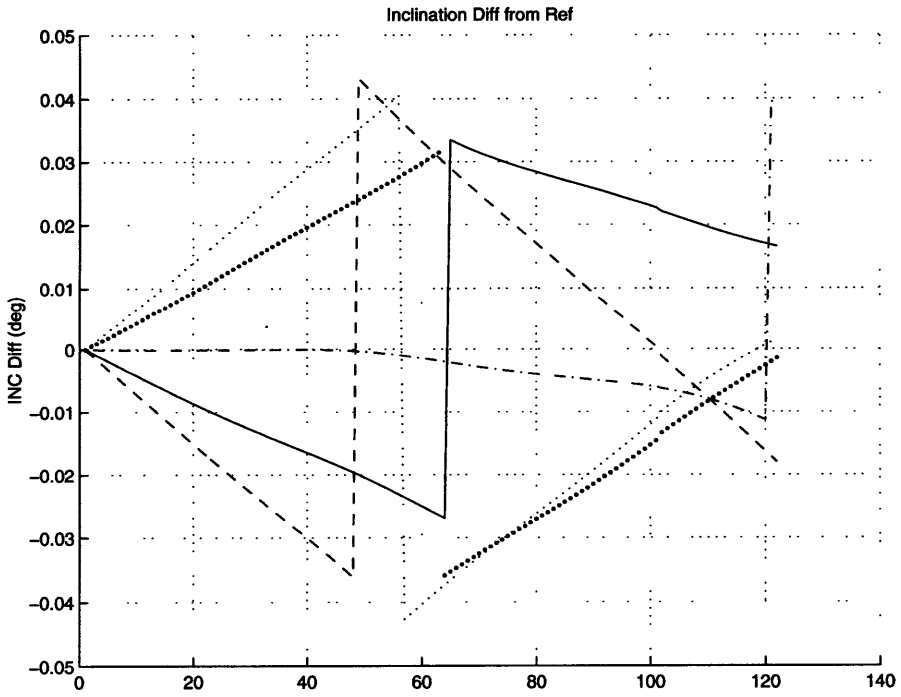

Figure C-5: 2 year inclination error history for Borealis node at noon plane

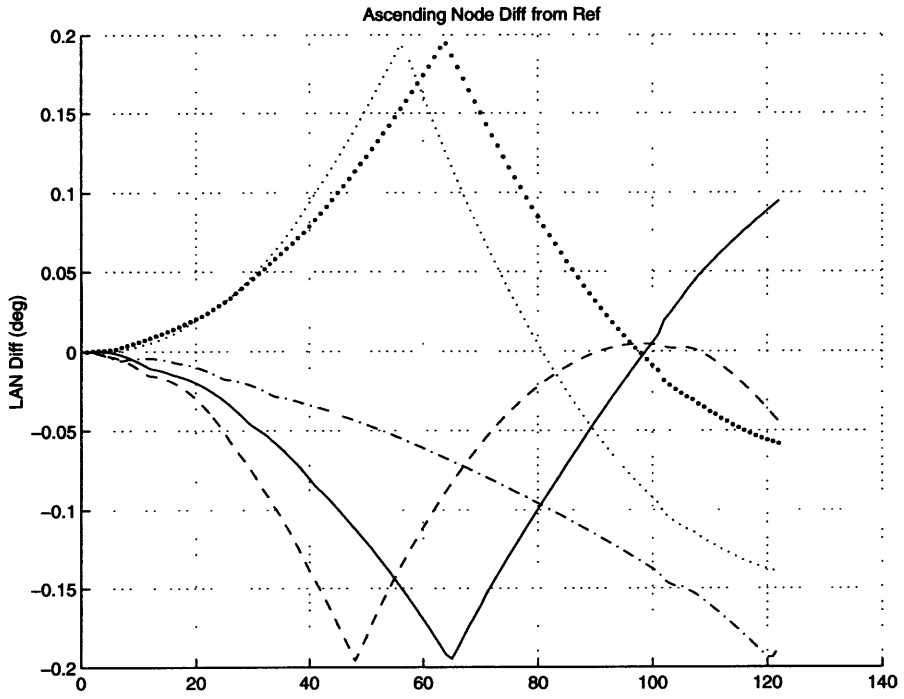

Figure C-6: 2 year ascending node error history for Borealis node at noon plane

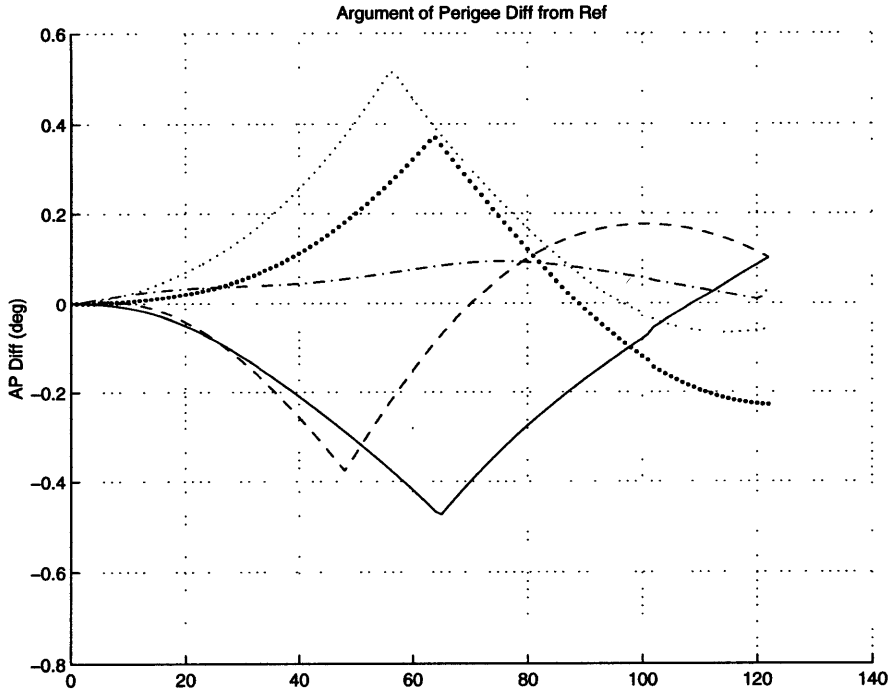

Figure C-7: 2 year argument of perigee error history for Borealis node at noon plane

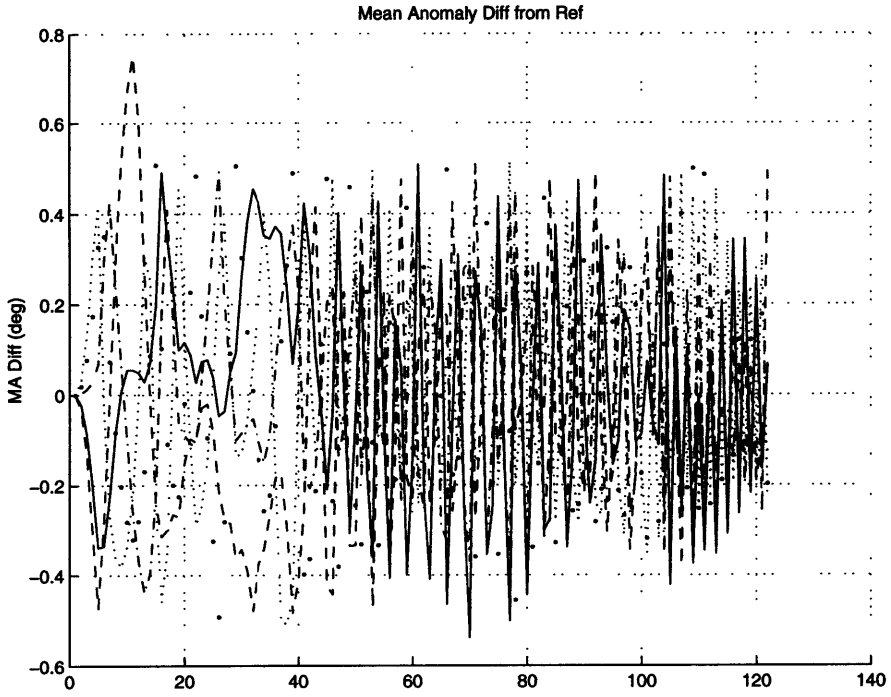

Figure C-8: 2 year mean anomaly error history for Borealis node at noon plane

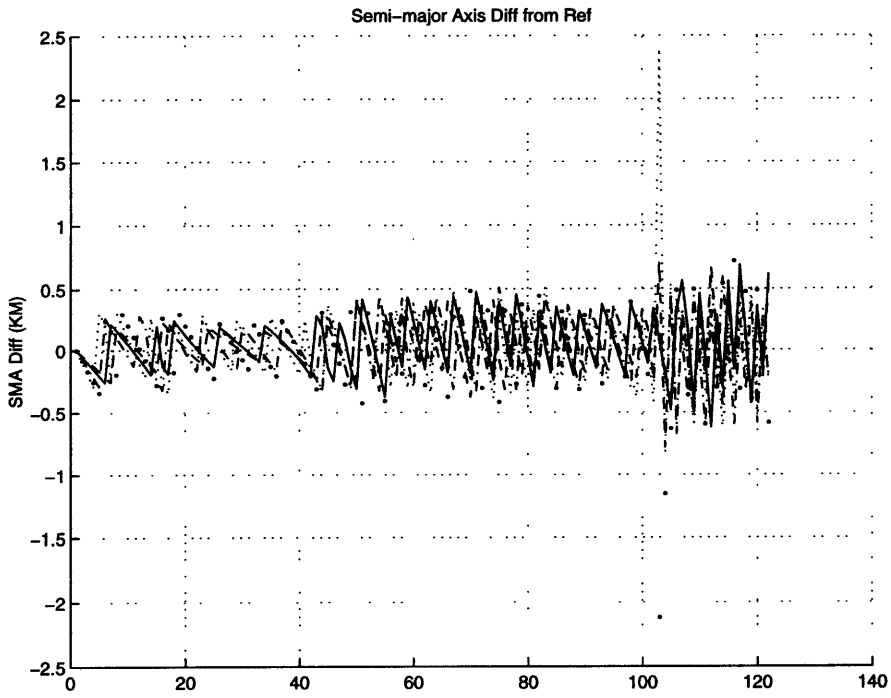

Figure C-9: 2 year semi-major axis error history for Borealis node at midnight plane

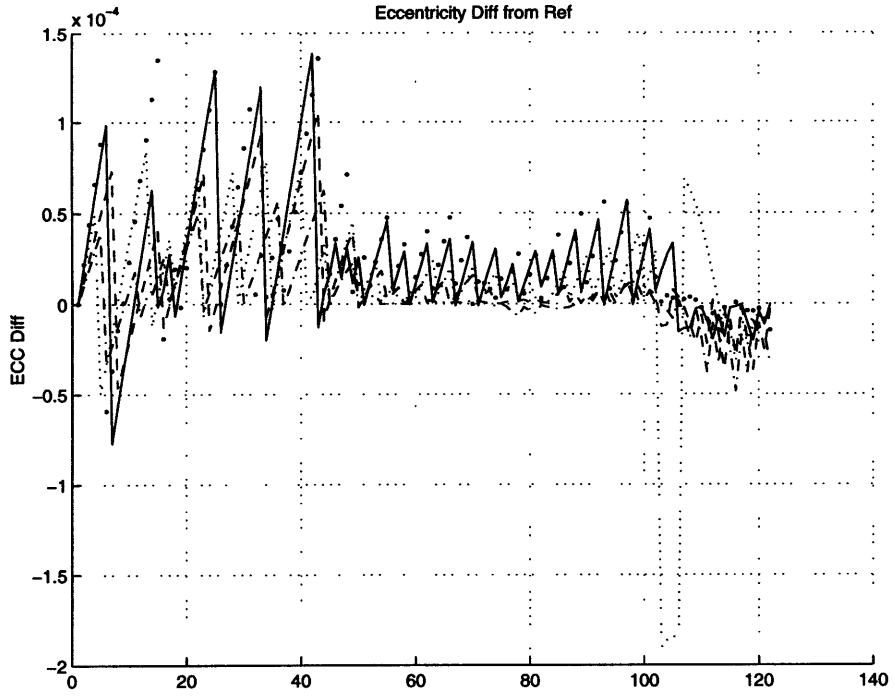

Figure C-10: 2 year eccentricity error history for Borealis node at midnight plane

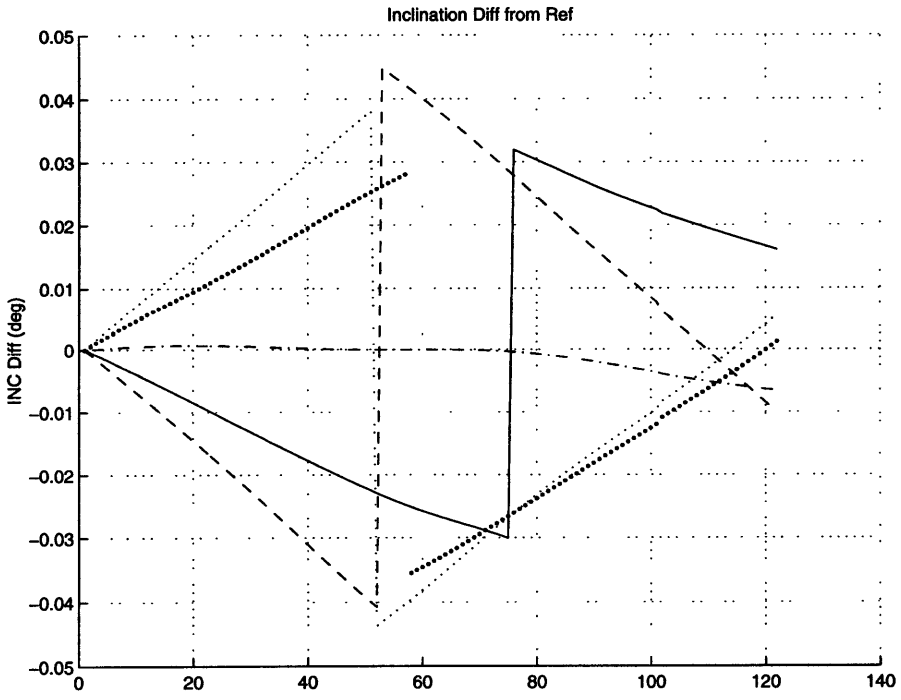

Figure C-11: 2 year inclination error history for Borealis node at midnight plane

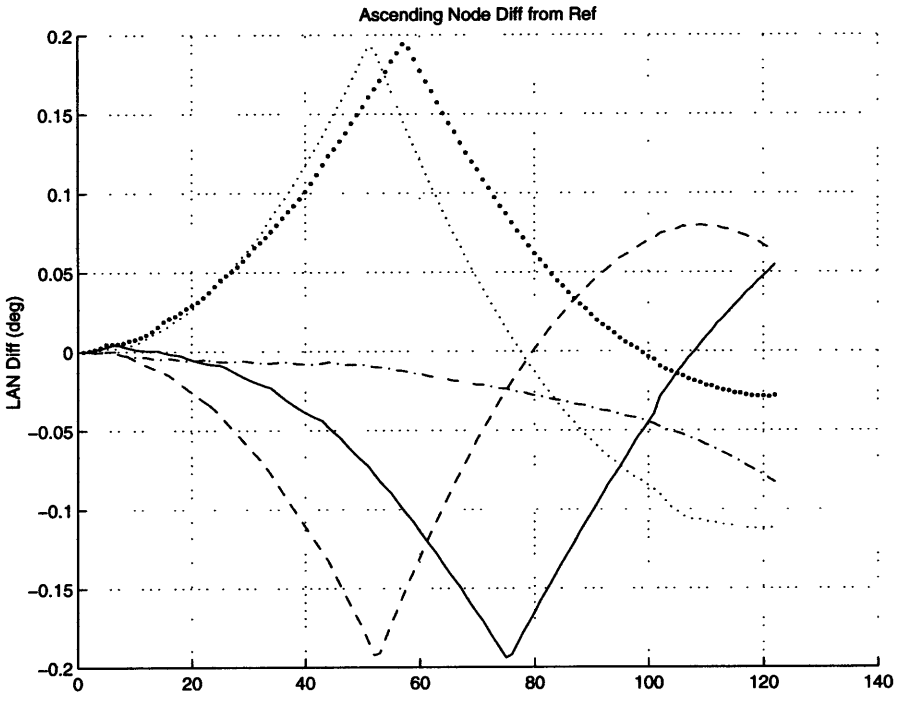

Figure C-12: 2 year ascending node error history for Borealis node at midnight plane

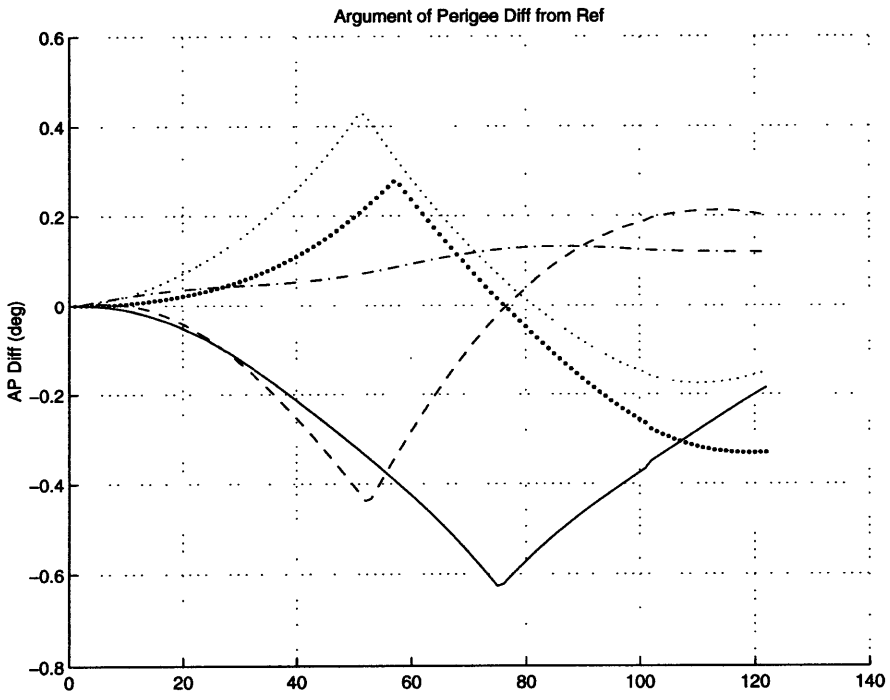

Figure C-13: 2 year perigee error history for Borealis node at midnight plane

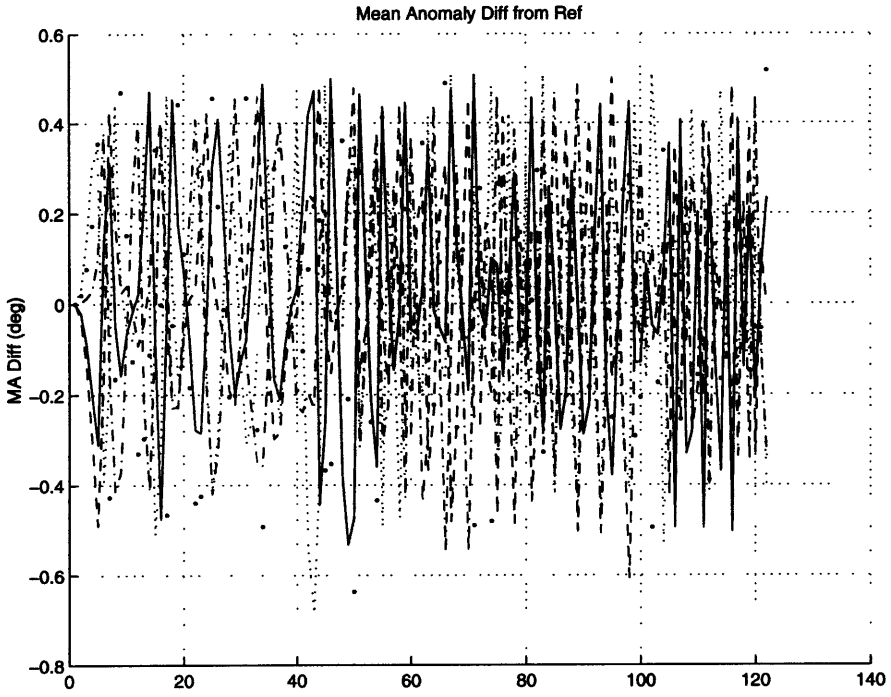

Figure C-14: 2 year mean anomaly error history for Borealis node at midnight plane

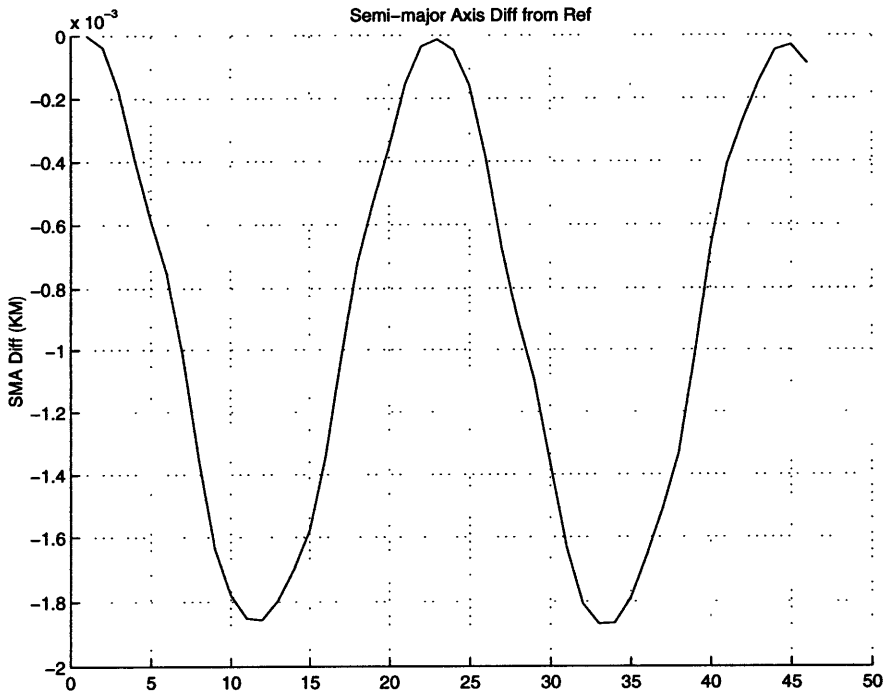

Figure C-15: 5 year semi-major axis error history for Concordia plane

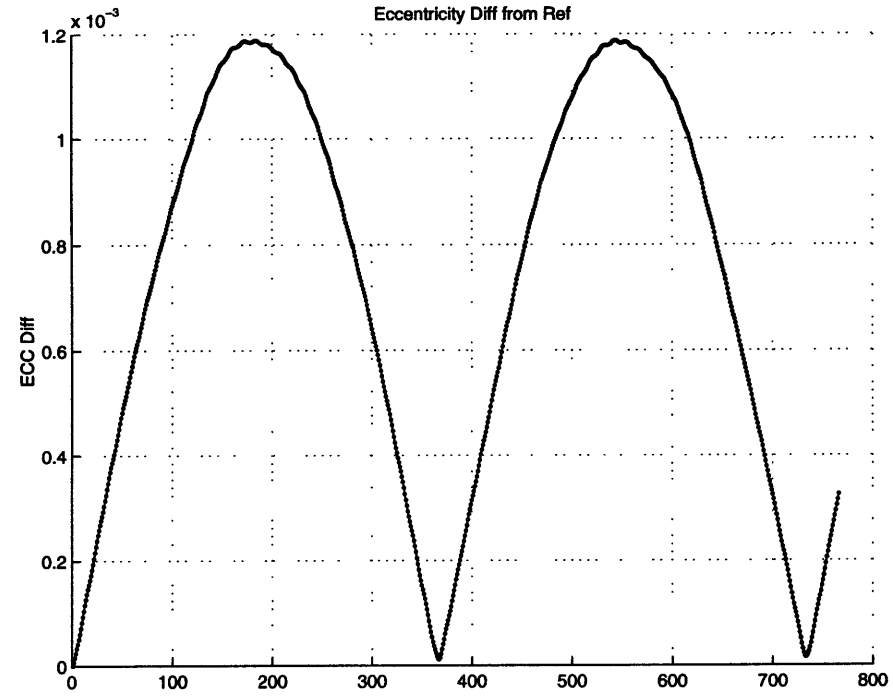

Figure C-16: 5 year eccentricity error history for Concordia plane

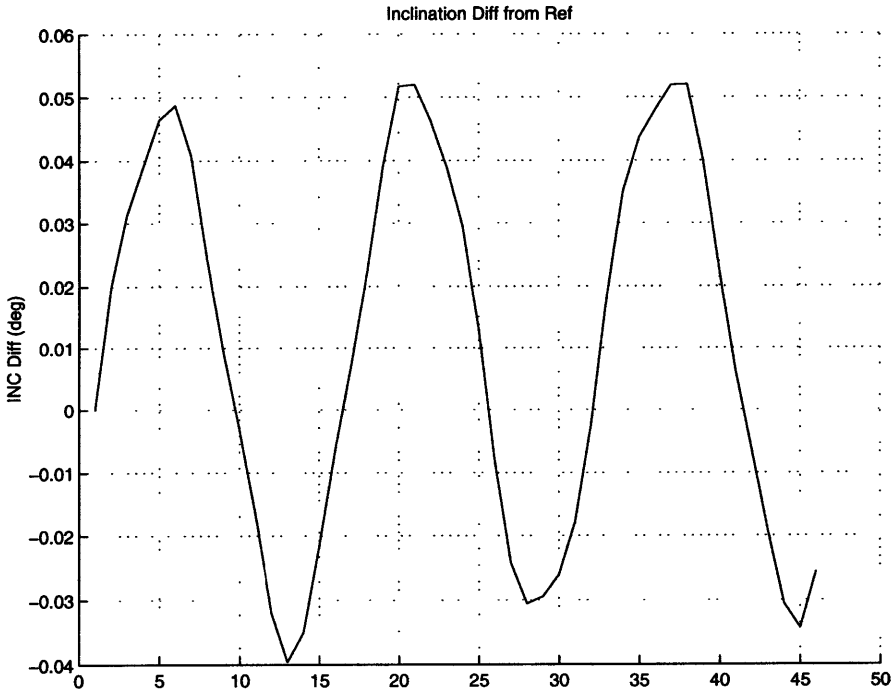

Figure C-17: 5 year inclination error history for Concordia plane

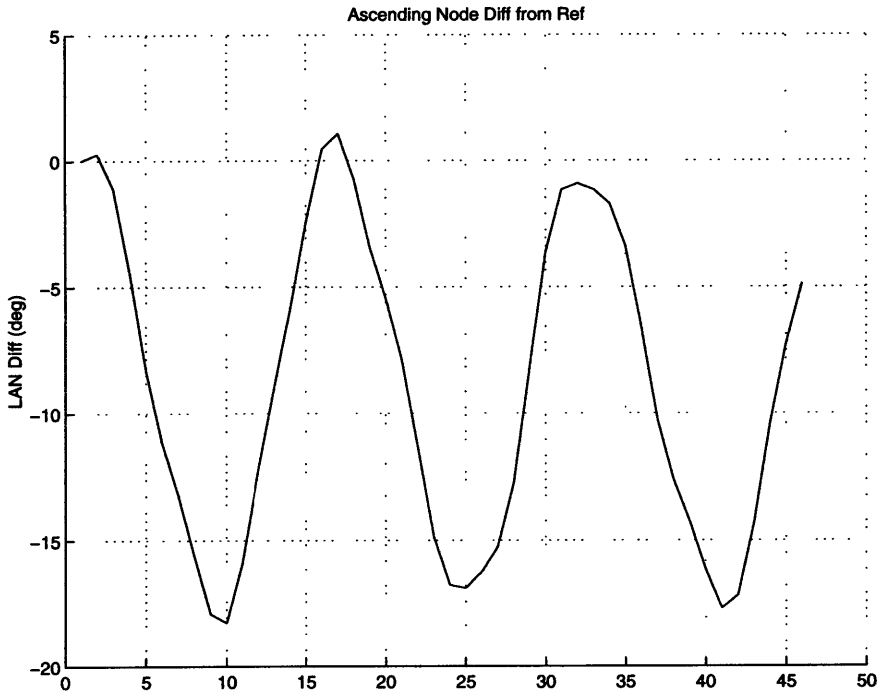

Figure C-18: 5 year ascending node error history for Concordia plane

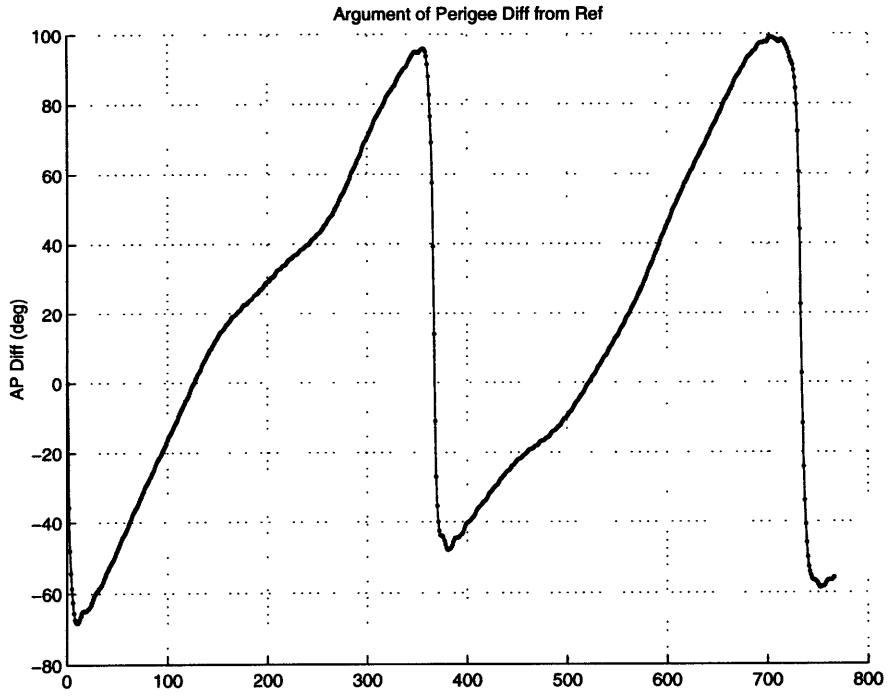

Figure C-19: 5 year argument of perigee error history for Concordia plane

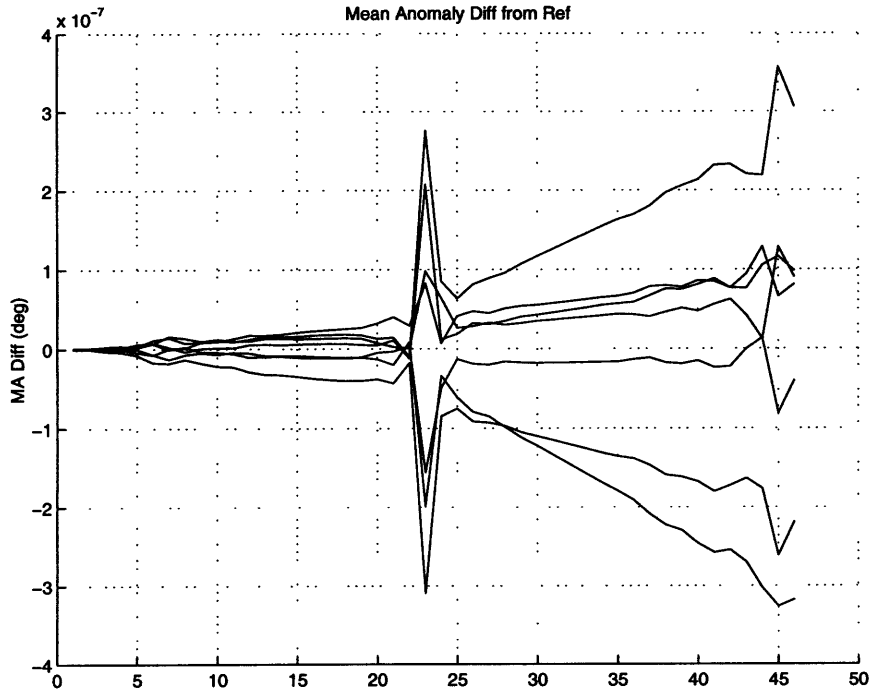

Figure C-20: 5 year mean anomaly error history for Concordia plane

Appendix D

Simulation Two

This appendix contains all of the output plots for the second of the three simulations of Chapter 6. It includes coverage and the element histories of the satellites in each Borealis plane. Concordia has been omitted, as it is the same as for the first run.

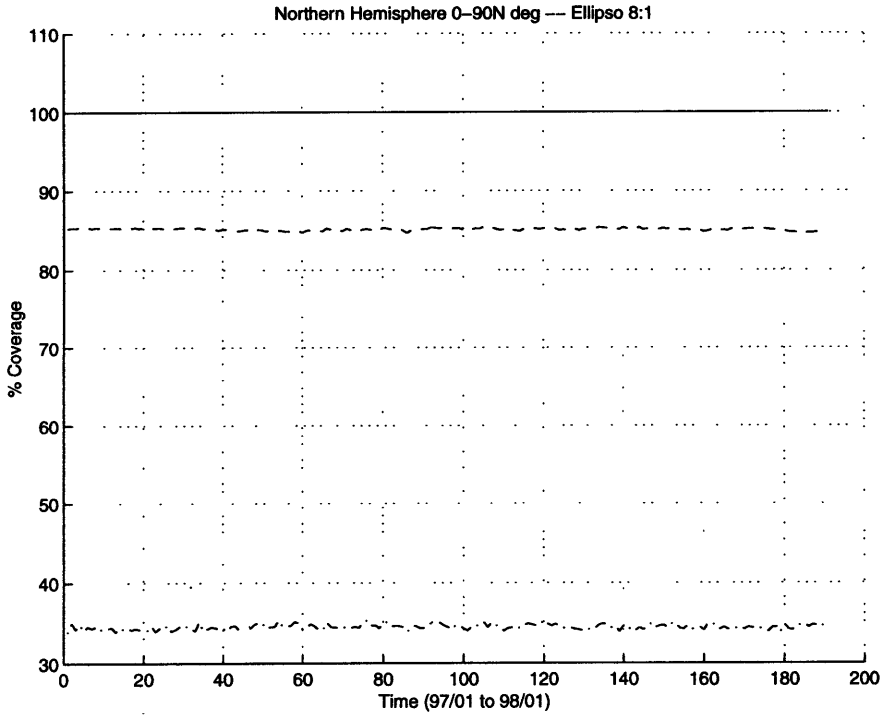

Figure D-1: Coverage history for Ellipso for one year

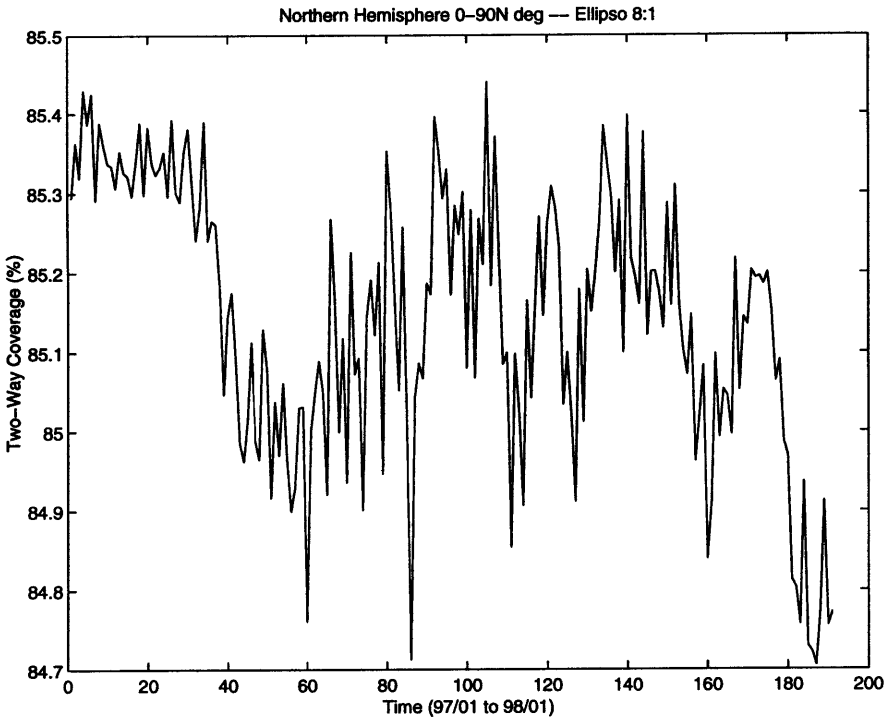

Figure D-2: Two-way coverage history for Ellipso for one year

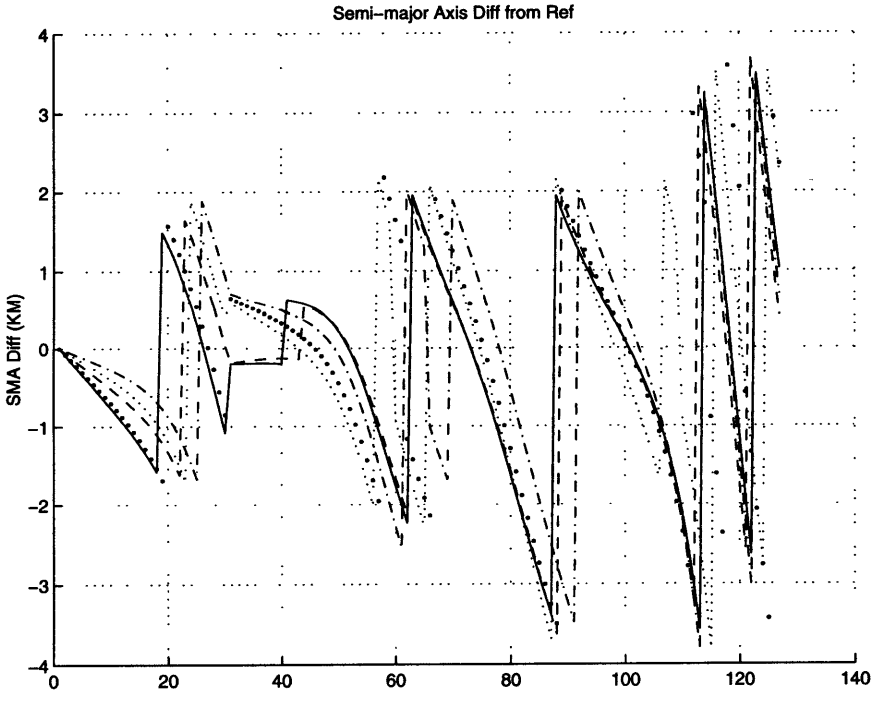

Figure D-3: 2 year semi-major axis error history for Borealis node at noon plane

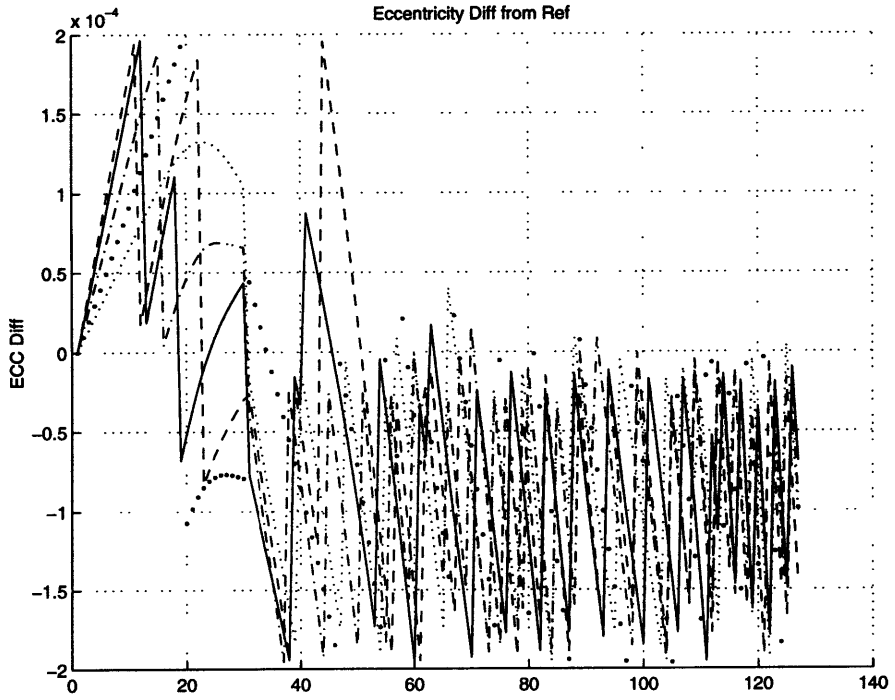

Figure D-4: 2 year eccentricity error history for Borealis node at noon plane

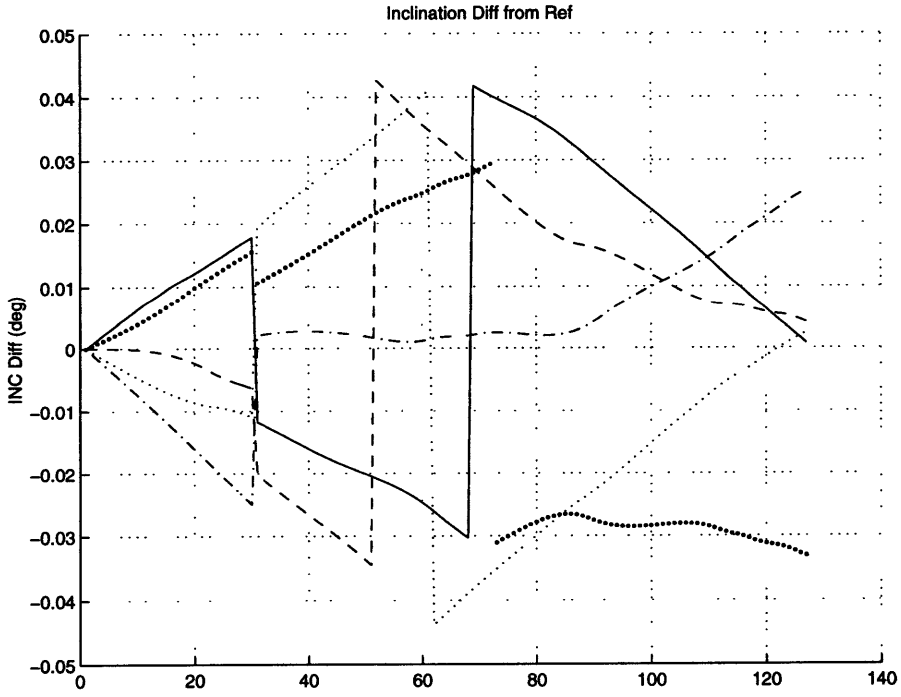

Figure D-5: 2 year inclination error history for Borealis node at noon plane

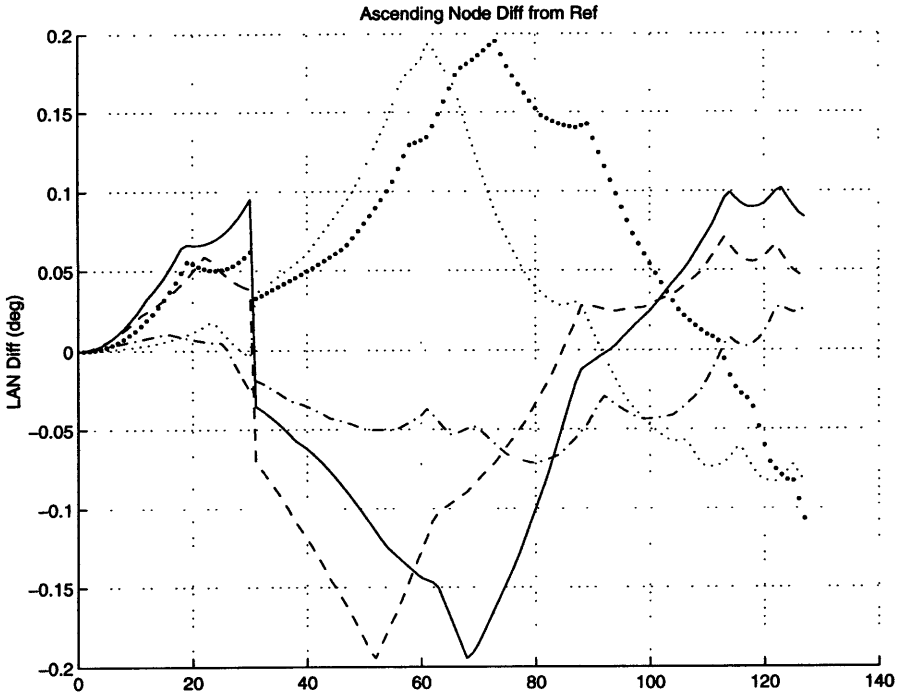

Figure D-6: 2 year ascending node error history for Borealis node at noon plane

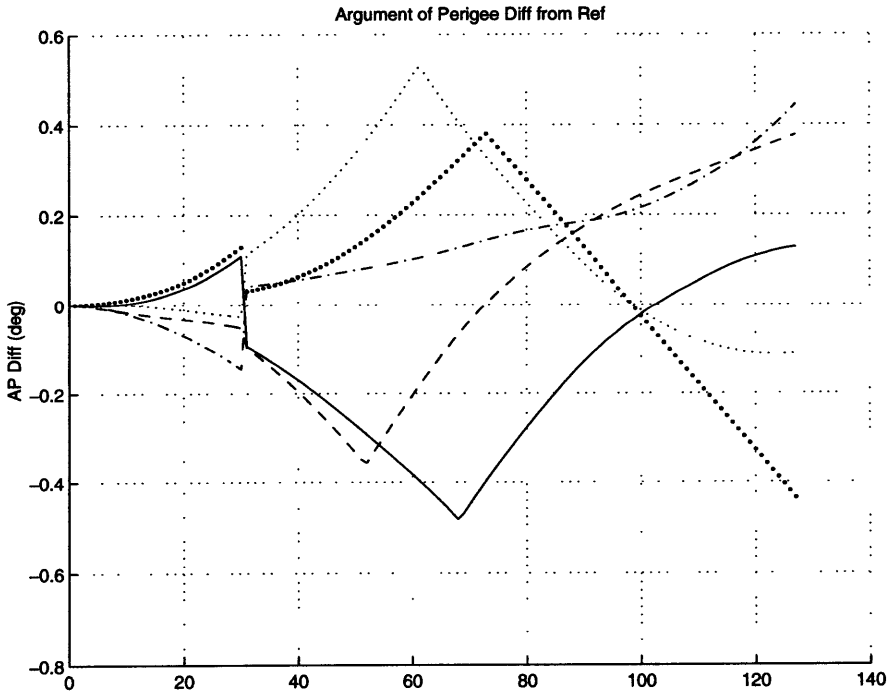

Figure D-7: 2 year argument of perigee error history for Borealis node at noon plane

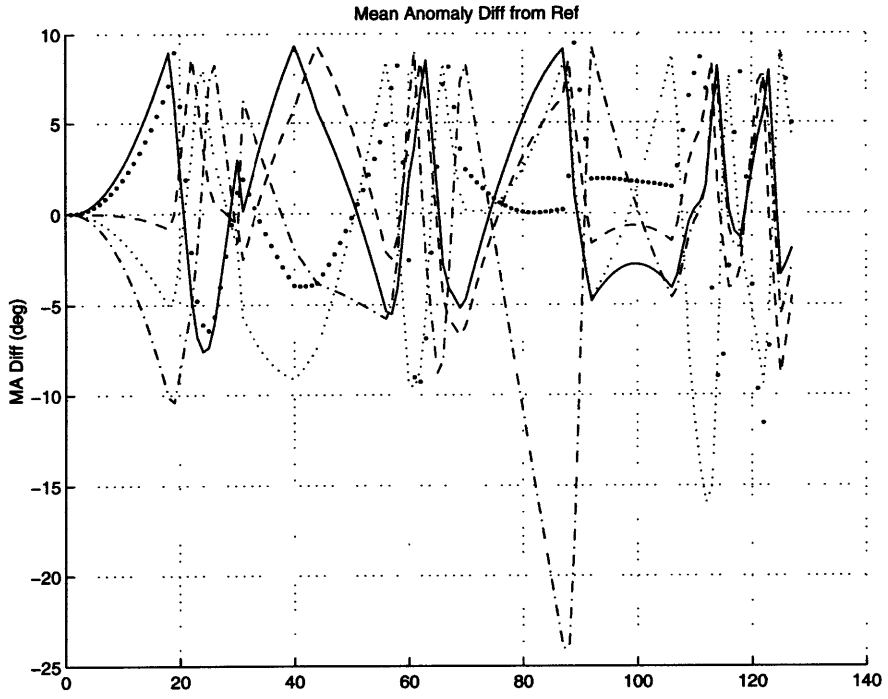

Figure D-8: 2 year mean anomaly error history for Borealis node at noon plane

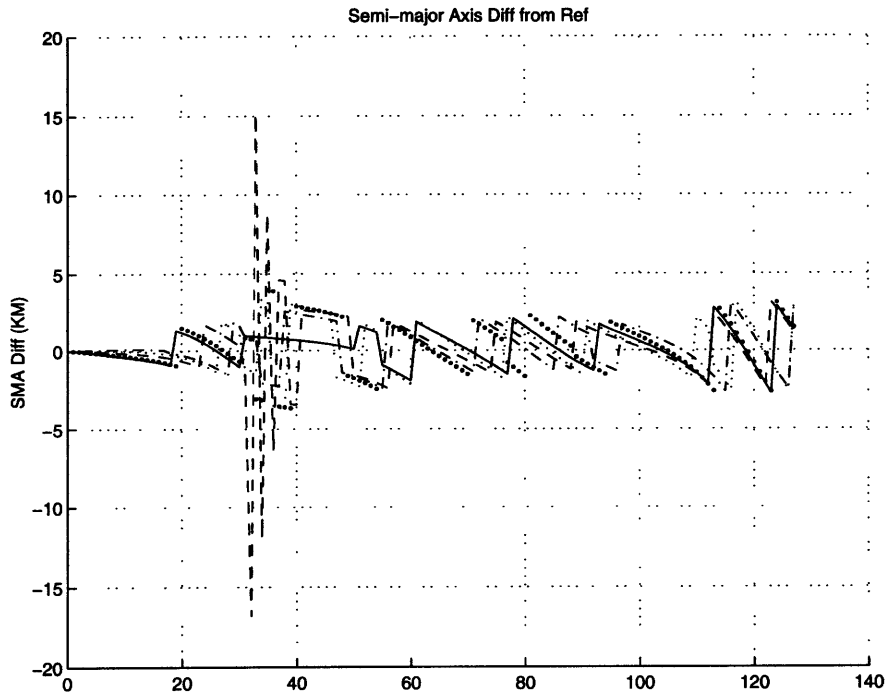

Figure D-9: 2 year semi-major axis error history for Borealis node at midnight plane

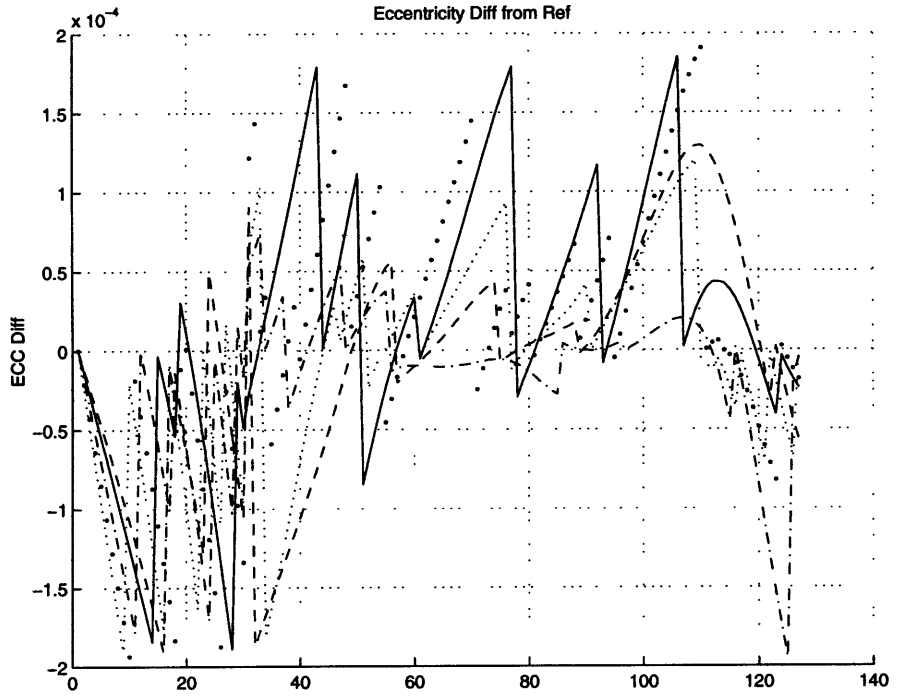

Figure D-10: 2 year eccentricity error history for Borealis node at midnight plane

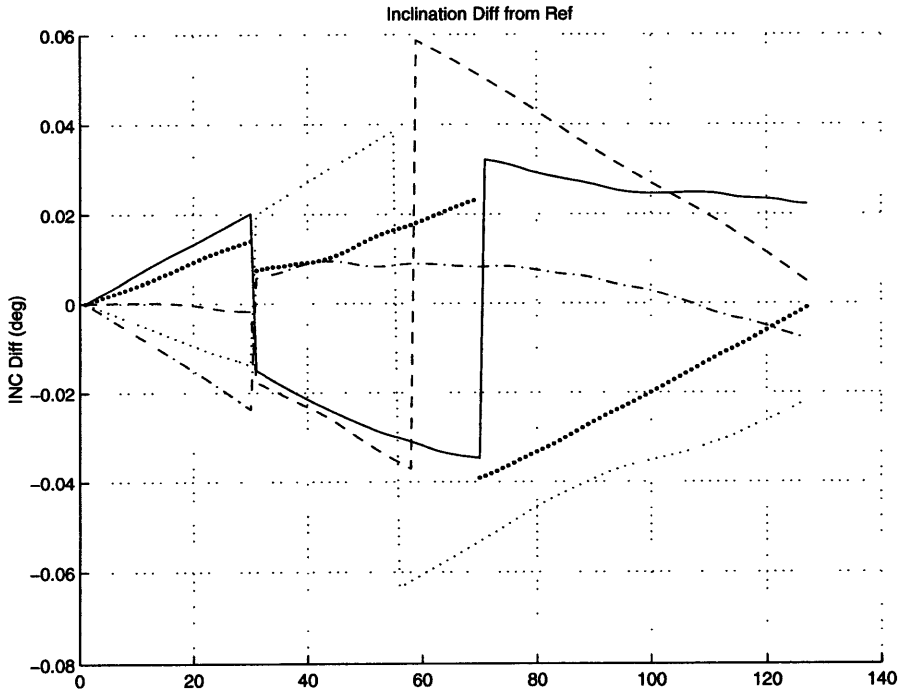

Figure D-11: 2 year inclination error history for Borealis node at midnight plane

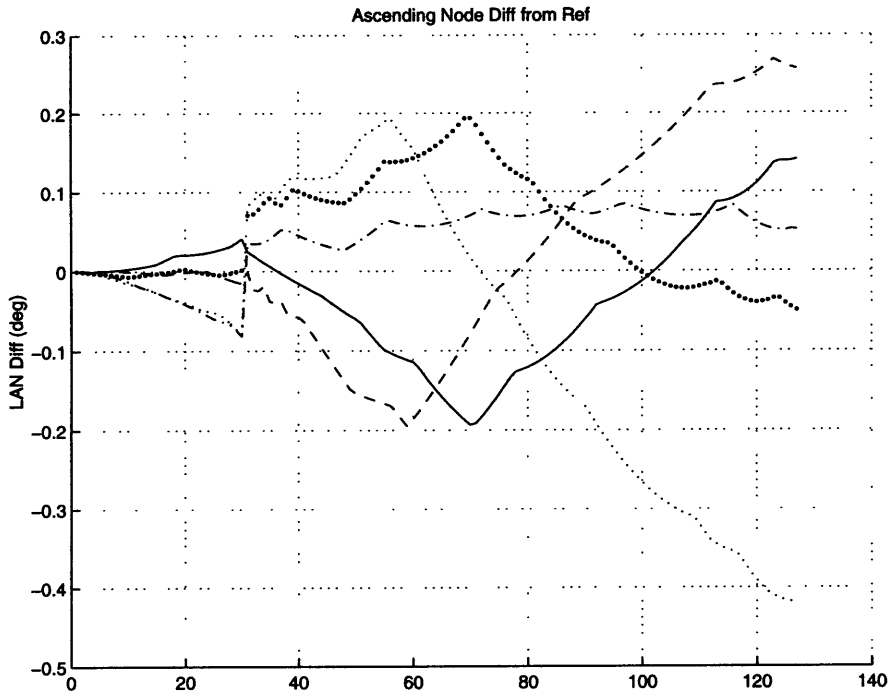

Figure D-12: 2 year ascending node error history for Borealis node at midnight plane

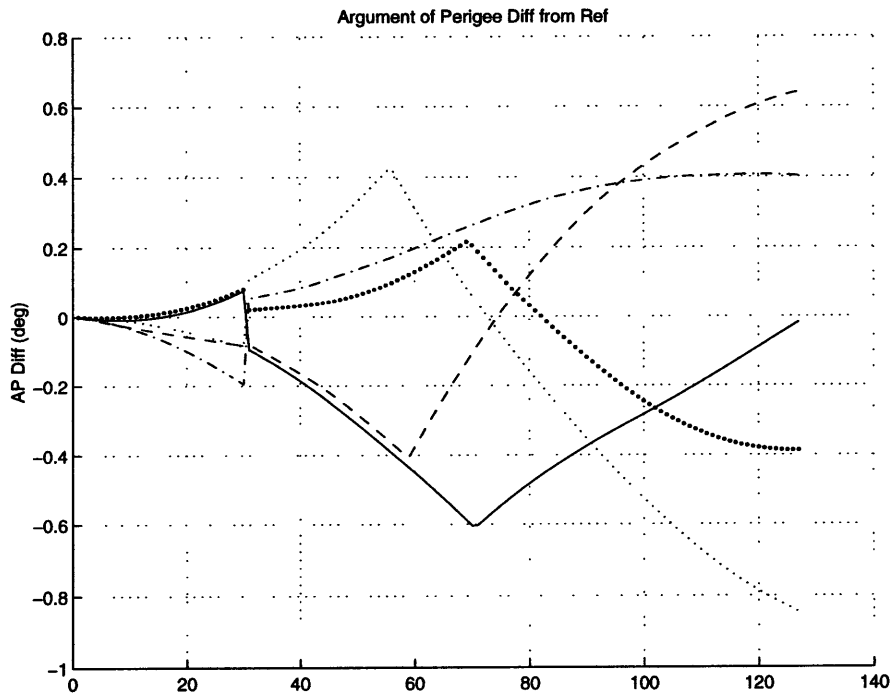

Figure D-13: 2 year perigee error history for Borealis node at midnight plane

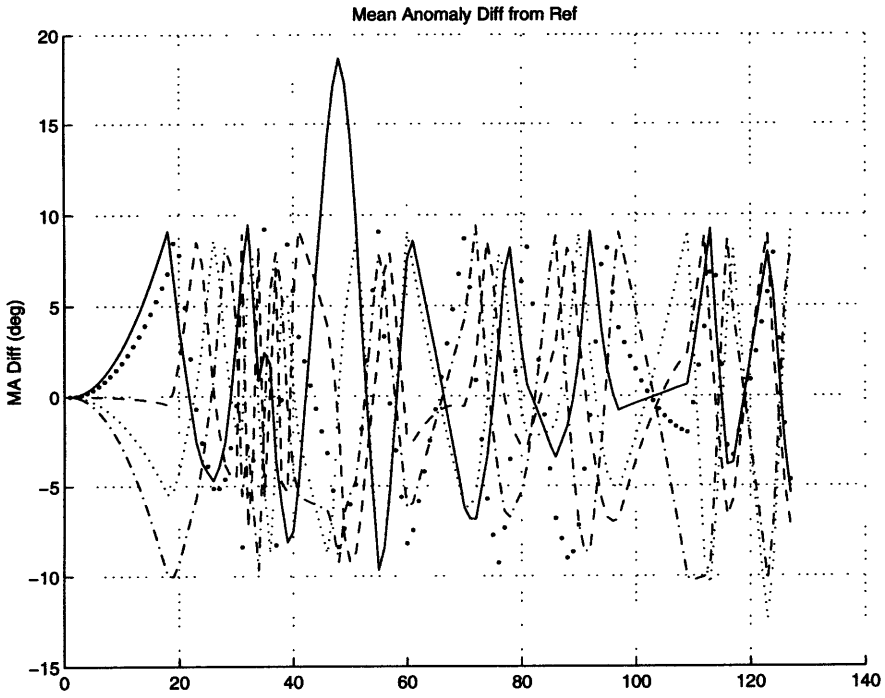

Figure D-14: 2 year mean anomaly error history for Borealis node at midnight plane

Appendix E

Simulation Three

This appendix contains all of the output plots for the first of the three simulations of Chapter 6. It includes coverage and the element histories of the satellites in each plane.

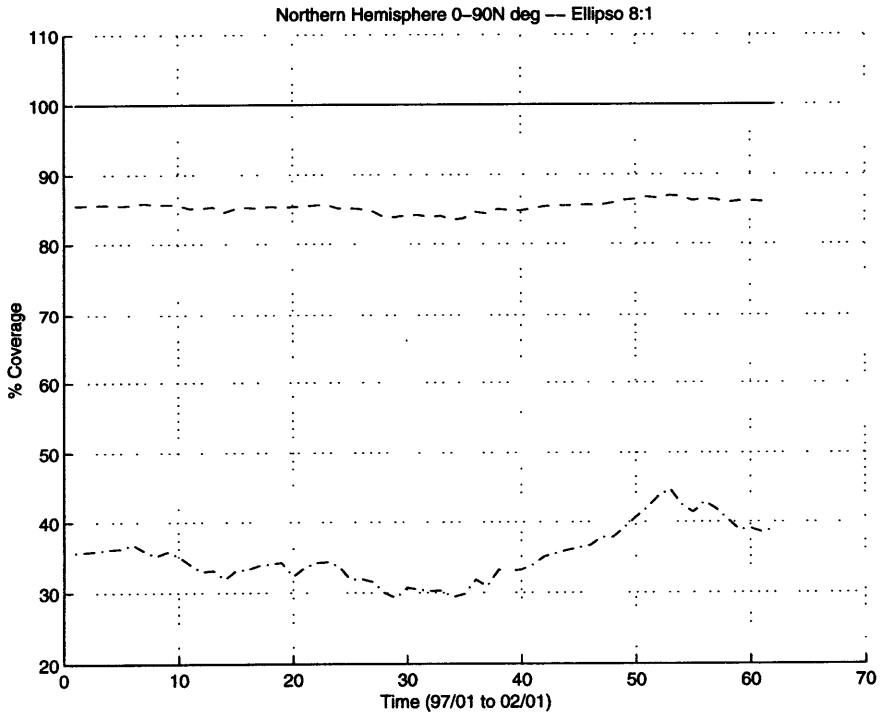

Figure E-1: Coverage history for Ellipso for one year

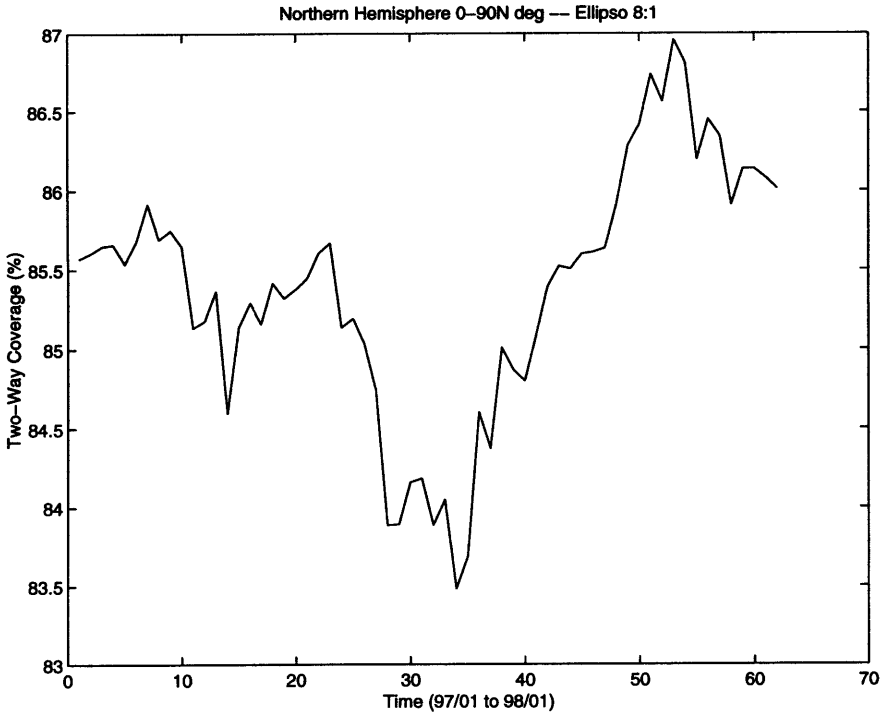

Figure E-2: Two-way coverage history for Ellipso for one year

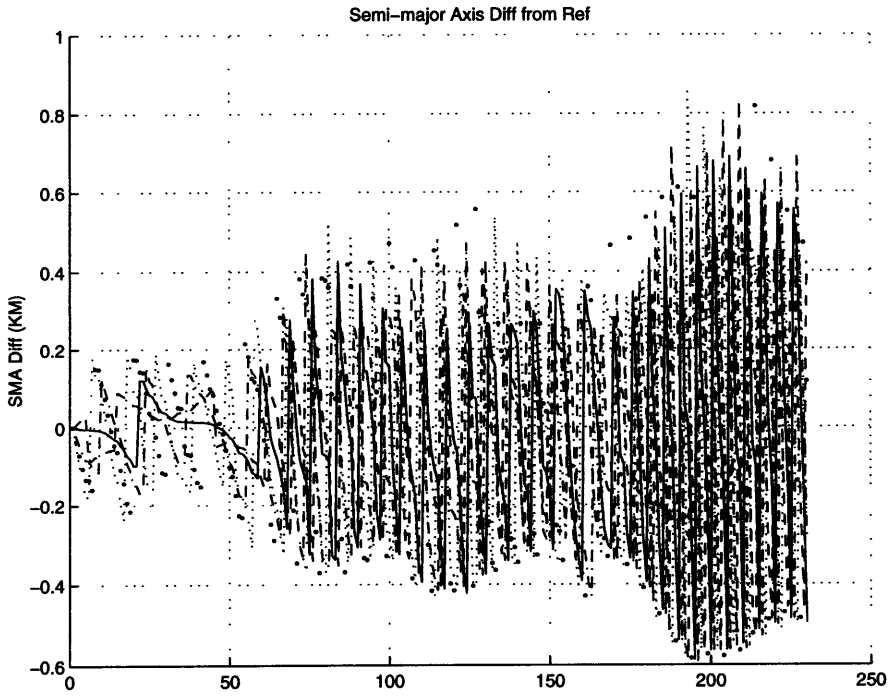

Figure E-3: 2 year semi-major axis error history for Borealis node at noon plane

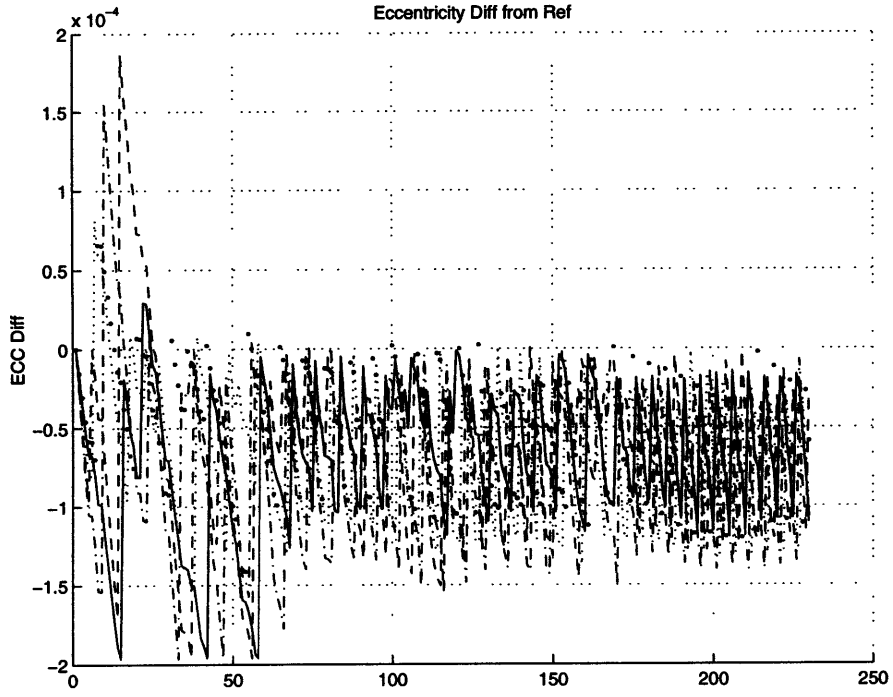

Figure E-4: 2 year eccentricity error history for Borealis node at noon plane

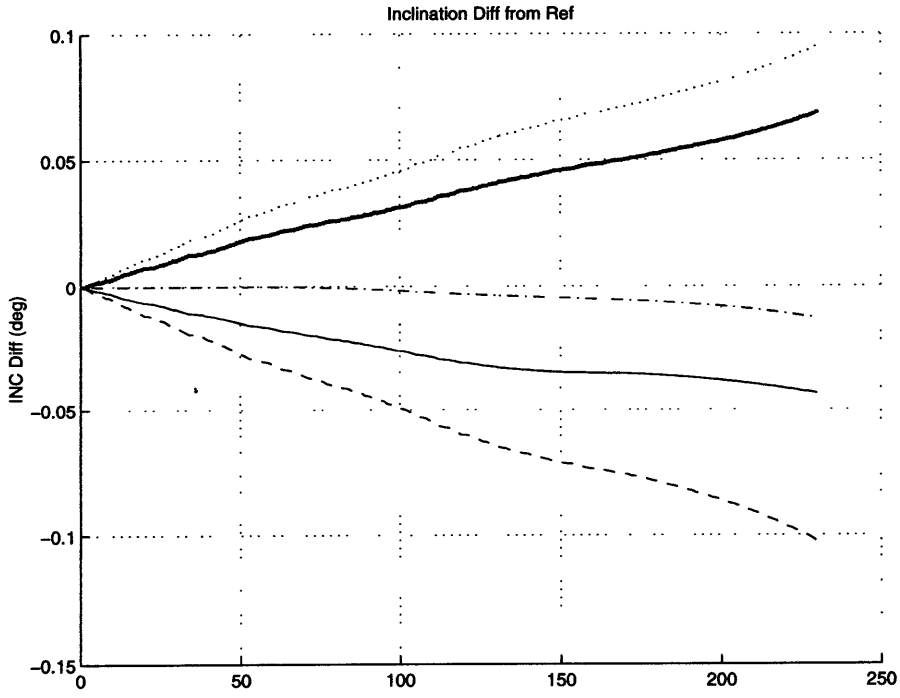

Figure E-5: 2 year inclination error history for Borealis node at noon plane

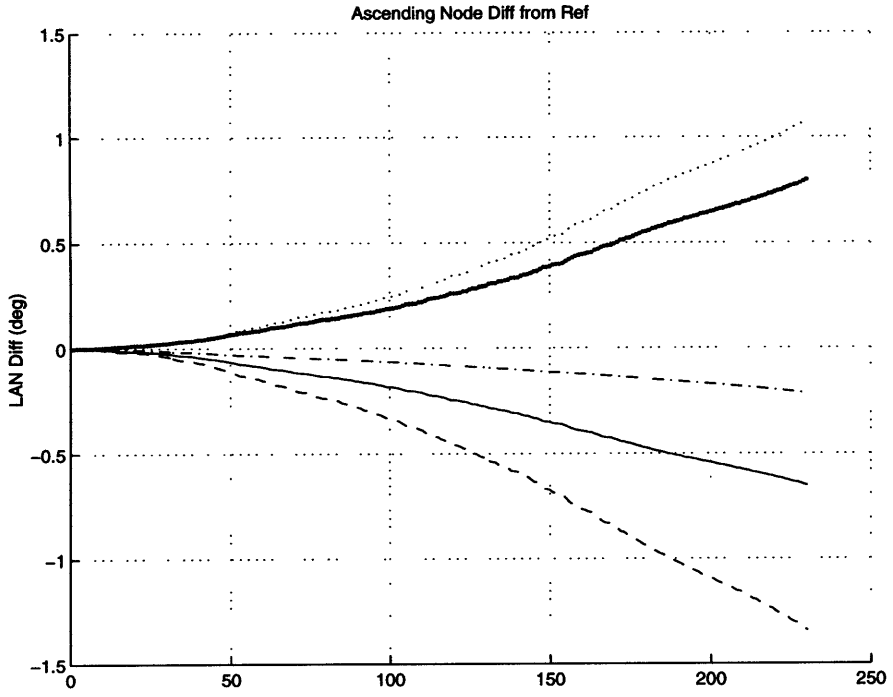

Figure E-6: 2 year ascending node error history for Borealis node at noon plane

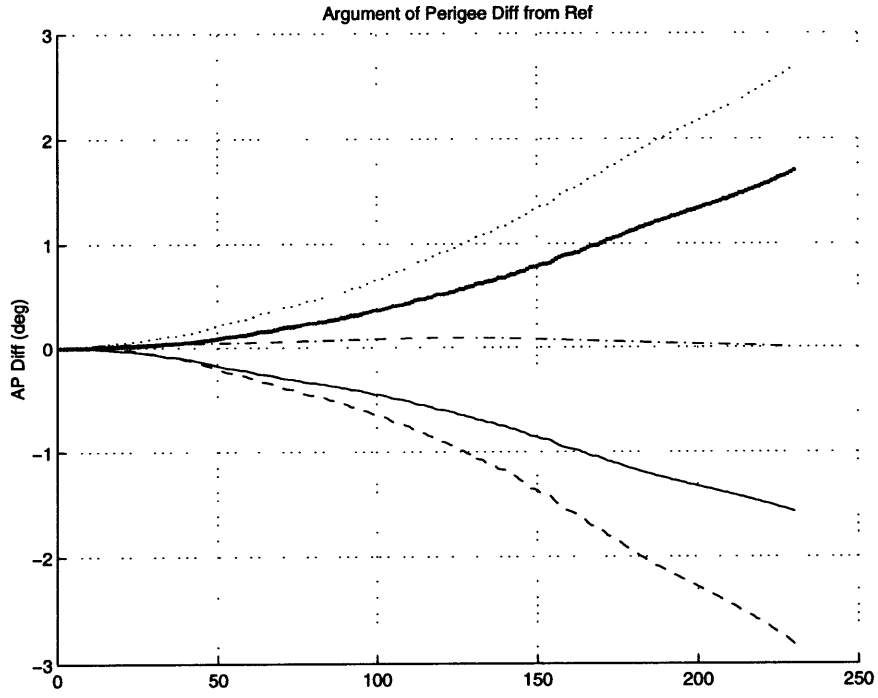

Figure E-7: 2 year argument of perigee error history for Borealis node at noon plane

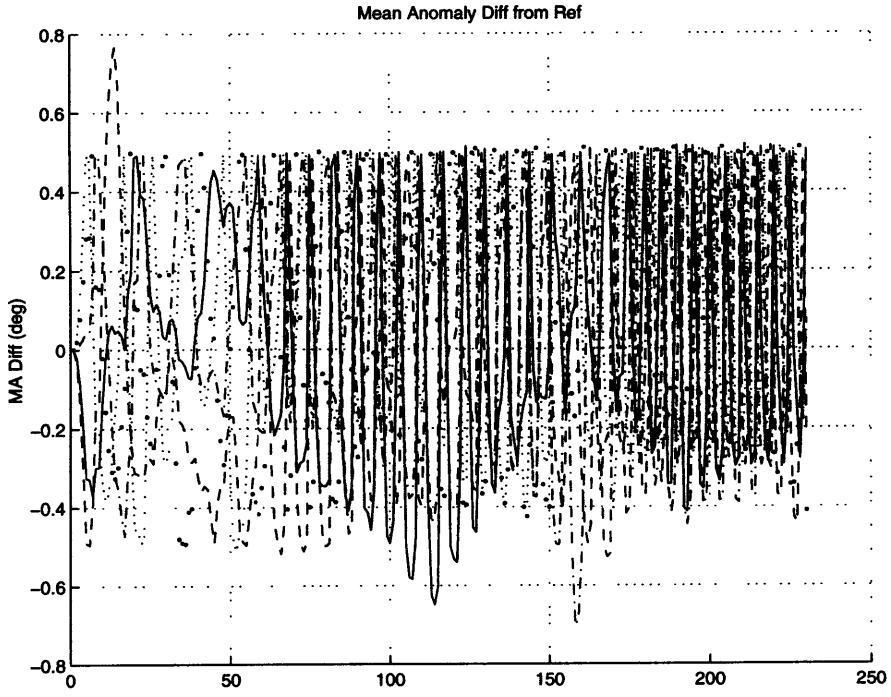

Figure E-8: 2 year mean anomaly error history for Borealis node at noon plane

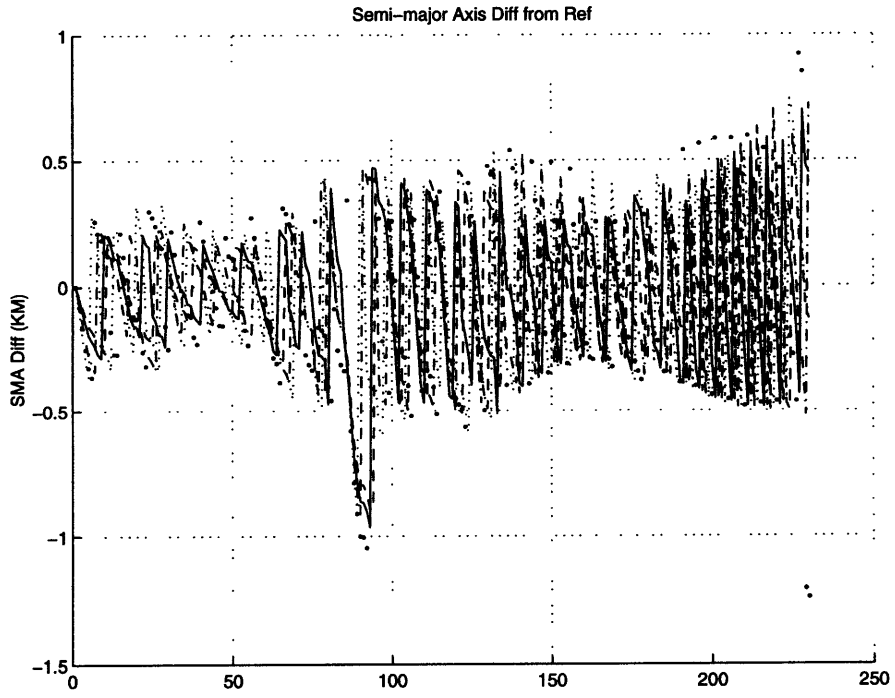

Figure E-9: 2 year semi-major axis error history for Borealis node at midnight plane

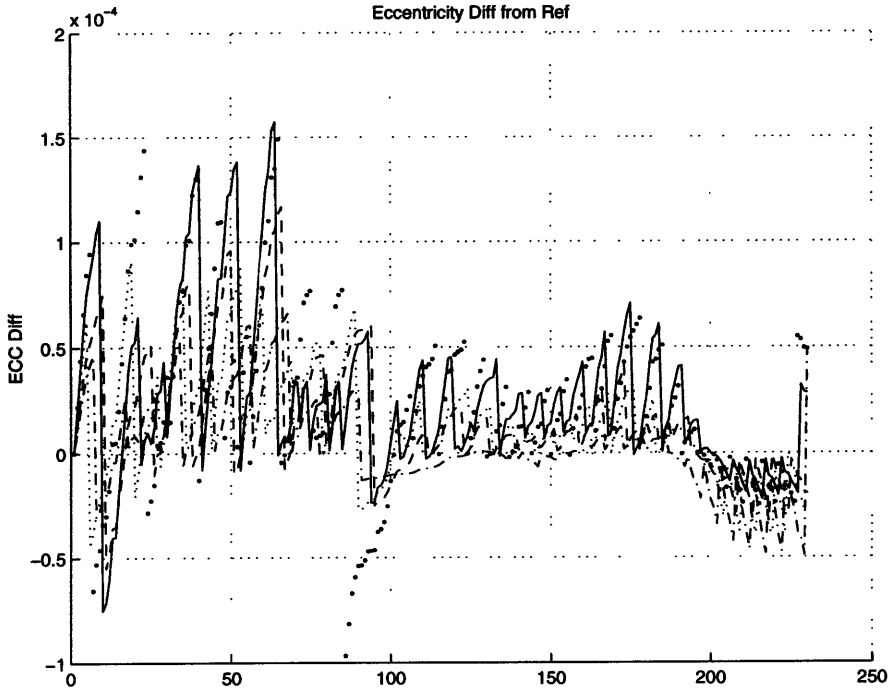

Figure E-10: 2 year eccentricity error history for Borealis node at midnight plane

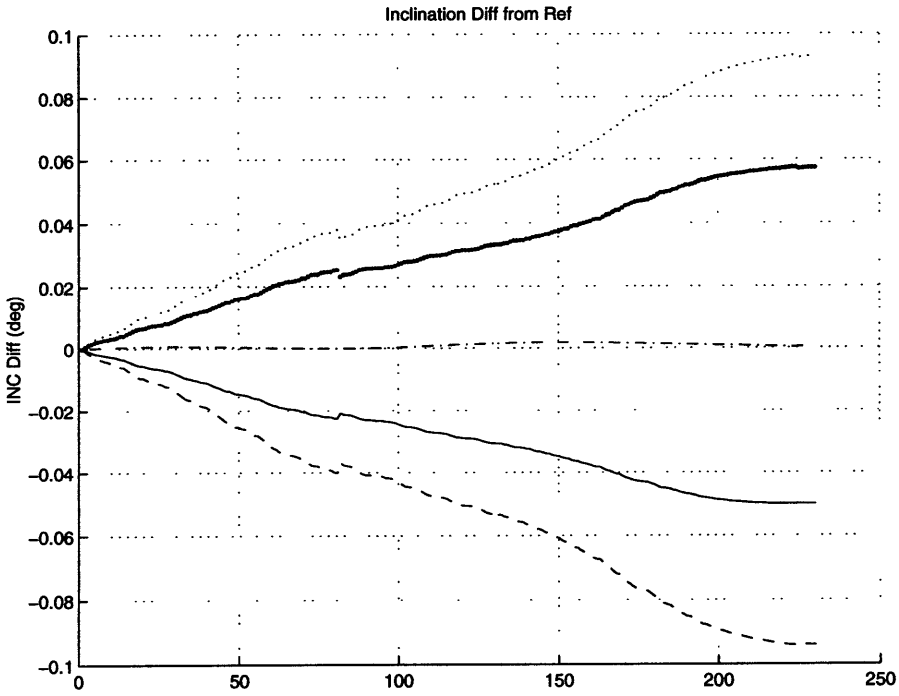

Figure E-11: 2 year inclination error history for Borealis node at midnight plane

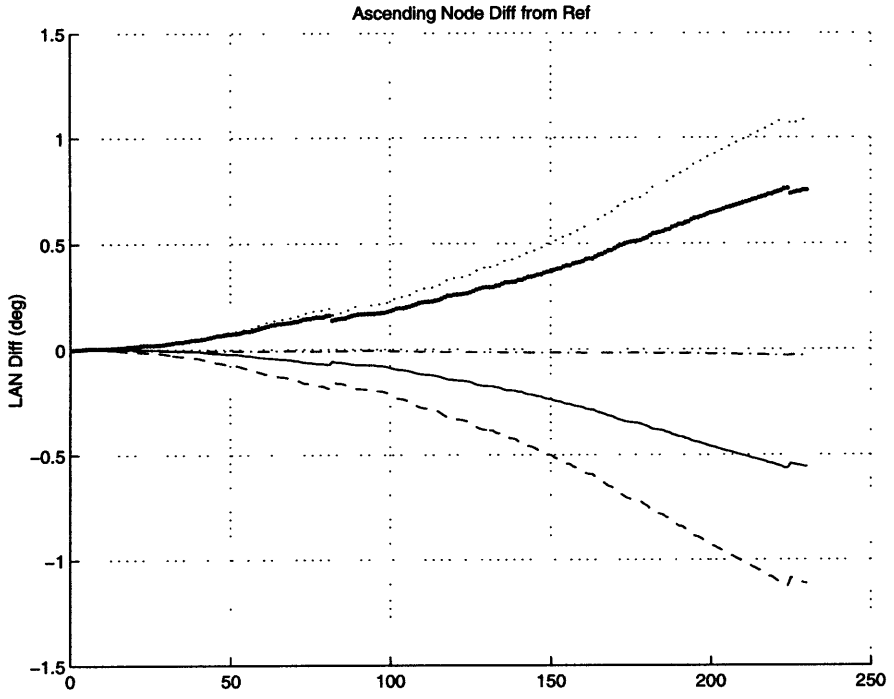

Figure E-12: 2 year ascending node error history for Borealis node at midnight plane

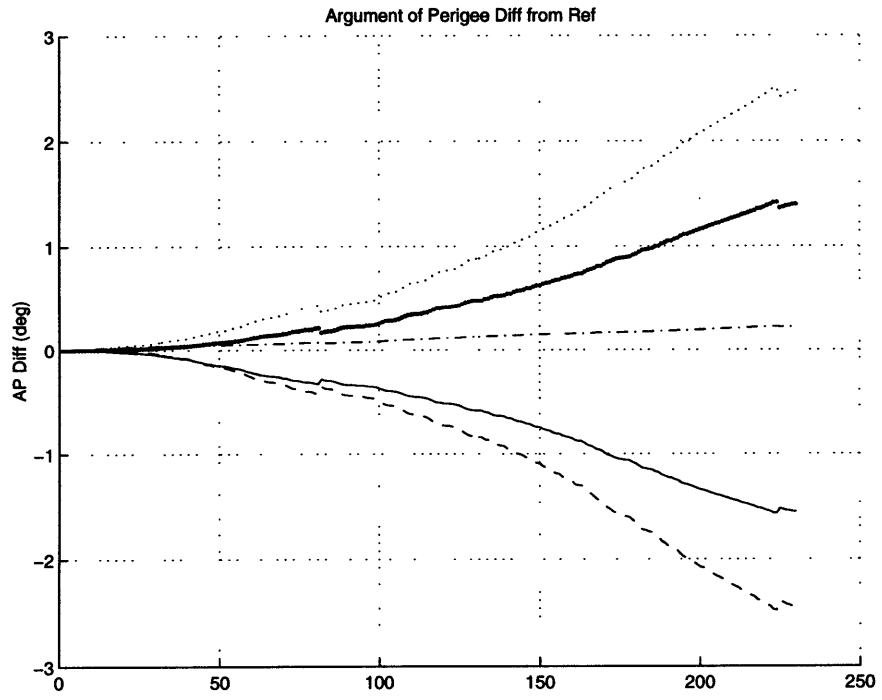

Figure E-13: 2 year perigee error history for Borealis node at midnight plane

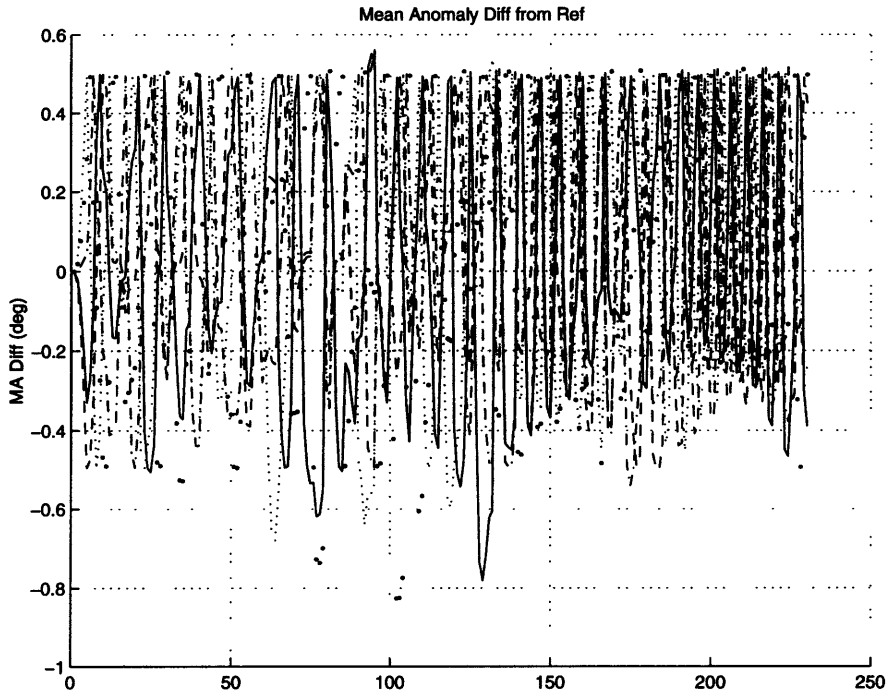

Figure E-14: 2 year mean anomaly error history for Borealis node at midnight plane

Appendix F

Analytic Coverage Driver

This appendix describes the driver for the analytic coverage software which may be used to confirm that the coverage calculations are being performed correctly. The program is called test_coverage and is located in the "mpi/c_src" subdirectory of the ASKS directory. The program requires the presence of "analytic_9.3" and "trig" to compile properly. To create the program, type "make test" at the prompt in this directory.

The driver creates the base configuration for six different constellations and calls the analytic coverage routines to calculate the coverage averaged over one period of the satellite orbits. The constellations chosen are:

1. Iridium
2. Globalstar
3. GPS
4. Ellipso, 81:10 repeat cycle
5. Ellipso, 115:14 repeat cycle
6. Ellipso, 8:1 repeat cycle

Choice	Steps	C	C_2	C_3	C_4	C_5	C_6	C_7	Time (sec)
1	20	100	79.7814	28.7278	14.8946	9.91539	7.11655	4.20013	22
2	20	100	100	95.615	77.9167	45.4821	21.6342	6.46261	6
3	2	100	100	100	100	100	100	96.7684	21
4	50	100	82.7165	32.954	7.27275	0.697123	0.02527	0	1
5	50	100	80.8085	30.7751	6.2842	0.23554	0	0	1
6	50	100	85.74	36.1752	7.78433	0.33769	0	0	1

Table F.1: Output data for analytic coverage driver

The n–way coverage is calculated up to a maximum level of seven. It also outputs the time required to determine the coverage. Elevation angle and latitude restrictions vary appropriately with the constellation.

The program is executed by typing at the prompt:

> test_coverage *constellation–choice steps–per–period*

The results for some test cases are listed in Table F.1. The number of time steps per period listed in Table F.1 for the various constellations are not intended as recommendations for actual analysis; they were chosen simply to cause the coverage calculations to be completed quickly. In addition, the listed values for time required for each computation will, of course, vary depending on the computer system and the process load, but does give some qualitative measure of the expected run-time for each configuration.

Bibliography

[1] M. E. Ash, 2 August 1974. Lincoln Laboratory internal memo.

[2] Ghassem Asrar and David J. Dokken. *State of Earth Science for Space: Past Progress, Future Prospects.* American Institute of Physics, Woodbury, NY, 1995.

[3] Richard H. Battin. *An Introduction to the Mathematics and Methods of Astrodynamics.* AIAA, New York, NY, 1987.

[4] Gerald Berman and K. D. Fryer. *Introduction to Cominatorics.* Academic Press, New York, NY, 1972.

[5] W. N. Barker S. J. Casali and R. N. Wallner. The accuracy of general perturbation and semianalytic ephemeris theories. *AAS / AIAA Astrodynamics Conference held in Halifax, Nova Scotia*, 14–17 August 1995. AAS Paper 95-432.

[6] R. G. Casten and R. P. Gross. Satellite cumulative earth coverage. *Proceedings of the AAS / AIAA Astrodynamics Specialist Conference held in Lake Tahoe, Nevada*, 3–5 August 1981. AAS Paper 81-125.

[7] Dennis Diekelman. Personal communication, 10 Jul 1997.

[8] John Draim, 5 March 1997. Fax to Draper Laboratory.

[9] John E. Draim. A common-period four-satellite continuous global coverage constellation. *Journal of Guidance, Control, and Dynamcics*, 10:492–499, 1987.

[10] L. W. Early. A portable orbit generator using semianalytical theory. *Proceedings of the AIAA / AAS Astrdynamics Specialist Conference held in Williamsburg, VA*, 18–20 August 1986. AIAA Paper 86-2164.

[11] T. Garrison, M. Ince, J. Pizzicaroli, and P. Swan. Iridium constellations dynamics : The systems engineering trades. *Proceedings of the 46th Inernational Astronautical Conference held in Oslo, Norway*, 2–6 October 1995. IAF Paper 95-U.2.04.

[12] Frank Gobetz. Satellite networks for global coverage. *Advances in the Astronautical Sciences*, 9:134–145, 1963.

[13] Robin M. Green. *Spherical Astronomy.* Cambridge University Press, Cambridge, England, 1985.

[14] Elizabeth Hayes. An algorithm for the computation of coverage area by earth observing satellites. *Proceedings of the AIAA / AAS Astrdynamics Specialist Conference held in Williamsburg, VA*, 18–20 August 1986. AIAA Paper 86-2067.

[15] Janis Indrikis and Robert Cleave. "space eggs: Satellite coverage model for low earth orbit constellations". In *Proceedings of the Fifth Annual Conference on Small Satellites*, Boston, 26–29 March 1991. AIAA / Utah State University, Academic Press.

[16] Jr. Joseph G. Neelon, Paul J. Cefola, and Ronald J. Proulx. Automated station-keeping for satellite constellations. *Proceedings of the AAS / AIAA Astrdynamics Specialist Conference held in Sun Valley, Idaho*, 4–7 August 1997. AAS Paper 97-731.

[17] Brian L. Kantsiper and Stanley I. Weiss. An analytic approach to calculating earth coverage. *Proceedings of the AAS / AIAA Astrdynamics Specialist Conference held in Sun Valley, Idaho*, 4–7 August 1997. AAS Paper 97-620.

[18] Thomas J. Lang. Conjunction / interference between leo and geo comsats. *Proceedings of the AAS / AIAA Astrodynamics Specialist Conference held in Sun Valley, Idaho*, 4–7 August 1997. AAS Paper 97-668.

[19] Wiley J. Larson and James R. Wertz. *Space Mission Analysis and Design*, chapter 7, pages 157–196. Space Technology Series. Microcosm and Kluwer Academic Publishers, Torrance, California, second edition, 1993.

[20] D. F. Lawden. Optimal trajectories for space navigation. 1963.

[21] Mark G. Matossian. Improved candidate generation and coverage analysis methods for design optimization of symmetric multi-satellite constellations. *Proceedings of the 47th Inernational Astronautical Conference held in Beijing, China*, 7–11 October 1996. IAF Paper 96-A.3.09.

[22] J. W. Middour. An efficient technique for computation of satellite earth coverage. *Proceedings of the 27th Aerospace Sciences Meeting held in Reno, Nevada*, 9–12 January 1989. AIAA Paper 89-0452.

[23] Giovanni Palmerini. Design of global coverage constellations based on elliptical orbits. *Proceedings of the AIAA / AAS Astrdynamics Specialist Conference held in San Diego, CA*, pages 589–594, 29–31 July 1996. AIAA Paper 96-3637.

[24] Nino Pino. Personal communication, 10 Jul 1997.

[25] Chris Sabol. Application of sun-synchronous critically inclined orbits to global personal communications systems. Master's project, Massachusetts Institute of Technology, Department of Aeronautics and Astronautics, November 1994.

[26] C[hris] Sabol, J[ohn] Draim, and P[aul] Cefola. Refinement of a sun-synchronous, critically inclined orbit for the ellipso personal communication system. *AAS / AIAA Astrodynamics Conference held in Halifax, Nova Scotia*, 14–17 August 1995. AAS Paper 95-340.

[27] N[aresh] Shah, R[on] Proulx, B[rian] Kantsiper, P[aul] J. Cefola, and J[ohn] Draim. Automated station-keeping for satellite constellations. *Proceedings of the AAS / AIAA Astrdynamics Specialist Conference held in Sun Valley, Idaho*, 4–7 August 1997. AAS Paper 97-623.

[28] Naresh H Shah. Automated station-keeping for satellite constellations. Master's project, Massachusetts Institute of Technology, Department of Aeronautics and Astronautics, June 1997.

[29] Dan Smith. Operations innovations for the 48-satellite globalstar constellation. *Proceedings of the AIAA / AAS Astrdynamics Specialist Conference held in San Diego, CA*, pages 537–542, 29–31 July 1996. AIAA Paper 96-1051.

[30] J[ames] J. Spilker and Bradford W. Parkinson. *Overview of GPS Operation and Design*, volume 1 of *Global Positioning System: Theory and Practice*, chapter 1, pages 29–56. American Institute of Aeronautics and Astronautics, Washington, DC, 1994.

[31] Michael Violet. The development and application of a cost per minute metric for the eavluation of mobile satellite systems in a limited-growth voice communications market. Master's project, Massachusetts Institute of Technology, Department of Aeronautics and Astronautics, September 1995.

[32] J. G. Walker. Some circular orbit patterns providing continuous whole earth coverage. *Journal of the British Interplanetary Society*, 24:369–384, 1971.

[33] J. G. Walker. Continuous whole earth coverage by circular orbit satellites. *Proceedings of the International Conference on Satellite Systems for Mobile Communications and Surveillance*, pages 369–384, 13–15 March 1973.